Macromolecules

Perspective

Cite This: Macromolecules 2018, 51, 6157−6189

Grafting Polymers *from* Cellulose Nanocrystals: Synthesis, Properties, and Applications

Sandra Wohlhauser,[†] Gwendoline Delepierre,[†] Marianne Labet,[£] Gaëlle Morandi,[‡] Wim Thielemans,[£] Christoph Weder,[†] and Justin O. Zoppe*[,†]

[†]Adolphe Merkle Institute, University of Fribourg, Chemin des Verdiers 4, 1700 Fribourg, Switzerland

[£]Renewable Materials and Nanotechnology Research Group, Chemical Engineering, KU Leuven, Campus Kulak Kortrijk, Etienne Sabbelaan 53, 8500 Kortrijk, Belgium

[‡]Laboratoire Polymères, Biopolymères, Surfaces, Normandie Université, INSA de Rouen, Avenue de l'Université, 76801 Saint-Étienne-du-Rouvray Cedex, France

Supporting Information

ABSTRACT: Over the past 10 years, the grafting of polymers from the surface of cellulose nanocrystals (CNCs) has gained substantial interest in both academia and industry due to the rapidly growing number of potential applications of surface-modified CNCs, which range from building blocks in nanocomposites and responsive nanomaterials to antimicrobial agents. CNCs are rod-like nanoparticles that can be isolated from renewable biosources and which exhibit high crystallinity, tunable aspect ratio, high stiffness, and strength. Upon drying, the abundance of surface hydroxyl groups often leads to a degree of irreversible aggregation, as a result of strong hydrogen bonding. Moreover, their relatively hydrophilic character renders CNCs incompatible with hydrophobic media, e.g., nonpolar solvents and polyolefin matrices. By grafting macromolecules from their surface, CNCs can be imparted with surface characteristics and other physicochemical properties that are reminiscent of the grafted polymer. This has allowed the design of nanoscale building blocks whose readily tunable properties are useful for the formation of both colloidal dispersions and solid state materials. In this Perspective, we provide an overview of the morphology and surface chemistry of CNCs and detail various techniques to manipulate their surface chemistry via polymer grafting *from* approaches. Moreover, we explore the most common polymerization techniques that are used to graft polymers from the surface and reducing end groups of CNCs, including surface-initiated ring-opening polymerization (SI-ROP), surface-initiated free (SI-FRP), and controlled (SI-CRP) radical polymerization. Finally, we provide insights into some of the emerging applications and conclude with an outlook of future work that would benefit the field.

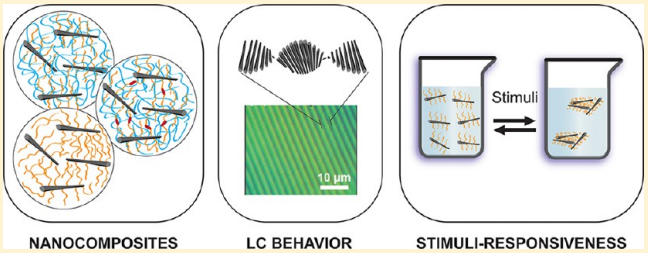

1. INTRODUCTION

During the last 3 decades, nanomaterials have emerged to play an ever increasing role in the material science field and are nowadays commonly found in our daily lives.[1] Nanomaterials display interesting and often unique mechanical, optical, and/or electronic properties, as a result of their high surface area as well as their specific structural features, that are not available in micro- and macroscale analogues. Cellulose-based nanocrystals and -fibrils have emerged as a particularly widely used class of building blocks for structural as well as advanced functional materials.[2−8] Cellulose, a linear homopolysaccharide composed of β-D-anhydroglucopyranose units, is the most abundant organic polymer on Earth and a promising renewable resource for the future production of biobased materials and fuels.[9] Cellulose is found in a wide variety of species, such as higher plants, tunicates, algae, fungi, bacteria, invertebrates, and amoeba. In nature, cellulose is found in hierarchically structured multicomponent materials, which at the lowest hierarchical level feature assemblies that contain individual cellulose in a uniaxially ordered (semi)crystalline organization. Careful disintegration schemes permit accessing cellulose nanocrystals (CNCs) and cellulose nanofibrils (CNFs), whose properties (e.g., crystallinity, morphology, aspect ratio, and surface chemistry)[10] depend on the requirements for use in polymer nanocomposites, colloidal liquid crystals, hydrogels, and multiresponsive materials.[2,8,11−14]

CNCs are rod-like nanoparticles that can be isolated from renewable biosources, and which exhibit high crystallinity, tunable aspect ratio, and high stiffness and strength. Typical dimensions are lengths in the range from 50 nm to more than 1 μm and widths of 5−50 nm, depending on the source material.[5,10] In contrast to many other nanorods, CNCs appear to be physiologically benign.[15−17] CNCs are commonly obtained by strong acid-catalyzed hydrolysis, with sulfuric acid as the most commonly used acid, which selectively degrades the amorphous regions of

Received: April 6, 2018
Revised: June 28, 2018
Published: July 26, 2018

DOI: 10.1021/acs.macromol.8b00733
Macromolecules 2018, 51, 6157−6189

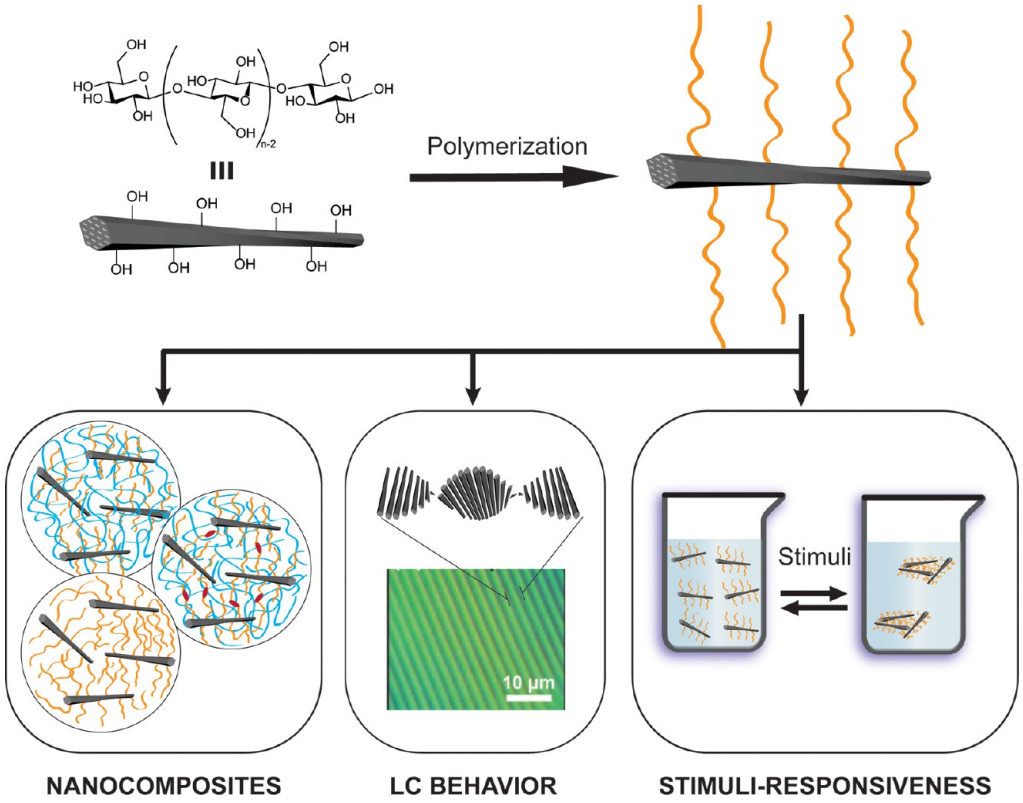

Figure 1. Schematic representation of CNC transformation into polymer-modified CNCs, which are useful for the formation of nanocomposites containing one or multiple components, display LC behavior, or exhibit stimuli-responsive behavior. (The center graphic in the bottom row was adapted from ref 31. Copyright 2017 Wiley-VCH Verlag GMbH & Co. KGaA.)

macroscopic cellulose fibers, while the crystalline domains stay intact. Hydrolysis with sulfuric acid also introduces anionic sulfate half-ester groups on the surface of the CNCs, which are essential for their colloidal stability in water, on account of electrostatic repulsions. This effect also likely plays an important role in their spontaneous assembly into chiral nematic (*a.k.a.* cholesteric) colloidal liquid crystal (LC) phases, in addition to their inherent chirality.[18−20] CNCs hydrolyzed by sulfuric acid typically show, however, a limited thermal stability, which is apparent by significant coloration when processed at elevated temperatures and presents an obstacle for the fabrication of polymer nanocomposites.[21,22] This problem can be overcome by hydrolyzing cellulose pulp with phosphoric acid, which affords CNCs with a low concentration of phosphate surface groups and which offer an attractive combination of adequate dispersibility in polar solvents and improved thermal stability.[21] The production of CNCs has also evolved at the industrial scale in some countries such as Canada, the United States, Israel, and Sweden, even though it is still developing.[23]

The CNC surfaces also contain many hydroxyl (−OH) groups, which allow many types of chemical modifications and enable a broad range of nanomaterials that cover a wide spectrum of properties and functions, ranging from stimuli-responsiveness to antimicrobial capabilities.[8,12] In addition, surface chemical modifications allow transforming the rather hydrophilic CNCs into hydrophobic particles, and thus facilitate their use in hydrophobic media.[24−26] One of the primary challenges in the chemical modification of CNCs is to carry out successful reactions without impacting their intrinsic properties, notably the dimensions, crystallinity, and intrinsic mechanical properties.[7]

Surface modification by graft polymerization proved to be a robust approach, in which some of the physical and chemical properties can be tailored at will.[4,27−29] Graft polymerization of surfaces can be performed by using "grafting *to*", "grafting *from*", or "grafting *through*" methods. The grafting *through* method involves the functionalization of solid substrates with polymerizable functional groups, e.g., acrylic moieties, followed by polymerization *in situ*. While the grafting *to* method involves the connection of preformed polymeric chains with the surface through reactive end groups, the grafting *from* strategy concerns the growth of polymer chains via surface-initiated polymerization either from a substrate containing functional groups capable of initiating the polymerization reaction, or by immobilization of an active initiator species to the substrate surface. Due to the steric hindrance often encountered while utilizing the grafting *to* approach, the grafting *from* approach has the advantage of well-controlled polymer graft lengths and high polymer tether grafting density.

As the latter strategy has been widely employed to modify CNCs toward multicomponent colloids and, more recently, one component-nanocomposites (OCNs), in which no polymer matrix is required and the final materials do not usually suffer from phase separation issues, this will be the focus of our Perspective (Figure 1). Our aim is to provide a concise overview of the field of grafting polymers *from* the surface of CNCs, while highlighting some noteworthy contributions over the past decade, since the pioneering work of Habibi et al. in 2008,[30] who introduced ε-caprolactone grafting from CNCs via surface-initiated ring-opening polymerization (SI-ROP). In the following sections, the physicochemical properties of CNCs, various chemical modification pathways known to graft polymers

DOI: 10.1021/acs.macromol.8b00733
Macromolecules 2018, 51, 6157−6189

from the surface of the CNCs and applications of polymer-modified CNCs (CNC-*g*-polymer) will be described and the opportunities and challenges that have emerged in the field will be discussed.

2. MORPHOLOGY AND SURFACE CHEMISTRY OF CNCS

The semicrystalline nature of cellulose fibers, in which the crystalline regions are held together by strong inter- and intramolecular hydrogen bonds, gives rise to their unique mechanical properties and is the naturally selected main structural component of the primary cell wall in higher plants.[9] Although less understood from a structural standpoint due to their disordered morphology, the noncrystalline, or "amorphous," regions of cellulose are thought to be advantageous in terms of water transport in plants.[32] This inherent architecture of cellulose fibers is what ultimately allows the nanoscale crystalline regions to be selectively extracted from macroscopic fibers through acid-catalyzed hydrolysis. Thus, before moving forward into methodologies to modify the surface of CNCs with polymer grafts, it is imperative to first discuss the structure of cellulose, its crystalline domains and the various extraction methods to produce CNCs, which lead to strikingly different surface chemistries and reactivity.

2.1. Morphology. Cellulose is the trivial name for the linear homopolysaccharide polymer composed of β-D-anhydroglucopyranose and linked by $\beta(1-4')$ glycosidic (ether) bonds. The repeating anhydroglucopyranose unit (referred to as AGU)[33] in cellulose is a six-membered closed ring form of D-glucose in the chair conformation with the anomeric carbon (C1) in the β-position (Figure 2).[34] The $\beta(1-4')$ glycosidic bond between

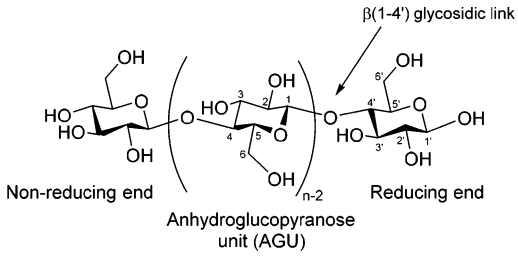

Figure 2. Molecular structure of cellulose, with the anhydroglucose repeating unit in the chair conformation, the glycosidic bond, as well as reducing and nonreducing chain ends.

the different AGUs results in a twist along the length of the chain, which can be defined by the glycosidic torsion angles ϕ = H1−C1−O4′−C4′ and ψ = C1−O4′−C4′−H4′.[35] It has to be noted that the definition of these angles is not standardized in the literature, so comparisons of values reported for different sources needs to take into account the angle definitions used.[35−37]

While the ring structure of the AGU is confined to the chair conformation with the C−O bonds in the equatorial position, free rotation can occur around the C5−C6 bond, resulting in different conformations of the hydroxymethyl group relative to the glucose ring. The position of the hydroxymethyl group relative to the glucopyranose ring can be described by the angles χ = O5−C5−C6−O6 and χ' = C4−C5−C6-O6.[5,38] Three energetic minima can be found when the angles are both 60° (*gauche*−*gauche* conformation, *gg*), 60°−180° (*gauche*−*trans*, *gt*), and 180°−60° (*trans*−*gauche*, *tg*).[5,36,37] The free rotation around the C5−C6 bond with the resulting freedom of positioning of O6 enables different hydrogen bonding patterns, including in cellulose crystals.[37,39]

Until recently, seven different crystal allomorphs of cellulose were thought to exist: I_α, I_β, II, III_I, III_{II}, IV_I, and IV_{II}. While cellulose II is thermodynamically the most stable form, native cellulose was thought to exist in polymorphs I_α (found in bacterial cellulose and algae, triclinic unit cell) and I_β (higher plants, monoclinic unit cells).[40,41] Recent findings from solid-state NMR spectroscopic investigations suggest, however, that native plant cellulose is structurally polymorphic and differs greatly from I_α and I_β, as evidenced by seven unique sets of ^{13}C chemical shifts.[42,43] While five of these sets are attributed to interior cellulose chains within microfibrils, two are assigned to surface chains and such structural complexity arises from interactions with matrix polysaccharides unique to higher plant celluloses. Nevertheless, cellulose I_α has been found to be metastable and can be partially transformed into I_β by annealing above 260 °C or treatment with gases and organic solvents.[44−46] Cellulose II is obtained by recrystallization of cellulose after dissolution, thus attaining the thermodynamic minimum. The other allomorphs are local minima in the highly regular hydrogen bonded network of cellulose chains. All allomorphs, despite some having parallel and others antiparallel chain alignment, have a pseudo 2_1 helical conformation of cellulose chains as a result of intrachain O3H−O5′ hydrogen bonding.[47] Disruption of any cellulose crystal structure can thus be expected to be linked to disruption of this intrachain hydrogen bond, a fact supported by the ability of cellulose to attain a random coil conformation when dissolved.[48] The various cellulose polymorphs have unique X-ray diffraction signatures corresponding to the spatial crystal arrangements in their structure.[9] The crystal packing of cellulose's polymorphs differ in the unit cell dimensions and, may present variations in the chain polarity, which result in changes in the properties of cellulose, such as its rigidity, thermal stability, solubility, or reactivity.[49]

Cellulose chains are synthesized by cellulose synthase enzymes arranged in complexes located at the plasma membrane. This cellulose synthase complex (CSC) produces elementary cellulose protofibrils with a width of 3−4 nm.[50] These CSCs sit at the end of the growing fibrils.[51,52] The CSC can take different forms with three rows of ordered particles, as seen in the algae *Oocytis apiculata*,[51] other linear complexes, as in tunicates and the algae *Valonia* and *Erythrocladia*,[53] while in higher plants as well as the green algae *Micrasterias* a hexameric rosette complex containing six particles, each featuring six cellulose synthases, have been reported.[53,54] The protofibrils are arranged into semicrystalline microfibrils with diameters up to 20 nm.[55,56] The ratio of crystalline to amorphous domains and the ratio of I_α to I_β found in the crystalline domains is dependent on the source of cellulose.[5,7,39,57]

CNCs are commonly represented as ribbons with either a parallelepiped or a hexagonal cross-section (Figure 3); the shape and the number of individual cellulose molecules varies greatly with the cellulose source. Native cellulose microfibrils in plants and bacteria have long been thought to consist of 36 chains, but recent advances in the structural characterization of CSCs suggest that an 18-chain model may be a more accurate depiction.[58] On the other hand, solid-state NMR spectroscopic experiments indicate that primary cell wall cellulose microfibrils are composed of at least 24 chains, which may be due to coalescence of multiple microfibrils synthesized by neighboring CSCs.[42,59] The exact number of cellulose chains within native cellulose microfibrils still remains a highly debated research topic.

As the main differences between the I_α and I_β structures have been shown to lie in the conformation of the AGU and the $\beta(1-4')$ linkages by NMR spectroscopy and X-ray and neutron

DOI: 10.1021/acs.macromol.8b00733
Macromolecules 2018, 51, 6157−6189

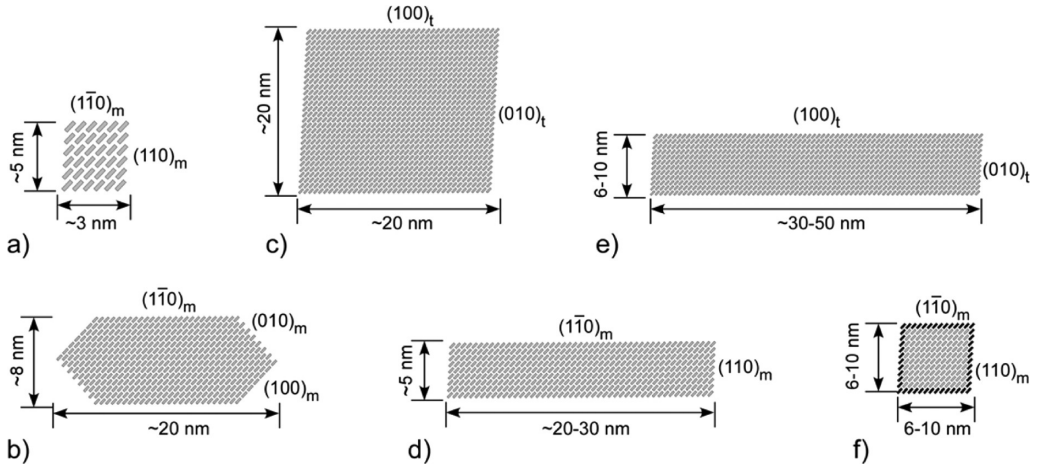

Figure 3. Schematic representation of idealized cellulose cross sections showing the faces of cellulose nanocrystals with the crystal planes (*t* = triclinic, m = monoclinic unit cell) and the crystal structure. Each gray box represents the cross-section of a cellulose chain viewed in the direction of its long axis. Representations for CNC extracted from (a) wood, (b) tunicate, (c) *Valonia*, (d) *Micrasterias*, (e) reference bacterial cellulose from *Acetobacter*, and (f) bacterial cellulose from *Acetobacter* produced in the presence of mannan. Reproduced from ref 7 with permission. Copyright 2011 The Royal Society of Chemistry.

diffraction,[57,60] one could assume that the availability and reactivity of the surface −OH groups between both allomorphs are similar. Crystal structure diffraction studies indicate the hydroxymethyl conformation to occur in the *tg* conformation with hydrogen bonding to exist between O3H−O5′ and O2H−O6′ of cellulose chain aligned next to each other, whereas hydrogen bonding between stacked chains is virtually nonexistent.[57] The 2-fold helical twist of the cellulose chain due to the $\beta(1-4')$ linkage (Figure 2) results in an alternation of primary and secondary −OH groups pointing out of the crystal along a single cellulose chain.

To assess surface reactivity, one needs to consider that surface groups are not as confined as the same groups within the CNCs. Indeed, ^{13}C solid state NMR studies suggest that the hydroxymethyl groups on the surface chains pointing outward display a different conformation (*gg*) than the hydrogen-bonded primary −OH groups inside the CNCs (*tg*).[38,60] One can also envision that the ability to change the conformation of the hydroxymethyl group will depend on the level of interference of the solvent in the hydrogen bonding of the hydroxymethyl group with other groups in the crystal surface.

Experimental observations suggest that the surface reactivity of the surface −OH groups follows O2 > O6 > O3 for native cotton and cotton-like (i.e., linen, ramie, sisal and wood) celluloses, whereas it follows O6 > O2 > O3 for *Valonia ventricosa* cellulose as a consequence of a higher degree of intramolecular hydrogen bonding between O3H and O5′H and the higher crystalline order leading to a reduction in the absolute availability of O2H by inaccessibility in the interior of the crystalline region (Figure 2).[61] This may be considered further confirmation of the *gg* conformation of the surface hydroxymethyl group as the intramolecular O2H−O6 hydrogen bond is not possible in this conformation. Surface reactivity also needs to consider the reaction mechanism. After activating surface hydroxyl groups, the O2 position cannot react under S_N2 conditions as the CNC crystal inhibits Walden inversion and only O6 can be expected to react. This can also be seen when surface alcohol groups have been replaced by chloride.[62] Finally, the reactivity of the −OH groups at the surface of cellulose seems also to be affected by the reaction media, i.e., the −OH groups at position 6 are the most available for reaction in homogeneous solutions following the order O6 > O2 > O3 due to steric reasons, while for heterogeneous modifications the −OH groups at position 2 become the most reactive species with the following order O2 > O6 > O3.[63]

2.2. Surface Chemistry. Chemical reactions carried out at solid−liquid interfaces differ from homogeneous reactions in that adsorption is a prerequisite for the chemical reaction to occur and functional groups on surfaces have fewer degrees of freedom as discussed above.[64] With an understanding of cellulose crystal morphology and surface −OH group reactivity, one must also be aware of the factors involved in CNC processing that affect their surface chemistry.

By far the most common method to extract CNCs from cellulosic raw materials is sulfuric acid-catalyzed hydrolysis.[2,3,5−7] After delignification of the native material and removal of hemicelluloses, this typically involves exposing high purity cellulose fibers to a 55−65 wt % sulfuric acid solution for 30−60 min at temperatures ranging from 35 to 70 °C. During this process, sulfuric acid reacts with a fraction of the −OH groups at the surface of the crystalline regions to form sulfate half-esters, which are typically present at a concentration in the range of 150−400 mmol/kg.[65] Upon purification by multiple centrifugation steps and dialysis against deionized water, these sulfate half-ester groups are negatively charged, yielding highly stable CNC dispersions due to electrostatic repulsions. As mentioned above, CNCs hydrolyzed by sulfuric acid typically display a limited thermal stability.[21,22] The sulfate half-esters can be removed by hydrolytic or solvolytic desulfation procedures,[66,67] but this modification comes at the expense of a reduced dispersibility.

It is also possible to employ hydrochloric (HCl)[68] or hydrobromic (HBr)[69] acid for the hydrolysis. In some cases, CNCs with a very low surface charge are produced; these charges likely originate from a small amount of carboxylate groups (*ca.* 20−30 mmol/kg).[65] Accordingly, CNCs produced by HCl- or HBr-based hydrolysis methods also have the disadvantage of low colloidal stability due to the lack of sufficient electrostatic repulsive forces that consequently allow hydrogen bonding between adjacent nanoparticles. Such dispersion aggregation is obviously problematic for subsequent surface modification. Phosphoric acid hydrolysis, introduced by Camarero Espinosa et al.,[21] affords

DOI: 10.1021/acs.macromol.8b00733
Macromolecules 2018, 51, 6157−6189

CNCs that feature a small concentration of phosphate groups (*ca.* 11 mmol/kg). In this case, each phosphate group at the CNC surface provides two acidic −OH groups and the CNCs display an interesting combination of good colloidal and thermal stability.

Other means to prepare CNCs include endoglucanase-mediated hydrolysis,[70] mechanochemical activation, and phosphotungstic acid hydrolysis,[71] ammonium persulfate (APS) oxidation,[72] and (2,2,6,6-tetramethylpiperidin-1-yl)oxyl (TEMPO)-mediated oxidation followed by cavitation.[73] The latter two methods yield CNCs functionalized with a high concentration of surface carboxylate groups (*ca.* 1.12−1.74 mmol/g for TEMPO-mediated oxidation),[73] which not only promote good dispersibility but also offer alternative surface chemical modification pathways.[24,25]

Regardless of the method utilized to produce CNCs, it is clear that anionic surface charges provide the colloidal stability necessary to prevent a certain degree of aggregation in both water and polar aprotic solvents, such as *N*,*N*-dimethylformamide (DMF) and dimethyl sulfoxide (DMSO).[74] The surface charges also affect the ease at which CNCs can be freeze-dried, and at the same time, they use up some of the surface −OH groups that could be used for later functionalization. In addition, the counterions of the surface charges strongly influence the redispersibility of dried CNCs by ultrasonication, especially on material with a moisture content lower than 4 wt % due to the presence of stronger intermolecular hydrogen bonds between CNCs.[75,76] Thus, using hydrolysis protocols that impart "just the right amount" of surface charges to promote colloidal stability appears advisable if subsequent surface modification reactions are to be carried out.

2.3. Pretreatments of CNCs for Surface Chemical Modification. The presence of surface impurities, bound water, and excess counterions can have a significant impact on the success of surface functionalization reactions and their reproducibility, notably between different types or batches of CNCs.[77−79] Furthermore, many reaction pathways suitable for the modification of −OH groups are intolerant to water, so that CNCs must either be dried and redispersed or transferred into a dry organic solvent by other means. It is possible to freeze-dry the CNCs[80−85] or to exchange the solvent.[30,83,86−89]

If freeze-dried CNCs are to be surface-modified, the nanocrystals are often washed with organic solvents such as ethanol,[78,79] acetone,[77] or *n*-pentane[77] to remove impurities. This is accomplished by either Soxhlet extraction[78,79] or by several cycles of dispersing the CNCs in the solvent of choice and subsequent separation via centrifugation.[77] It was found that such pretreatments improved the reproducibility between grafting experiments.[77]

Solvent exchanges usually involve mixing an aqueous dispersion of the CNCs with a water-miscible organic solvent, usually acetone, centrifugation, replacement of the solvent, and multiple repetitions of this cycle, until the solvent is changed to the organic solvent, in which surface-initiated polymerization is often performed.[30,87,88,90,91] For example, Tian et al. compared the SI-ROP of ε-caprolactone (ε-CL) from freeze-dried CNCs and from solvent-exchanged CNCs and observed that the grafting density is higher from the solvent-exchanged nanocrystals than from those that were freeze-dried.[86] From these findings, it is clear that impurities adsorbed on the surface of CNCs are generally better removed by treatment with organic solvents. These impurities are likely byproducts formed by the hydrolysis of residual hemicellulose or lignin or perhaps the acid-catalyzed dehydration of mono- and oligosaccharides.[2,7]

3. SURFACE-INITIATED POLYMERIZATION *FROM* CNCS

Much of the research efforts directed toward the surface modification of CNCs have focused on tuning the physicochemical characteristics of their surface, while at the same time preserving their morphological integrity and crystallinity.[24,25,92] Indeed, if the functionalization chemistry is chosen to selectively modify the surface or the reducing end groups, the intrinsic crystallinity and crystal structure of the CNCs should be retained, which can be checked by X-ray diffraction studies.[24,30,82,83,86,93−96] In the present section, the methods most often utilized to modify CNCs via the grafting *from* approach, i.e., surface-initiated and reducing end-initiated polymerization, will be presented.

3.1. Surface-Initiated Ring-Opening Polymerization. Ring-opening polymerization (ROP) is a common technique to produce polymers from cyclic monomers such as lactones,[97,98] dilactones,[99] lactams,[100] cyclic carbonates,[101] cyclic ethers,[102] and oxazolines[102] (Figure 4). For some of these monomers, e.g., lactones and dilactones, the ROP can be initiated by −OH groups. Therefore, they are ideal candidates for the surface modification of not only CNCs, but also cellulose fibers and nanofibrils, as they also contain a high density of −OH surface groups. In this case, the cellulosic substrate acts as a macroinitiator and the polymerization process is most often referred to as SI-ROP.

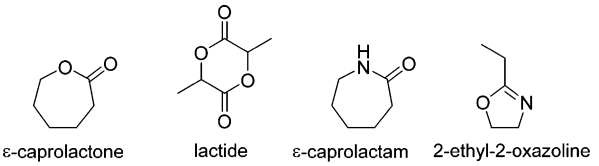

Figure 4. Examples of common monomers used for ROP.

CNC-g-polyesters. CNC-*g*-polyesters have been prepared by the SI-ROP of ε-caprolactone (ε-CL),[30,80−83,86,103−105] L-lactide (L-LA),[84,85,87,88,90,91,104,106−108] and D-lactide (D-LA)[89,105,109,110] from CNCs. The mechanism of the ROP of lactones and dilactones varies depending on the system used, i.e. the nature of the catalyst and the initiator.[111] The mechanism can be an anionic, a cationic, a monomer-activated or a coordination−insertion polymerization. In the case of SI-ROP from CNCs, the nanocrystals act as the initiator and the mechanism is only dependent on the catalyst. This reaction is water sensitive as water can also initiate the ROP of lactones. Therefore, the water, in which the nanocrystals are normally dispersed, needs to be removed as much as possible by means described in section 2.3.

Tin(II) 2-ethylhexanoate ($Sn(Oct)_2$)[30,77,80−88,90,91,103,105,106,108−110,112] is the most commonly used catalyst for the SI-ROP of (di)lactones. The reaction is usually performed in toluene, however it has also been carried out in ionic liquids (1-allyl-3-methylimidazolium chloride, [AMIM]Cl[113]), in DMSO,[108] or in bulk.[84] Typical conditions further are temperatures between 80 and 130 °C and a reaction time of typically 24 h. The grafted polymers have also been prepared under microwave irradiation.[81,112] Benzyl alcohol is sometimes used as a sacrificial initiator to produce free polymer in solution, which is easier to characterize than the grafts.[77,108] Of course, the comparison with free polymer that is produced "in parallel" is only sensible if one can safely assume that the kinetics of solution ROP are similar to SI-ROP from CNCs, which may or may not be the case.

In general, the nature of SI-ROP from CNCs makes the accurate characterization of grafted polymer molecular weight

DOI: 10.1021/acs.macromol.8b00733
Macromolecules 2018, 51, 6157−6189

Scheme 1. Mechanism of the SI-ROP of ε-CL from CNCs Using $Sn(Oct)_2$ as a Catalyst[a]

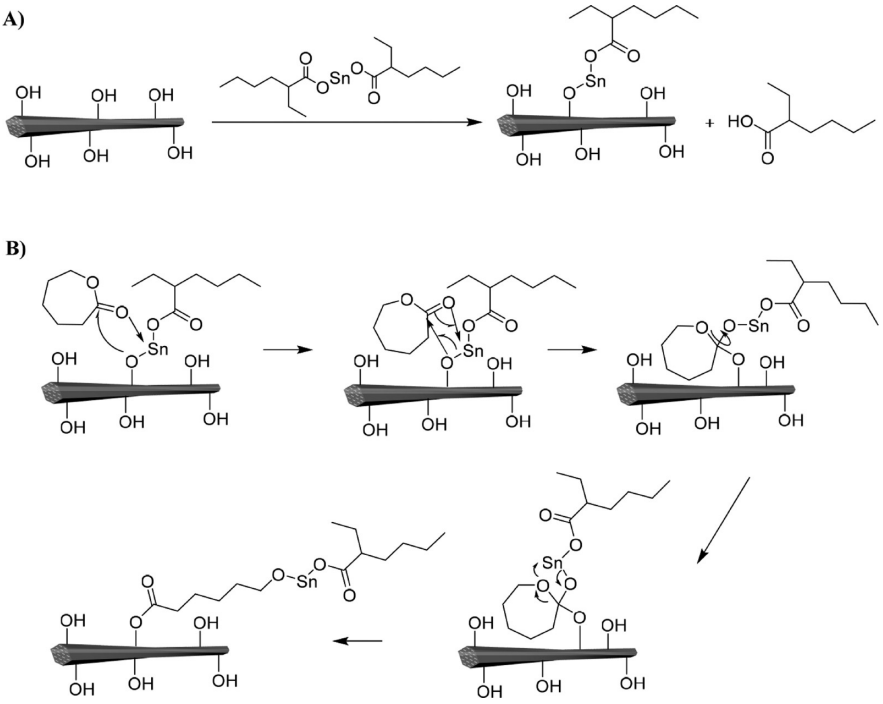

[a]Key: (A) Conversion of $Sn(Oct)_2$ into tin alkoxide. (B) Grafting of ε-CL from the surface of CNCs via coordination of tin alkoxide with the monomer.

and dispersity challenging, as the polymer must be degrafted before full molecular characterization is possible. Most degrafting schemes rely on hydrolytic cleavage of interfacial ester bonds, which, however, are also present in some of the polymer chains discussed here. This problem can potentially be addressed through the use of cleavable anchoring groups, such as those containing disulfides[114] or UV-sensitive moieties,[115] similar to the approached employed in the case of polymer-modified cellulosic substrates synthesized via surface-initiated controlled radical polymerization (SI-CRP).[28] Perhaps one could also take advantage of the high bond tension of the esters at the polymer-CNC interface, which are likely more sensitive to hydrolysis than esters along the polymer chain such that they could be cleaved by mechanochemical means, *e.g.*, by ultrasound.[116,117]

Some researchers have attempted to estimate the length of the polymer grafts based on the melting temperature determined by differential scanning calorimetry (DSC) using a correlation curve,[89,106,110] although this method does not account for potential differences in grafting density or effects of surface-confinement. Wu et al. proposed the use of FTIR data for poly(lactic acid) (PLA) brush quantification.[89] The approach relied on measuring FTIR spectra of physical mixtures of CNCs and PLA and creating a calibration curve based on the relative intensities of a characteristic band of PLA (i.e., 1454 cm^{-1}, corresponding to the CH_3 asymmetric stretching) and a characteristic band of the CNCs (i.e., 1428 cm^{-1}, corresponding to the CH_2 symmetric bending). The calibration curve was then employed to analyze CNC-*g*-PLA samples. While this method does not provide information on the molecular weight or grafting density of grafted polyesters, it permits to quantify the composition of PLA in CNC-*g*-PLA to be 25.3 wt % and estimate the molecular weight of the grafts to be 3.4 kDa.

Although the analysis of grafted CNCs in the liquid phase is usually impractical due to poor dispersibility in typical solvents,[106] some researchers managed to make stable colloidal dispersion of surface-modified CNCs in $CDCl_3$[105] or DMSO-d_6[107,118] (mixed with small amount of chloroform) in order to perform ^1H and ^{13}C NMR in well-stabilized dispersions. In this sense, the synthesis of CNC-*g*-PLA was evidenced by the appearance of resonance signals at 1.50−1.75 ppm (methyl protons),[105,107] 5.00−5.50 ppm (methine proton),[105,107] and 1.35 ppm (terminal methyl protons)[107] corresponding to PLA brushes. In the latter case, de Paula et al.[107] dispersed CNC-*g*-PLA in DMSO-d_6 with the addition of some chloroform and were able to directly calculate the degree of polymerization (DP) of PLA (=12) from the ^1H NMR spectra. This particular study highlights the limited DP one can achieve with SI-ROP from CNCs. In addition, the grafting of poly(ε-caprolactone) (PCL) from the surface of CNCs was confirmed in another study by the appearance of signals at 1.50−1.65 ppm, 2.23−2.32 ppm, and 4.07−4.11 ppm (methylene protons),[105] however, the DP of the polymer was not reported. It is important to note that the NMR results obtained from well-dispersed CNC-*g*-polymers may only provide partial information, which, unless appropriate separation protocols are used, is mainly related to free polymer molecules, while the polymer chains grafted from the dispersed contribute broader signals. Thus, the quantitative analysis of such NMR data is not always straightforward.

Regarding the mechanism of the SI-ROP catalyzed by $Sn(Oct)_2$, it is widely accepted that the reaction proceeds by a coordination−insertion mechanism. The first step is the conversion of the catalyst into a tin alkoxide to produce the active species, followed by the coordination of the monomer to the alkoxide through its insertion into the metal−oxygen bond (Scheme 1).[111]

Other metal-based catalysts that have been tested for SI-ROP of cyclic esters from CNCs include magnesium hydride (MgH_2)[107] and zinc oxide.[108] Zinc oxide seems to give similar

DOI: 10.1021/acs.macromol.8b00733
Macromolecules 2018, 51, 6157−6189

Scheme 2. Mechanism of the SI-ROP of ε-CL Using Citric Acid as a Catalyst

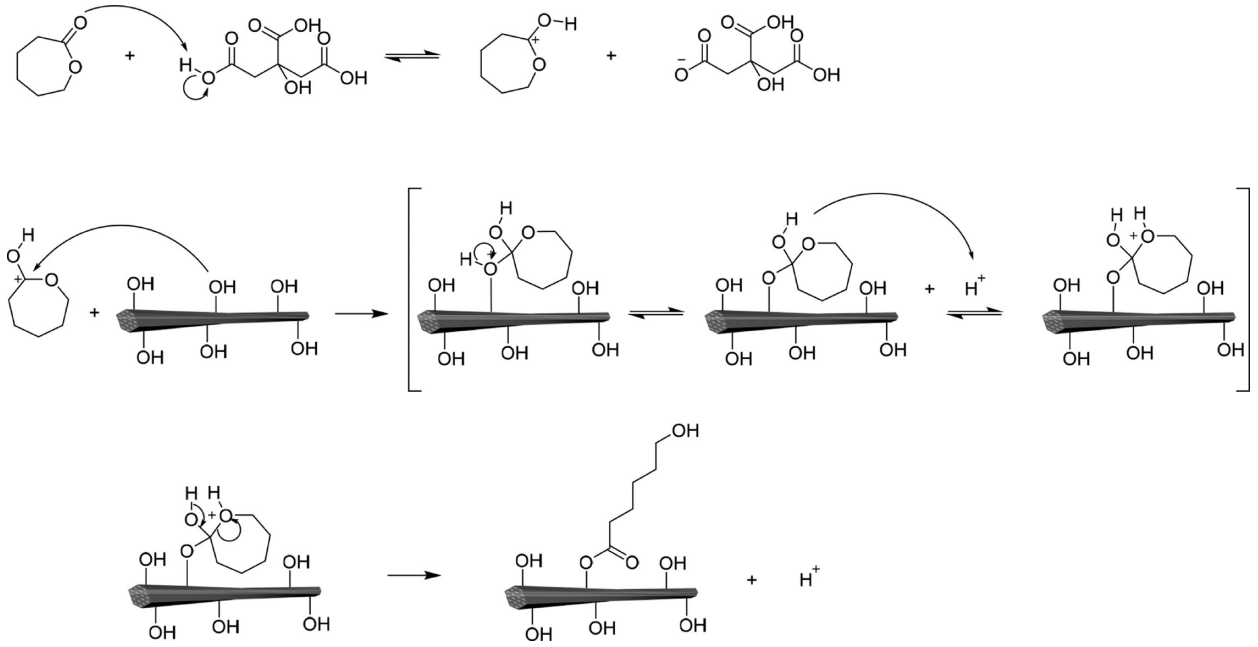

Scheme 3. SI-ROP of 2-Ethyl-2-oxazoline from Tosylated CNCs

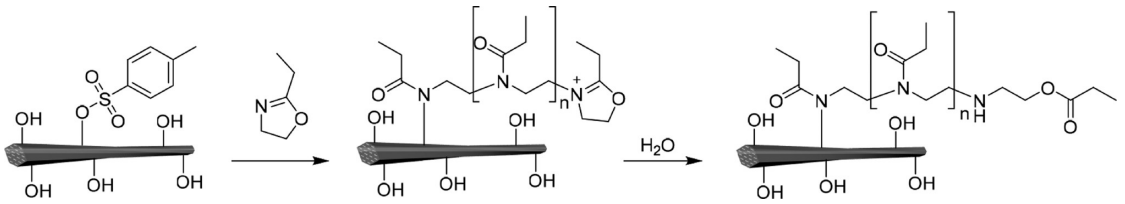

results in terms of monomer conversion and grafting yield as $Sn(Oct)_2$.[108] Organic catalysts such as 4-dimethylaminopyridine (DMAP),[83,113] citric acid,[78] and tartaric acid[83] have also been used for the SI-ROP of lactones from CNCs.

In the case of organic acids (citric acid and tartaric acid), the polymerization occurs through a monomer-activated mechanism,[119,120] in which the monomer is activated by a proton donated by the carboxylic acid. An −OH group of the cellulose, acting as a nucleophile, then reacts with this proton-activated monomer, leading to the formation of a hydroxyl-terminated ester via the ring-opening of the monomer. The propagation occurs as this newly formed hydroxyl-terminated species, acting as a new nucleophile, reacts with a new proton-activated monomer (Scheme 2). A few drops of HCl are sometimes added to the reaction medium at the end of the procedure to stop the reaction.[30,80,82,88−90] The grafted nanocrystals can be recovered by precipitation (in heptane,[80,82] deionized water,[113] or methanol[81,89,90,105,106,109,112]) and purified by Soxhlet extraction in toluene,[80,82] dichloromethane,[80,83,86] and/or tetrahydrofuran (THF)[77] to remove residual monomer, catalyst, and free homopolymer, in cases where a sacrificial initiator is used or impurities are present that initiate polymerization in solution.

Alternatively, they can be recovered by successive dispersion in methanol, ethanol, and acetone, each step followed by sedimentation via centrifugation.[87] Bitinis et al. noted that this second procedure allows the removal of the unwanted coproducts and unreacted reagents while losing fewer grafted nanocrystals in comparison to the purification performed via Soxhlet extractions.[87] However, when applying the same procedure with toluene, Habibi et al. could not recover the grafted nanocrystals via centrifugation as they remained highly stable in the supernatant.[30] This is likely due to the higher grafting yield obtained by Habibi et al.,[30] which was on the order of 85% in comparison to the 70% yield obtained by Bitinis et al.;[87] however, the molecular weight and grafting density of the tethered polymers was unknown.

CNC-g-polyoxazolines. The grafting of oxazolines via SI-ROP follows a cationic mechanism, and thus cannot be initiated from the −OH groups at the surface of CNCs; indeed a modification of the CNC surface through tosylation substitutes the nucleophilic −OH groups with electrophilic tosyl moieties.[121] In this case, tosylated CNCs act as the macroinitiator for the SI-ROP of 2-ethyl-2-oxazoline. It was shown that after tosylation, the modified CNCs can simply be mixed with the monomer and the SI-ROP readily takes place under microwave irradiation (completed in *ca.* 13 min). The reaction can be stopped by the addition of cold water and is subsequently washed with methanol (Scheme 3).

3.2. Surface-Initiated Free Radical Polymerization. One of the most commonly used approaches for the grafting of vinyl polymers from the surface of CNCs is surface-initiated free radical polymerization (SI-FRP). The polymerization starts by the activation of the initiator species, which will, often via hydrogen abstraction, generate a reactive radical on the surface of CNCs, from which monomers add to a propagating chain.[122] This method allows the facile growth of polymers at the CNC surface, along with free chains in solution, with relatively high molecular weight, even at low monomer conversions.

DOI: 10.1021/acs.macromol.8b00733
Macromolecules 2018, 51, 6157−6189

Scheme 4. Synthesis of CNCs Grafted with PAA via SI-FRP Using KPS as Radical Initiator

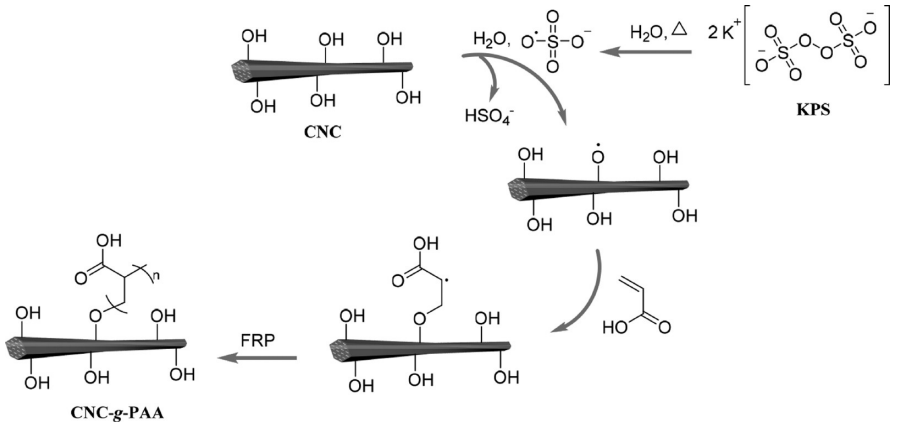

A wide variety of radical initiators have been demonstrated to be effective for the surface-initiated polymerization of vinyl monomers. Among the thermal initiators, potassium persulfate (KPS) is widely employed to decorate CNC surfaces with polymer chains, due to the stability of free radicals and compatibility with aqueous solutions. The radical formation starts in the aqueous phase by the thermal homolytic dissociation of the KPS peroxide bond, at temperatures ranging between 60 and 70 °C. The free sulfate radicals thus produced are capable of abstracting hydrogen atoms from the surface of the CNCs and thus generate the surface-bound initiating species (Scheme 4). Using this initiator, 2-(3-(6-methyl-4-oxo-1,4-dihydropyrimidin-2-yl)ureido)ethyl methacrylate (UPyMA) was successfully polymerized from the surface of CNCs, affording CNC-*g*-PUPyMA containing 6.9 wt % of polymer.[123] The presence of UPyMA units contributed significantly to the emulsion stabilizing ability of the nanoparticles (NPs) in comparison with pristine CNCs, which made them suitable to prepare high internal phase emulsions and macroporous hydrogels. Another example was reported by Wu et al., who used acrylic acid (AA) as the monomer.[124] The use of grafted poly(acrylic acid) (PAA) chains offered CNC-based hydrogels excellent water retention properties with a swelling ratio of 323 g/g in distilled water versus 33 g/g in sodium chloride (NaCl) solution.

A particular case of SI-FRP was described by Anirudhan et al., who reported the grafting of poly(methacrylic acid-*co*-vinylsulfonic acid) (P(MAA-*co*-VSA)) from the surface of magnetized CNCs.[125] First, magnetic CNCs were prepared by the chemical precipitation of magnetite (Fe_3O_4) onto the surface of CNCs. Then, the SI-FRP was carried out in the presence of KPS as initiator, the corresponding monomers and 2-(2-methylacryloyloxy)ethyl 2-methylacrylate (EGDMA) as cross-linker in water to form a three-dimensional network, which ultimately had a surface area that was five times larger than that of the parent CNCs.

Ammonium persulfate (APS) is another thermal initiator that has been used for the grafting from the surface of CNCs, in water, via SI-FRP; in this case, poly[2-(dimethylamino)ethyl methacrylate] (PDMAEMA) was used as the monomer.[126] The final product contained 11.7 wt % of polymer chains, which imparted stimuli-responsive properties to the CNCs.

In addition to the radical formation via thermal homolytic decomposition of the peroxide bond, persulfate initiators can also effectively generate free radicals in the presence of a reducing agent, such as oxyacids of sulfur (e.g., sulfite, bisulfite, thiosulfate, metabisulfite and dithionate), organic acids (e.g., ascorbic acid), metal ions (e.g., Fe^{2+} or Ag^{+}) or amines (e.g., TMEDA: *N*,*N*,*N*′,*N*′-tetramethylethane-1,2-diamine). This works by electron transfer from atoms or ions containing species that feature unpaired electrons and subsequent bond dissociation in the acceptor (persulfate) molecules.[127] These systems are referred to as redox initiators, redox catalysts or redox activators. They are often used at or below room temperature and are commonly employed in emulsion and aqueous polymerizations. This pathway has also been utilized for the formation of active radicals on the surface of CNCs by Zhou et al., where KPS and sodium bisulfite (SBS) were used as a redox initiator system to directly graft polyacrylamide (PAM) from the surface of CNCs dispersed in water.[128] The initiation reaction of this system is shown in Scheme 5.

Scheme 5. Radical Formation of the KPS/SBS Redox Initiator System

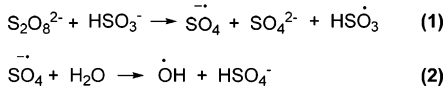

(1)

(2)

In this case, both radicals, formed through reaction 1 (Scheme 5), could activate CNCs via hydrogen abstraction at −OH groups on the surface. Upon addition of acrylamide (AM) monomer and *N*,*N*′-methylenebis(acrylamide) (NMBA) as a cross-linker, these surface radicals acted as the initiating sites for grafted PAM chains. Simultaneously, free radicals were also formed in solution promoting the polymerization of AM, which were also cross-linked by NMBA. Finally, a nanocomposite hydrogel based on CNC-*g*-PAM and PAM network was formed and showed well-dispersed modified-CNCs and enhanced interfacial adhesion between the two components.

The main advantage of using this type of initiator system is that the polymerization can be performed under mild conditions, as no heat is needed to promote the radical formation, which decreases the possibility of undesired side reactions while still obtaining high molecular weight polymers with a high yield. APS and TMEDA have likewise been used as a redox couple for the SI-FRP of *N*-isopropylacrylamide (NIPAM) from CNCs in order to form thermoresponsive hydrogels.[129] The initiation mechanism proceeds via a contact charge transfer complex and a cyclic transition state, from which two primary radicals are formed, one from the amine and another from persulfate, which both in turn initiate the polymerization process (Scheme 6).[130]

DOI: 10.1021/acs.macromol.8b00733
Macromolecules 2018, 51, 6157−6189

Scheme 6. Radical Formation of the APS/TMEDA Redox Initiator Couple[a]

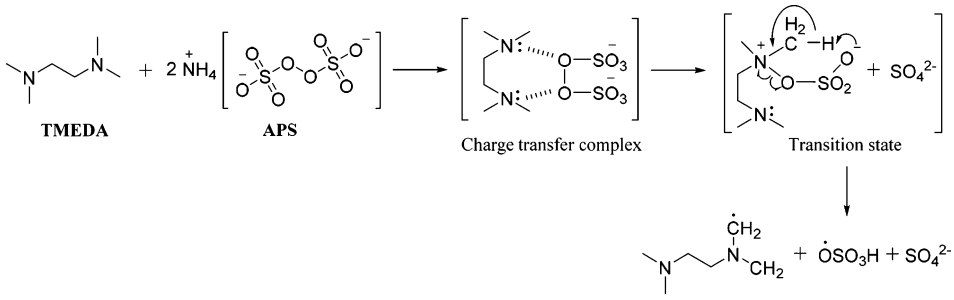

[a]Scheme adapted from ref 131.

Scheme 7. Mechanism of Ceric Ion Reduction, Leading to the Formation of CNC-Based Radicals[a]

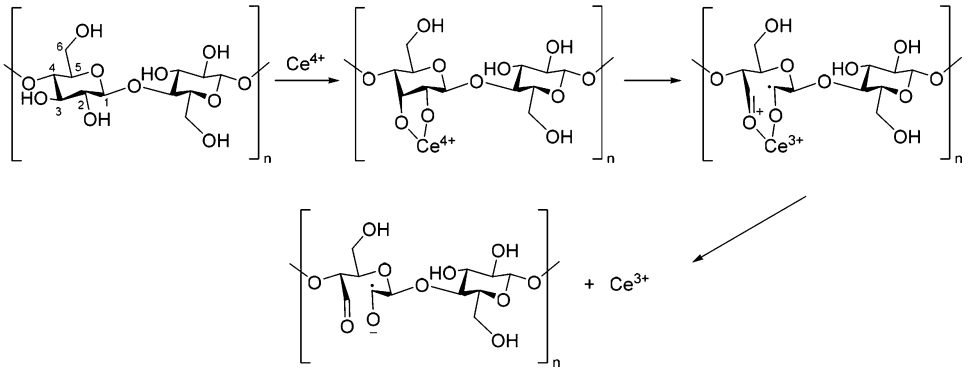

[a]Scheme adapted from ref 136.

Another technique, based on ceric-ion initiated polymerization and performed in aqueous solutions of nitric acid to modify the surface of CNCs, was first reported by Kan et al.[132] In this approach, ceric ions (Ce^{4+}) chelate with two adjacent −OH groups on the AGUs, possibly those at C2 and C3 positions. This step is followed by an electron transfer from the AGU to Ce^{4+}, leading to its reduction into Ce^{3+}, opening of the ring at C2 and C3 positions, and the formation of a radical species (Scheme 7). The ability to graft poly(4-vinylpyridine) (P4VP) from the surface of CNCs proved the effectivity of this chemistry on the surface of highly crystalline cellulose. Using similar chemistry, poly(glycidyl methacrylate) (PGMA)[133] and poly(methyl methacrylate) (PMMA)[134] have also been successfully grafted from the surface of CNCs.

In addition, Tang et al. carried out the synthesis of binary polymer brushes consisting of poly(oligoethylene glycol) methacrylate (POEGMA) and poly(methacrylic acid) (PMAA) from the surface of CNCs.[135] These brushes offered new properties to the final material that were effectively controlled by external stimuli such as pH and temperature. Initially, the OEGMA polymerization was performed via cerium-mediated reactions, followed by the subsequent sulfate-initiated MAA polymerization. Combining these two initiator systems allowed the authors to polymerize two vinyl monomers, with different intrinsic properties, from the surface of CNCs while assuring the accessibility to binding sites. Thus, cerium-initiated polymerization generated radicals at AGUs by ring-opening at the C2 and C3 positions and transforming their secondary alcohol, but without affecting their primary alcohols, which left the latter available for further radical-initiated polymerization through hydrogen abstraction. Indeed, it is believed that the ring opening of the AGUs at the C2−C3 position and the generation of aldehyde groups yields a material, which undergoes thermal degradation at a lower temperature, thus reduced thermal stability can be observed compared to pristine CNCs. This was demonstrated for CNC-*g*-POEGMA or CNC-*g*-P(OEGMA-*ran*-MAA) (T_d = 180 °C)[135] and CNC-*g*-PMMA (T_d = 250 °C).[134]

In general, the modification of CNCs via SI-FRP comes with the formation of a substantial amount of free (unattached) homopolymers in solution, which represents a loss of monomer and a reduction in grafting efficiency, which thus is the main drawback of this method. In addition, the successful removal of such species is in some cases tedious and challenging, depending on the reactants and the final product. The purification of hydrogels, for example, request the immersion of the material into an excess of water for a period between 48 and 72 h in order to remove any water-soluble fraction. It is usually followed by a drying process (50−70 °C) in vacuum for 48 h.[128,137] For the removal of metals, i.e., particles released from sonication probe, the common reported procedure implies the use of glass microfiber filter paper followed by extensive dialysis and ultrafiltration.[132,134] If the extraction of CNC-*g*-polymer from the reaction media is required, it generally proceeds via subsequent centrifugation and washing steps with one or more solvents (according to the affinity of interested species), which could be followed by dialysis and drying processes.[94,135]

Nevertheless, inorganic peroxides, such as KPS and APS, have shown their versatility as initiator species in SI-FRP based on the large variety of polymers that have successfully been grafted from the surface of CNCs. The main advantage of using this type of initiator system is that the grafting can be performed directly from the surface of pristine CNCs, i.e., without previous modification. For cases where the polymerization should be performed at ambient or lower temperatures, a

DOI: 10.1021/acs.macromol.8b00733
Macromolecules 2018, 51, 6157−6189

Scheme 8. Overview of the Most Common SI-CRP Strategies Illustrated by SI-ATRP of Sty,[141] S-RAFT of NIPAM,[142] and SI-NMP of Methyl Acrylate (MA)[143] on the CNC Surface

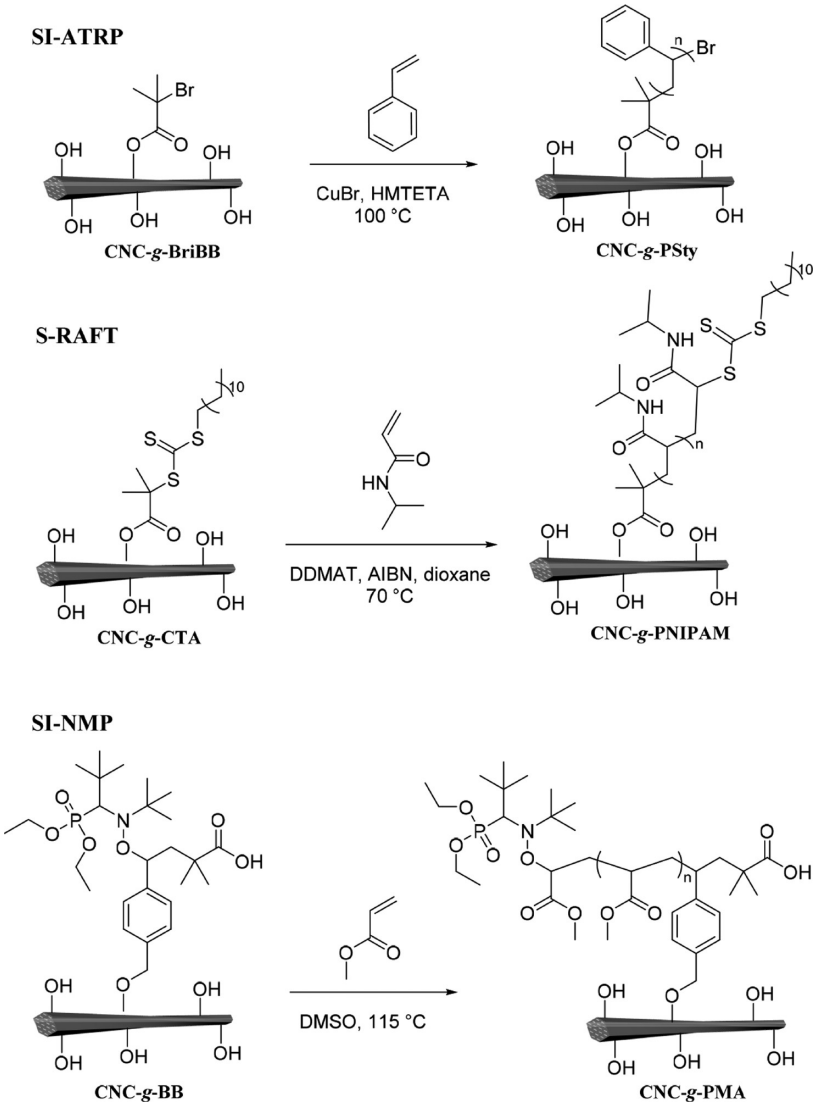

redox system involving any of these compounds can be used. In comparison to ceric ion SI-FRP, peroxy compounds have the advantage of not altering the structure of CNC surface chains, which usually results in nanomaterials with higher thermal stability, as previously discussed.

The SI-FRP methods presented above involved the formation of reactive species directly on the surface of CNCs, from which polymer chains were allowed to grow. Yang and co-workers reported a different approach, in which the CNC surface was chemically modified with reactive small molecules before polymerization.[137,138] A chemical entity containing end vinyl groups were covalently linked to the surface of CNCs by treatment with γ-methacryloxypropyl silane. Subsequently, radicals species were formed at the end vinyl groups in the presence of KPS initiator, thus creating propagating radicals, from which AA[137] or AM[138] monomers were polymerized until termination reactions occurred by recombination, indeed promoting the formation of cross-linked networks. On the basis of the high monomer-to-surface initiator ratio[137,138] employed and the final monomer conversion (*ca.* 99%),[137] the polymer grafted via this approach formed a dense shell around the CNC core due to either a high grafting density or a high molecular weight.

Espino-Perez et al. proposed the synthesis of CNC-*g*-polystyrene via reaction steps consistent with principles of green chemistry.[94] The protocol involved the ozonolysis of CNCs leading to peroxide groups at their surface, and the subsequent radical polymerization in the presence of KPS and styrene (Sty) monomers within a sodium acetate buffer solution (pH = 3.5). The thermally activated sulfate radicals reduced the peroxide groups, creating free radicals, which propagated to form tethered polystyrene (PSty) chains. The Sty/AGU ratio was estimated to be 0.24, which confirmed the low grafting efficiency on CNCs through this method due to the low hydroperoxidation efficiency during the ozonolysis treatment.

Another strategy for decorating CNCs with grafted vinyl polymers was presented by Lee et al.[139] The SI-FRP took place on the surface of CNCs containing trichloroacetyl groups in the presence of molybdenumhexacarbonyl ($Mo(CO)_6$) as initiator and 2-methacryloyloxyethyl phosphorylcholine (MPC) and stearyl methacrylate (SMA) as monomers in ethanol to yield CNC-*g*-P(MPC-*co*-SMA), with over 90% of monomers conversion.

More recently, a new free radical strategy was presented by Wohlhauser et al. where the initiator species was covalently

DOI: 10.1021/acs.macromol.8b00733
Macromolecules 2018, 51, 6157–6189

attached to the surface of CNCs.[93] This approach guarantees the presence of a high number of reactive sites at the surface of the substrate, although it does not avoid the formation of radicals in solution. In this work, PMMA and poly(hexyl methacrylate) (PHMA) were successful grafted from CNCs through an undemanding protocol, which involved the surface modification of CNCs with benzophenone moieties as photoinitiators and subsequent surface-photoinitiated FRP of methacrylates in DMF under UV-irradiation. Benzophenone is a Norrish Type II photoinitiator that undergoes intersystem crossing from its excited singlet state to the lowest energy reactive triplet, followed by the abstraction of aliphatic hydrogen from a nearby molecule or interface, yielding a ketyl radical and a carbon centered radical.[140] The SI-FRP is thus initiated by the carbon centered radical and can also result in the formation of free (unattached) polymer chains (initiated from a monomer or solvent molecule). Using this method, compositions containing 80 and 90 wt % of grafted polymers were prepared for both monomers. This was achieved by using DMF as solvent and variation of the monomer conversion. In comparison to previous studies, the fraction of polymer brushes on the surface of CNCs was very high, but given the mechanism, a substantial amount of polymer (between 24 and 48 wt %, relative to the initial monomer amount) was also produced as free (unattached) polymer.

In general, the polymer grafted on the surface of CNCs via free radical polymerization from covalently immobilized reactive species depends on factors related to the propagating radical, such as surface initiator efficiency, propagation rate and the monomer-to-surface initiator ratio. Indeed, additional studies are needed in the field to better understand the influence of these parameters. Another opportunity that currently remains in this field is the investigation of SI-FRP via the attachment of other conventional radical initiators (i.e., azo-containing initiators) and subsequent comparisons with polymer brushes obtained through the above-mentioned techniques.

3.3. Surface-Initiated Controlled Radical Polymerization. SI-CRP is an effective way to grow polymers when a precise control over polymer architecture, composition, molecular weight, and graft density is required.[28] In general, CRP reactions rely on the reversible deactivation of propagating chains, such that termination reactions are minimized, thus providing first order polymerization kinetics and low dispersity. Different SI-CRP methods can be performed, which depend on the type of initiator or so-called chain transfer agent (CTA) coupled to the surface, such as Cu-mediated SI-CRP, surface reversible addition−fragmentation chain transfer (S-RAFT) or surface-initiated nitroxide-mediated polymerization (SI-NMP), among others. Scheme 8 exemplifies the three most commonly used SI-CRP techniques, i.e. surface-initiated atom transfer radical polymerization (SI-ATRP), S-RAFT, and SI-NMP. In the following sections, a brief overview of each of these techniques will be provided.

3.3.1. Cu-Mediated SI-CRP. Of all SI-CRP techniques, those mediated by transition metal complexes, especially Cu species, as in SI-ATRP, have been the most widely employed to graft polymers from CNCs. The control in ATRP arises from the existence of a dynamic equilibrium between dormant and propagating species, thus lowering radical concentration and minimizing termination reactions.[144] The reversible deactivation occurs through the exchange of a halogen atom (Br or Cl) between a metal complex (based on Cu in most cases) and the propagating species. As the presence of residual metal in the final polymers may be a problem for some applications, techniques were then developed to decrease the required amount of catalytic system to ppm by (re)generating Cu(I) *in situ* activators by electron transfer (A(R)GET) ATRP.[145−147] CRP in the presence of Cu(0) was also reported with a debate on the model of the electron transfer mechanism, i.e. single-electron transfer living radical polymerization (SET LRP) and supplemental activator and reducing agent atom transfer radical polymerization (SARA ATRP).[148−150] As the present Perspective aims at reporting the different structures obtained from CNCs and their related properties rather than debating the mechanism, techniques involving Cu species are grouped under the generic term "Cu-mediated SI-CRP."

Conducting a Cu-mediated SI-CRP from CNC requires the preliminary introduction of initiating sites on their surface. This is usually achieved by reacting the numerous −OH functionalities on the CNC surface with 2-bromoisobutyryl bromide (BiBB) in a solvent (THF or DMF), usually in the presence of a base (triethylamine) and a catalyst (DMAP).[141,151−161] The extent of this modification can be tailored through the reaction duration and the amount of BiBB introduced.[162,163] Through a combination of active initiators and inactive "dummy" initiators, the overall grafting density can be controlled.[28] Over the years, strategies were developed to improve the CNCs dispersibility during the modification by either performing (1) solvent exchanges (rather than freeze-drying), which permitted avoiding a redispersion step of dried CNCs,[163,164] or (2) a chemical vapor deposition of BiBB on a CNC aerogel to partially hydrophobize the CNCs prior to a subsequent liquid phase reaction with BiBB.[165−169] Higher modification degrees (up to 15 wt % Br determined by elemental analysis) were then reached with lower BiBB excess.[165] Although less widely used, the incorporation of the initiating sites was also reported by reacting the −OH functions with α-bromoisobutyric acid activated with carbonyl diimidazole.[170,171] In another study, the use of 2-bromopropionic acid was proposed for the introduction of active sites on the CNCs surface with a yield of 46% and 2.86 wt % of Br content determined by elemental analysis.[95] The protocol involve a pretreatment of pristine CNCs with HCl, followed by one-step reaction, which combines Fischer esterification and acid hydrolysis.

In all the previous studies, the −OH functions were statistically and homogeneously modified on the entire nanocrystal surface. Recently, Zoppe et al. reported an approach to introduce initiating sites specifically on the reducing end groups of CNCs through their oxidation and reaction with ethylenediamine and subsequently 2-bromoisobutanoic acid *N*-hydroxysuccinimide ester.[172] This approach is discussed in further detail in section 3.4.

The CNC macroinitiators have been used in the Cu-mediated SI-CRP of various styrenic-, (meth)acrylic, or acrylamide-based monomers (Figure 5) with catalytic systems and solvents optimized for the various monomers employed (see Table S1). The polymerization control can be elucidated through the saponification of the grafted polymers (via either acidic or alkaline conditions) and further analysis of the degrafted polymer in solution; however the degrafting reactions require an extended reaction time (2 days to 3 weeks) and can potentially alter the polymer structure.[141,152−154,163,164,170,172] The versatility of Cu-mediated SI-CRP techniques and their high tolerance toward many functional groups has given access to CNCs grafted with a large variety of polymeric chains ranging from neutral PSty,[115,141,157,162] poly(alkyl ((meth)acrylate),[158,169,170] to cationic poly(amino(alkyl) methacrylate/methacrylamide)[155,172] or

DOI: 10.1021/acs.macromol.8b00733
Macromolecules 2018, 51, 6157−6189

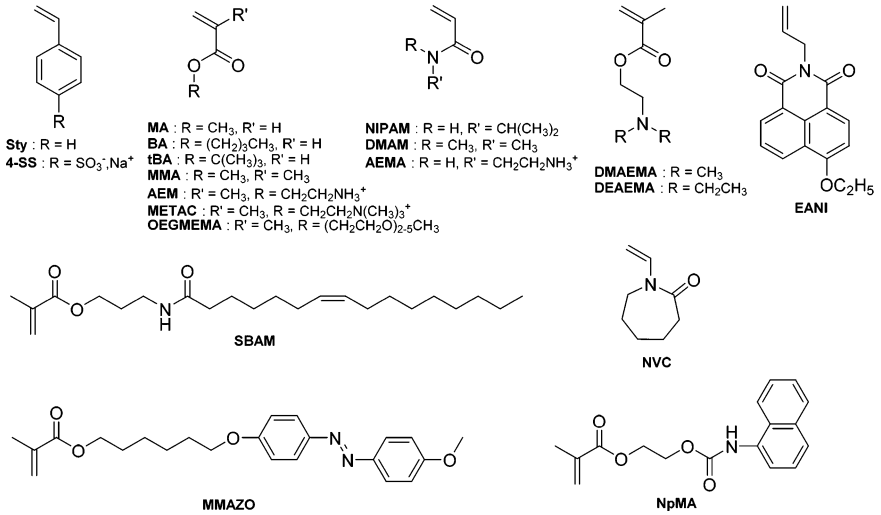

Figure 5. Monomers used in Cu-mediated SI-CRP from CNC macroinitiators; Sty;[115,141,157,162] 4-SS, sodium 4-vinylbenzenesulfonate;[172] MA;[158,170] BA, butyl acrylate;[169] tBA, *tert*-butyl acrylate;[165,168] MMA, methyl methacrylate;[169] AEM, 2-aminoethyl methacrylate;[155] METAC, [2-(methacryloyloxy)ethyl]trimethylammonium chloride;[172] OEGMEMA, oligoethylene glycol methyl ether methacrylate;[159,160] NIPAM;[153,154,163,164,172] DMAM, *N,N*-dimethylacrylamide;[173] AEMA, 2-aminoethyl methacrylamide;[155] DMAEMA, dimethylaminoethyl methacrylate;[152,166,167,171] DEAEMA, diethylaminoethyl methacrylate;[171] EANI, 4-ethoxy-9-allyl-1,8-naphtalimide;[154] SBAM, soybean amide methacrylate;[156] NVC, *N*-vinylcaprolactam;[161] MMAZO, 6-[4-(4-methoxyphenylazo)phenoxy] hexyl methacrylate;[151] NpMA, naphtyl methacrylate.[166]

anionic polystyrenesulfonate[172] and PAA (through the hydrolysis of poly(*tert*-butyl acrylate) (PtBA)).[165,168] Thermosensitive polymers, such as PNIPAM,[153,154,163,164,172] PDMAEMA,[152,166,167,171] poly(*N*-vinylcaprolactam) (PNVC),[161] or poly[(oligoethylene glycol) methyl ether acrylate] (POEGMEMA)[159,160] have also been grafted with this approach.

The use of a sacrificial initiator (i.e., free initiator species added to the reaction medium, usually EBiB, ethyl α-bromoisobutyrate) is common as it provides a simple means to monitor the polymerization process, allows targeting the DP, and also contributes to a better control by increasing the concentration of Cu(II) deactivator species in the reaction.[154,157,162,165,167−169] A good correlation between molecular weight of the free PSty chains (initiated from the sacrificial initiator) and the molecular weight of PSty grafts was demonstrated by incorporating *o*-nitrobenzyl photosensitive moieties between the CNC surface and the surface-grafted initiator, degrafting the PSty grafts under mild conditions (UV-irradiation) and comparing their molecular weight to the free chains (number-average molecular weight (M_n) = 8.5 kDa, dispersity ($Đ = M_w/M_n$) = 1.08 versus M_n = 10.1 kDa, $Đ$ = 1.07 for degrafted and free polymers, respectively).[115] In contrast, Zoppe et al. showed high dispersity of surface-grown PNIPAM, however this was likely due to insufficient amounts of CuX_2 deactivator species and complexation with NIPAM monomers, in addition to having been conducted in highly polar media.[163] Using a similar SI-AGET-ATRP approach with ascorbic acid as reducing agent, Wu et al. found that free PNIPAM chains had a bimodal molecular weight distribution, whereas cleaved PNIPAM chains were unimodal and had a lower dispersity.[154] In addition, a significantly higher M_n was observed for the free PNIPAM chains.

Monte Carlo simulations of surface-initiated polymerization from neutral planar substrates have shown that bulk polymers tend to grow at faster rates and with lower dispersity, however this is highly dependent on the grafting density of initiating sites.[174] Along with the importance of CuX/CuX_2 ratio,[28,29] it is clear that the monomer type/concentration, solvent and bulk vs solution synthesis all play a role in the control of Cu-mediated SI-CRP.[28] Thus, the assumption that the polymerization kinetics of surface-initiated polymers is similar to that of free polymers is not always valid.

In general, Cu-mediated SI-CRP conducted in higher polarity solvents, such as water, tend to yield polymers with higher dispersity, as a result of high rates of activation.[175] Such high dispersity implies higher rates of termination and the loss of active polymer chain ends, thus low overall control. The kinetics of Cu-mediated SI-CRP conducted at high monomer concentrations in less polar solvents or in bulk, *e.g.*, Sty, tend to resemble those of solution Cu-mediated CRP.[115] Such aspects are important considerations when more complex architectures are required, such as block copolymer brushes from CNCs, for example, in which good control and high chain-end fidelity are critical for success.

The impact of the CNC surface charges on SI-ATRP control was also investigated through the initiation of a DMAM polymerization from CNCs with various charge densities.[173] It was demonstrated that electrostatic interactions lead to an enrichment of catalytic species on the surface and increased the initiator efficiency, but at the expense of a higher dispersity. A qualitative model of catalyst enrichment for SI-ATRP from CNCs is shown in Figure 6. Since Cu(II) halide species readily dissociate in aqueous environments, divalent Cu^{2+}/ligand complexes can strongly interact with sulfate half-ester groups on the surfaces of the CNCs, which in turn has a negative impact on deactivation of growing polymer chains. Therefore, low charge density CNCs are advantageous if low dispersity of grafted chains is required in the final hybrid materials; however, a lower initiator efficiency can be expected.

It was also recently demonstrated that a controlled Cu-mediated SI-CRP of MA can be photoinduced from modified CNCs in a commercial UV nail box.[158] The CNCs were previously modified with BiBB, then the polymerization of the monomer proceed under UV irradiation at 360 nm during 90 min in the presence of a sacrificial initiator. The analysis of the free PMA synthesized simultaneously in solution demonstrated first order kinetics and, thus, good control. The use of this technique

DOI: 10.1021/acs.macromol.8b00733
Macromolecules 2018, 51, 6157−6189

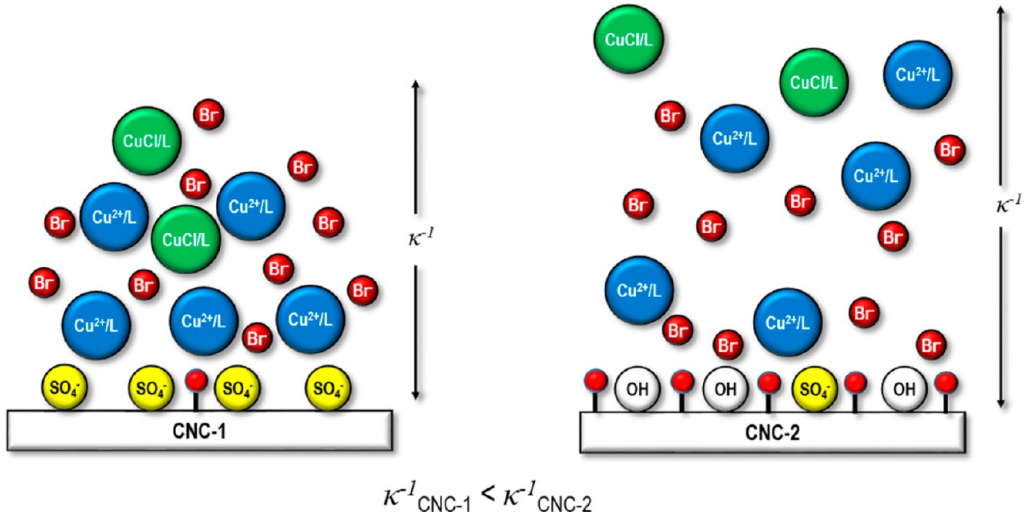

Figure 6. Qualitative model describing the composition of the interfacial region around CNCs prior to polymer brush growth from CNCs with high (CNC-1) and low (CNC-2) density of surface sulfate groups. (small red circle = initiator, L = ligand, κ^{-1} = Debye length). Reprinted with permission from ref 173. Copyright 2016 American Chemical Society.

Scheme 9. (A) R-Group vs Z-Group CTA Immobilization Strategies, (B) S-RAFT of VAc from CNCs Using the R-Group Approach,[179] and (C) S-RAFT of Acrylamide from CNCs Using Free macroCTA and Surface Free Radicals Generated by CAN[96]

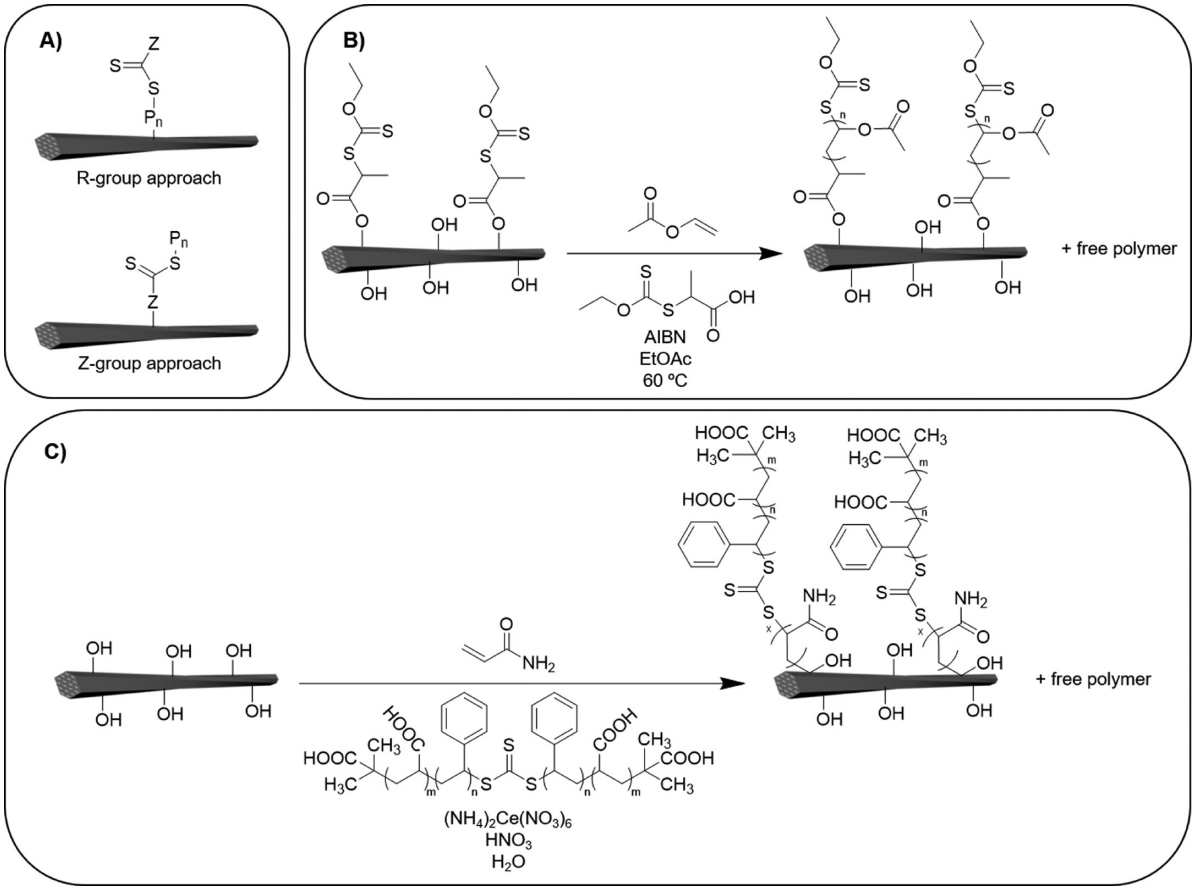

allowed high grafting density in short reaction times and a straightforward purification due to the significant reduction in the amounts of Cu and ligand employed in comparison with a traditional Cu-mediated CRP. The authors observed an increase of the glass transition temperature (T_g) of CNC-*g*-PMA compared with the free PMA, indicative of reduced chain mobility when tethered to the CNC surface. The development of such user-friendly SI-CRP techniques opens up a wide range of synthetic possibilities for grafting polymers from CNCs.

Even though the above-mentioned techniques has been widely used in the field of grafting polymers from CNCs, the removal of Cu residues after the polymerization is still challenging and needs more investigation. Several purification methods are used in solution polymerization but they are difficult to

DOI: 10.1021/acs.macromol.8b00733
Macromolecules 2018, 51, 6157–6189

employ when the reaction involves CNCs, e.g., purification over silica or neutral alumina columns.[144] The (re)generation of Cu(I) in solution partially solved this problem, since much lower amounts of Cu are used in the reaction. Nevertheless, in case of biomedical applications, the removal of trace amounts of Cu appears to be crucial.

Dialysis has been used to remove Cu after polymerization reactions.[176] Prior to dialysis, Rosilo et al. performed several centrifugations of CNC-*g*-poly(*N*,*N*-dimethylaminoethyl methacrylate) in different organic solvents, i.e., MeOH, DMF, and dioxane.[167] In both cases, the approaches used may not be sufficient to remove the adsorbed Cu on the surface of the grafted CNCs. In another study, Morandi et al. proposed two subsequent Soxhlet extractions on freeze-dried samples in dichloromethane and ethanol for the removal of Cu traces. The blue color, related to the Cu adsorbed on the surface of the CNCs, was removed by this treatment. Nevertheless, no quantitative analysis of remaining traces of Cu was performed after this process. Another method to remove Cu could involves stirring the grafted CNCs with an ion-exchange resin.[177] Or, as discussed in section 3.2, the particles could be removed by filtering the modified CNCs through glass microfiber filter paper.[132]

3.3.2. Surface-RAFT Polymerization. Reversible addition−fragmentation chain transfer polymerization (RAFT) involves a reversible chain transfer process and is carried out in the presence of a CTA, in addition to a free radical initiator. Such CTAs are often based on dithiocarbamates, dithiocarbonates, or dithioesters and contain so-called R- and Z-groups. The function of the CTA is to mediate addition, fragmentation and chain transfer reactions, resulting in an overall controlled molecular weight and dispersity. During RAFT polymerization, radicals either reversibly react with the CTA or monomers. Consequently, S-RAFT polymerization is conducted by the prior immobilization of either free radical initiators or CTAs to the substrate surface. If the CTA is attached to the substrate surface, it can be tethered so as to present either the R- or Z-group, the former of which being the most commonly utilized. Scheme 9 shows (A) the two different CTA immobilization strategies and examples of S-RAFT from CNCs using (B) the R-group approach and (C) surface free radicals and free CTA.

One of the first studies utilizing S-RAFT to modify CNCs was reported by Zeinali et al., in which PNIPAM and random copolymers of PNIPAM and PAA (P(NIPAM-*ran*-AA)) were grafted via the immobilization of the CTA with the R-group approach.[142] The CTA, 2-(dodecylthiocarbonothioylthio)-2-methylpropionic acid (DDMAT), was grafted to CNC −OH groups via DMAP-catalyzed esterification in the presence of *N*,*N*′-dicyclohexylcarbodiimide (DCC) in chloroform. A sulfur content of 2.1 wt %, determined by elemental analysis, confirmed the successful attachment of the CTA. S-RAFT polymerizations of NIPAM and NIPAM-*ran*-AA were conducted with 2,2′-azobis(2-methylpropionitrile) (AIBN) in dioxane and in the presence of free CTA, i.e., DDMAT. The authors obtained statistical copolymer grafts using different monomer feed ratios, in which the CNC hybrids were characterized by FTIR, dynamic light scattering (DLS) and thermal analysis. From the results of DSC experiments, the authors concluded that as the ratio of AA was increased, while the heat capacity variation (ΔC_p) decreased. In comparison to free (co)polymers, those grafted from CNCs displayed higher T_g due to surface chain confinement.

Similar block copolymers were grafted from CNCs coated with a cross-linked poly(2-hydroxyethyl methacrylate) (PHEMA) shell by immobilization of the CTA, S-(thiobenzoylthioglycolic) acid.[178] CNCs were first coated with PHEMA cross-linked with ethylene glycol dimethacrylate (EGDMA), using a free radical approach with AIBN in solution, to increase the −OH groups content on the surface. From X-ray photoelectron spectroscopy (XPS) analysis of CTA-modified CNC/PHEMA particles, the surface S content was determined to be 1.8%. In this case, the authors likely obtained a higher grafting density of PNIPAM-*block*-PAA chains due to grafting from a cross-linked PHEMA network at the surface of CNCs. In other work, PMMA was grafted from CNCs using 4-cyano-4-(phenylcarbonothioylthio)pentanoic acid (CPADB) functionalized CNCs.[118] Here the authors determined a sulfur content of 2.9 wt % by elemental analysis and estimated that 1 out of 6 AGUs was modified with CPADB, which is one of the highest values reported so far for CTA-functionalized CNCs. The authors further utilized ^{1}H NMR spectroscopy in DMSO-d_6 in the presence of an ionic liquid to observe CPADB-functionalized CNCs.

Boujemaoui et al. investigated the grafting of vinyl acetate (VAc) via S-RAFT and the interchange of xanthates (MADIX) polymerization.[179] The xanthate-based CTA, 2-((ethoxycarbonothioyl)thio)propanoic acid, was attached to CNCs either by Steglich esterification or a two-step approach, the latter of which resulted in a lower grafting yield of poly(vinyl acetate) (PVAc). The kinetics of the S-RAFT process was monitored using sacrificial CTA and demonstrated good control over the molecular weight and dispersity. However, for all the aforementioned studies, little is known regarding the molecular weight, dispersity and grafting density of the tethered polymers.

S-RAFT of various acrylamides from CNCs has also been mediated by free macromolecular CTAs and conducted utilizing free radical initiators, such as ceric(IV) ammonium nitrate (CAN) (Scheme 9C).[96,180] In these cases, macromolecular CTAs with molecular weight between 1.4 and 2 kDa were used to mediate S-RAFT polymerization of AM[96,180] and DMAM[180] from CNCs, in which surface radicals were generated as shown in Scheme 7. PAM chains were cleaved from the surface of CNCs and determined to have M_n = 14 kDa and $Đ$ = 1.28, the latter demonstrating involvement of the macromolecular CTA.[96] In addition, increased S contents were observed for the polymer-modified CNCs, which indicated that at least some of the grafted PAM chains were end-capped with macromolecular CTA moieties.

In a unique approach, poly[poly(ethylene glycol)ethyl ether methacrylate] (PPEGEEMA) and PDMAEMA were grafted from a difunctional CNC macroinitiator via a combination of S-RAFT and SI-ATRP.[176] The difunctional CNC macroinitiator was obtained by first transforming the −OH groups on the CNC surface into reactive amines, and then, transforming them into bromoisobutyryl functionalities and azo initiator sites via consecutive reactions with α-bromoisobutyric acid (BIBA) and 4,4′-azobis(4-cyanovaleric acid) (ACVA), respectively. The subsequent step involved the growth of PPEGEEMA brushes from the surface of modified CNCs via S-RAFT polymerization, followed by the grafting of PDMAEMA via SI-ATRP. The polymerizations were sequentially performed in this way to avoid potential destruction of the azo initiator sites by the SI-ATRP processes. Free PPEGEEMA formed in solution via RAFT had a M_n of 4.7 kDa and $Đ$ of 1.2. After SI-ATRP, PDMAEMA chains were successfully cleaved from the CNCs by acid hydrolysis, yielding M_n in the range of 4.2−7.7 kDa and $Đ$ of 1.2−1.3, depending on the SI-ATRP reaction time between 5 and 30 min. However, under such conditions (64 wt % of sulfuric acid, 3 h, 45 °C), the reported size-exclusion chromatography (SEC)

DOI: 10.1021/acs.macromol.8b00733
Macromolecules 2018, 51, 6157−6189

results likely represented a mixture of cleaved PDMAEMA and PPEGEEMA or their corresponding hydrolysates, *e.g.* PMAA. There is still much to learn about S-RAFT from CNCs, given the complexity of the RAFT process and the lack of knowledge on the kinetics of such polymerizations conducted from CNCs.

3.3.3. Surface-Initiated NMP. Similar to Cu-mediated SI-CRP, surface-initiated nitroxide-mediated polymerization (SI-NMP) mechanistically depends on the reversible activation−deactivation of propagating polymer chains by a deactivating species, in this case a nitroxide radical. In general, alkoxyamines, such as TEMPO and *N-tert*-butyl-*N*-[1-diethylphosphono(2,2-dimethylpropyl)] nitroxide (DEPN), are commonly used for SI-NMP. Roeder et al. were the first to use SI-NMP to graft polymers from CNCs.[143] The authors first functionalized CNCs with 4-(diethoxyphosphinyl)-2,2,5,5-tetramethyl-3-azahexane-N-oxyl, *a.k.a.* BlocBuilder, and subsequently grafted PMA and PMMA from CNCs in the presence of sacrificial BlocBuilder initiators (see Scheme 8). The grafting yields obtained were 75−80 wt %. The authors were unable to cleave the grafted PMA or PMMA from the CNC surfaces, despite several attempts. However, SI-NMP conducted in the presence of sacrificial BlocBuilder allowed SEC analysis of free polymers. While free PMA showed M_n values from 3.3 to 43.7 kDa and $Đ$ of 1.35−1.4, the free PMMA had a M_n in the range of 30.8−140 kDa and similar dispersity, despite similar monomer conversion. These results suggested that higher sacrificial initiator efficiency was obtained for PMA.

The same group later employed the same approach to graft a variety of methacrylamides, such as DMAEMA, DEAEMA and *N*-[3-(dimethylamino)propyl] methacrylamide (DMAPMAM), from CNCs.[181] In addition to elemental analysis and thermal analysis, these CNC hybrids were characterized by cross-polarization magic-angle spinning (CP-MAS) ^{13}C NMR spectroscopy. The latter technique revealed that the composition depended on the reaction time, however molecular weight and dispersity of the grafted polymers were not reported. The highest grafting yield was obtained for SI-NMP of DEAEMA from CNCs, *i.e.*, 65 wt %. Overall, little is known regarding the kinetics of SI-NMP from CNCs in comparison to solution NMP, which leaves plenty of research opportunities for this field.

3.4. Polymer Grafting from the Reducing End Groups of CNCs. Individual cellulose chains contain chemically distinct end groups, commonly referred to as the nonreducing end and the reducing end. The directionality of cellulose chains is a direct result of the mechanism of the cellulose biosynthesis.[58] This reducing end can be reversibly converted between an aldehyde and a cyclic hemiacetal under a variety of conditions. Thus, site-specific, or "patchy" CNCs can be obtained by modifying this reducing end through aldehyde-selective reaction pathways. CNCs with end-tethered polymers chains present an interesting alternative to uniformly modified CNCs for certain applications, in which their self-assembly can be exploited toward structural hierarchies with unique properties, including both assemblies on surfaces and in nanocomposite materials.[8] Depending on the molecular weight of end-tethered polymers, one can see such anisotropic colloidal building blocks as somewhat analogous to rod−coil block copolymers.[182]

Different procedures have been established in order to attach a small molecule or initiator to the reducing end groups of CNCs. Arcot et al. reported a method to introduce thiol groups on the reducing ends of the CNCs by reductive amination in an aqueous medium.[183] The authors synthesized thiolated cellulose nanocrystals (CNC-SH) by using 6-amino-1-hexanethiol hydrochloride ($NH_2(CH_2)_6SH{\cdot}HCl$), a reducing agent (Cn, sodium cyanoborohydride; Ac, sodium triacetoxyborohydride; or Pc, 2-picoline-borane complex) and an aqueous CNC dispersion at different pH (5, 7 or 9.2) values. The CNC-SH were then functionalized with silver nanoparticles (AgNPs) in order to characterize the successful reducing end group modification, qualitatively using transmission electron microscopy (TEM) and quantitatively using XPS. The authors determined that the highest yield of functionalization was obtained when using basic conditions.

The same group later introduced a second thiolation procedure with shorter reaction times, milder conditions, and higher colloidal stability of the modified CNCs.[184] Usuda and coworkers had previously demonstrated the selective oxidation of reducing ends to carboxylates with sodium chlorite ($NaClO_2$), which gives access to a wider variety of potential modification chemistries.[185] Thus, the reducing ends were first reacted with $NaClO_2$ to generate carboxylate functionalized CNC reducing ends (CNC−COOH). After this oxidation step, a mild activation step of the carboxyl group was carried out mediated by *N*-hydroxysuccinimide (NHS) and *N*-(3-(dimethylamino)propyl)-*N*-ethylcarbodiimide hydrochloride (EDC), which was followed by a nucleophilic substitution with $NH_2(CH_2)_6SH{\cdot}HCl$, resulting in CNC-SH.

Gruber et al. proposed a different reducing end group functionalization strategy via hydrazone linkages.[186] The authors used 4-hydrazino-benzoic acid or radical initiators 4,4′-azobis(4-cyanopentanoic dihydrazide) and 4-carboxyphenylazomethylmalonodinitrile to form the hydrazone linkage, which resulted in a phenylcarboxylate terminated CNC with a yield of 44.6%. Similar yields with the conversion of 4-hydrazinobenzoic acid were obtained for the other initiators. The authors hypothesized that the low yield was due to the poor accessibility of the reducing end groups. If one considers individualized CNCs to consist of 18-chains,[58] this would imply a maximum of 18 reducing end groups at one end of the cellulose I crystal. Given the rod-like shape of CNCs, the reducing end-groups are likely distributed heterogeneously. This may lead to varying degrees of reducing end group accessibility for chemical reactions, however this remains to be explored.

Gruber and coworkers grafted PAM by SI-FRP from different azo initiators discussed in section 3.2 and shown in Table 1.[186] The molecular weight of the polymers were determined by SEC measurements after degrafting the PAM from the CNCs. The authors observed high molecular weights for PAM, but only a small amount of the initiators reacted to yield the polymer-grafted CNCs. Initiator efficiencies for surface-initiated polymerizations are reported to be very low, *e.g.*, 5−30%.[28]

Recently, Zoppe et al. reported a route to functionalize the end groups with an SI-ATRP initiator containing α-bromoisobutyryl groups.[172] The reducing ends were first oxidized with $NaClO_2$ and further modified with ethylenediamine (EDA), following the work of Arcot et al.[184] Subsequently, primary amine groups were reacted with 2-bromoisobutanoic acid *N*-hydroxysuccinimide ester (NHS-BiB) to yield the ATRP initiator-functionalized reducing end groups. Although the authors were unable to quantify the success of the initiator modification reactions with conventional techniques, such as FTIR, XPS and elemental analysis, they subsequently grafted a variety of polymers from the functionalized reducing end groups of CNCs via SI-ATRP. The monomers investigated included NIPAM, METAC, and 4-SS. Thermogravimetric analysis (TGA), FTIR, and XPS were used to qualitatively analyze the

DOI: 10.1021/acs.macromol.8b00733
Macromolecules 2018, 51, 6157−6189

Table 1. Polymerization of Different Monomers from the CNC Reducing Ends[172,186]

Initiator	Technique	Link	Monomer	Structure
4,4'-Azobis(4-cyanopentanoic dihydrazide)	SI-FRP	Hydrazone	AM	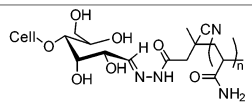
p-Carboxyphenylazomethylmalonodinitrile	SI-FRP	Hydrazone	AM	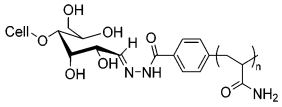
NHS-BiB	SI-ATRP	Diacetamide	NIPAM	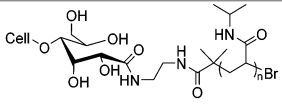
			METAC	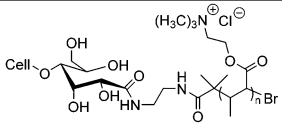
			4-SS	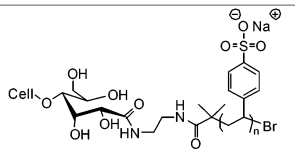

successful grafting of the CNCs. In order to directly visualize the selective modification of CNC reducing ends with grafted polymers, patchy CNC/PMETAC hybrids were labeled with gold nanoparticles (AuNPs) and observed by cryo-TEM (Figure 7).

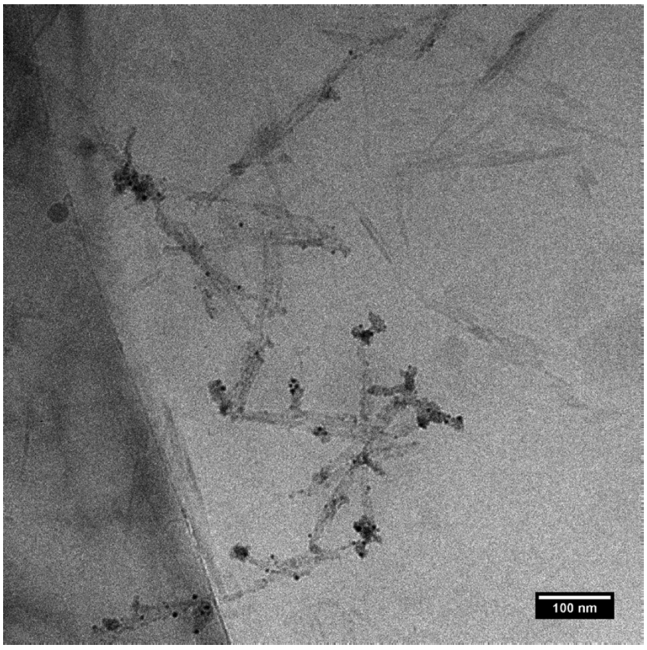

Figure 7. Cryo-TEM micrograph of patchy CNC/PMETAC hybrids labeled with AuNPs. Reprinted with permission from ref 172. Copyright 2017 American Chemical Society.

This image supports the point that the authors successfully achieved the preferential modification of the CNC ends, but nevertheless, optimization of the reaction conditions for both the end group functionalization and the AuNPs adsorption is necessary in future work, since it was clear that not all CNCs were successfully functionalized. Moreover, better characterization techniques are needed to quantify the number of initiators on the CNC reducing end groups.

4. EMERGING APPLICATIONS AND PROPERTIES OF POLYMER-MODIFIED CNCS VIA "GRAFTING *FROM*"

The rapidly growing academic and commercial interest in CNCs and hybrid nanomaterials thereof has driven their suggested use in unprecedented applications.[3,5,7,8,24,26,92] These include Pickering emulsions, nanotemplates for functional materials, supercapacitors, biosensors, drug delivery, and enantioselective catalysis. Here, we will focus on some of the emerging applications of polymer-modified CNCs, in which the grafting from approach, where high grafting density and molecular weight, is a priori advantageous over other polymer grafting strategies. In the following sections, applications in hybrid colloidal liquid crystals (LC), stimuli-responsive nanohybrids, nanocomposites and hydrogels as well as their unique properties will be discussed.

4.1. Self-Assembly, Hybrid Colloidal Liquid Crystals, and Optical Properties. CNCs have the intriguing ability to form chiral nematic LC phases, which depend on several factors, notably aspect ratio, surface charge density, ionic strength, external fields and solvent conditions.[31] Above a critical concentration, CNCs undergo a phase transition from an isotropic phase to a chiral nematic (cholesteric) liquid-crystalline phase (Figure 8).[187] The rods align preferentially with their long axes along a director. Each director of every pseudolayer (defined as an infinitesimally thin layer taken perpendicularly to the helicoidal axis) is slightly rotated around the helicoidal axis for each subsequent layer. The vertical distance required to complete a 360° rotation of the director is defined as the pitch.[188,189] When the suspension is left to dry on a substrate, the chiral nematic structure that forms upon increasing sample concentration is maintained after complete evaporation of the solvent, resulting in a film whose pitch

DOI: 10.1021/acs.macromol.8b00733
Macromolecules 2018, 51, 6157–6189

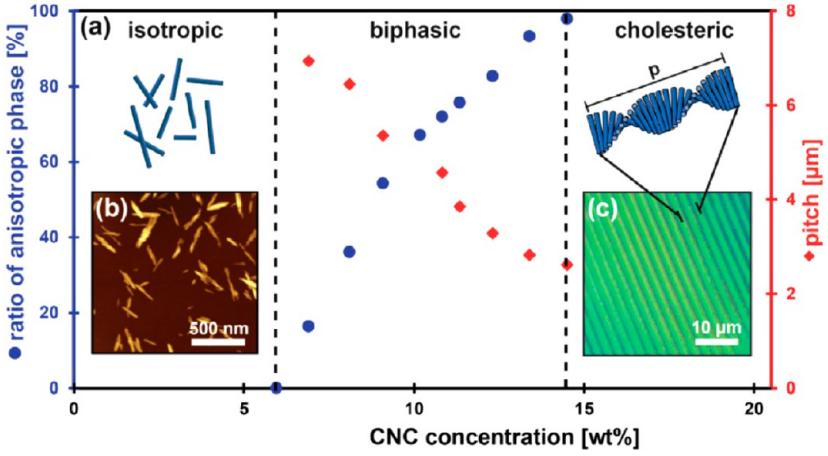

Figure 8. Schematic representation of the self-assembly of a CNC suspension upon evaporation to form a structurally organized array. (A) Phase diagram showing the transition from isotropic to cholesteric phase upon increase of CNC concentration. (B) Atom force microscopy image of individual CNCs. (C) Polarized optical microscopy (POM) image of a typical fingerprint pattern of the cholesteric phase. Reprinted with permission from ref 31. Copyright 2017, Wiley-VCH Verlag GmbH & Co. KGaA, Weinheim, Germany.

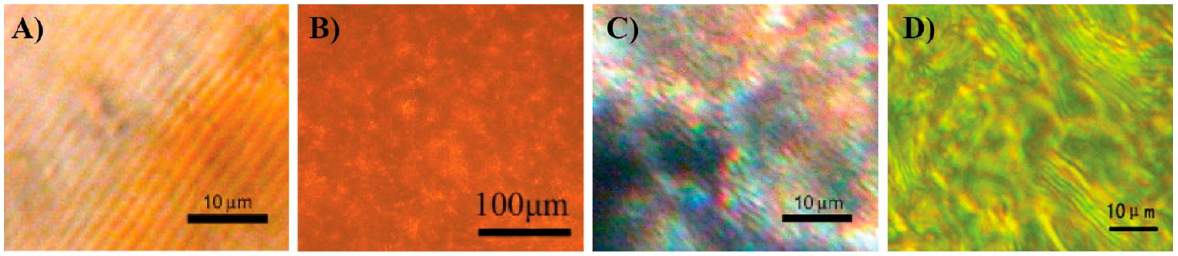

Figure 9. POM images showing (A) the fingerprint texture of pure CNC in water (3.1 wt %), and the fingerprint of different polymer-modified CNCs in their zone of anisotropic phase, i.e., (B) CNC-*g*-PMMAZO in chlorobenzene (5.1 wt %), (C) CNC-*g*-PSty in DMF (5.7 wt %), and (D) CNC-*g*-PDMAEMA in water (4.7 wt %, after 3 days) scale bar 10 μm for A, C and D and 100 μm for B. Adapted with permission from ref 141 (A, C) and ref 151 (B), copyright 2008 Elsevier Ltd., and ref 152 (D), copyright 2009, Springer Science+Business Media B.V.

dimension decreases to the submicrometer scale.[31] By exerting control over the drying conditions, the film can be homogeneous in thickness while retaining the long-range order of the CNCs.[190] Thus, the film behaves as a photonic crystal, and only light that is circularly polarized with the same handedness as the colloidal helices is reflected, in this case left-handed circularly polarized light.[188] These attractive properties of the self-assembled CNCs give a wide variety of interesting applications, such as devices for optical encryption, sensors, mesoporous chiral nanotemplates, and security coatings.[188,189,191,192]

Grafting polymers from the surface of CNCs, without a doubt, will affect their assembly behavior. Self-assembly of polymer-tethered CNCs is of great interest since more complex assemblies can be targeted through entropy-driven processes. Furthermore, their self-assembly can be potentially obtained in a variety of solvents, since the dispersibility of the CNCs can be tuned by surface modification. Such grafted-CNCs could give rise to a variety of CNC-based functional materials and templates based on colloidal LC assemblies. Nevertheless, self-assembly of polymer-grafted CNCs has not been widely explored to date, since the grafts likely alter the packing density of the CNCs, where they may behave more like spherical objects upon reaching a certain graft molecular weight and grafting density.[193] However, by using grafting to approaches, Jean et al. showed that polyetheramine-modified CNCs self-assembled into chiral nematic phases, albeit at a lower critical concentration in comparison to unmodified CNCs.[194]

Zhang and co-workers investigated the thermotropic and lyotropic LC phase behavior of CNC-*g*-PMMAZO,[151] CNC-*g*-PSty,[141] and CNC-*g*-PDMAEMA[152] (Figure 9). The CNC-*g*-PMMAZO showed a smectic to nematic transition at 95 °C and a nematic to isotropic transition at 135 °C in the absence of a solvent.[151] Furthermore, for these grafted CNCs, the POM image reveals a lyotropic LC phase in chlorobenzene above a concentration of 5.1 wt %. The authors reported a chiral nematic liquid crystalline behavior for the CNC-*g*-PSty, in both the lyotropic (DMF) and thermotropic states.[141] In the latter case, chiral nematic phases were observed upon cooling CNC-*g*-PSty to 163 °C, highlighting the potential of generating thermotropic LC phases based on CNCs grafted with nonmesogenic polymers. The authors later grafted thermosensitive PDMAEMA from CNCs.[152] They observed the fingerprint pattern for the CNC-*g*-PDMAEMA in the anisotropic phase, indicating chiral organization in aqueous media. The spacing of the fingerprint lines in aqueous suspensions could be tuned by changing the temperature. Below the lower critical solution temperature (LCST) of PDMAEMA, the polymer brushes existed in an extended conformation and therefore increased the spacing of the fingerprint, the opposite of which occurred above the LCST. Such systems are of great potential in developing colloidal analogues of stimuli-responsive molecular mesogens. The ability to externally manipulate the LC phases of CNCs in a reversible manner opens a number of interesting possibilities, including templating chiral 3D nanostructures,[192] optical sensors,[31] nanocomposite liquid crystalline elastomers (LCEs),[195] and multiresponsive supracolloidal systems.[196]

4.2. Stimuli-Responsive Nanohybrids. Biopolymers in living organisms are ubiquitously involved in dynamic systems

DOI: 10.1021/acs.macromol.8b00733
Macromolecules 2018, 51, 6157–6189

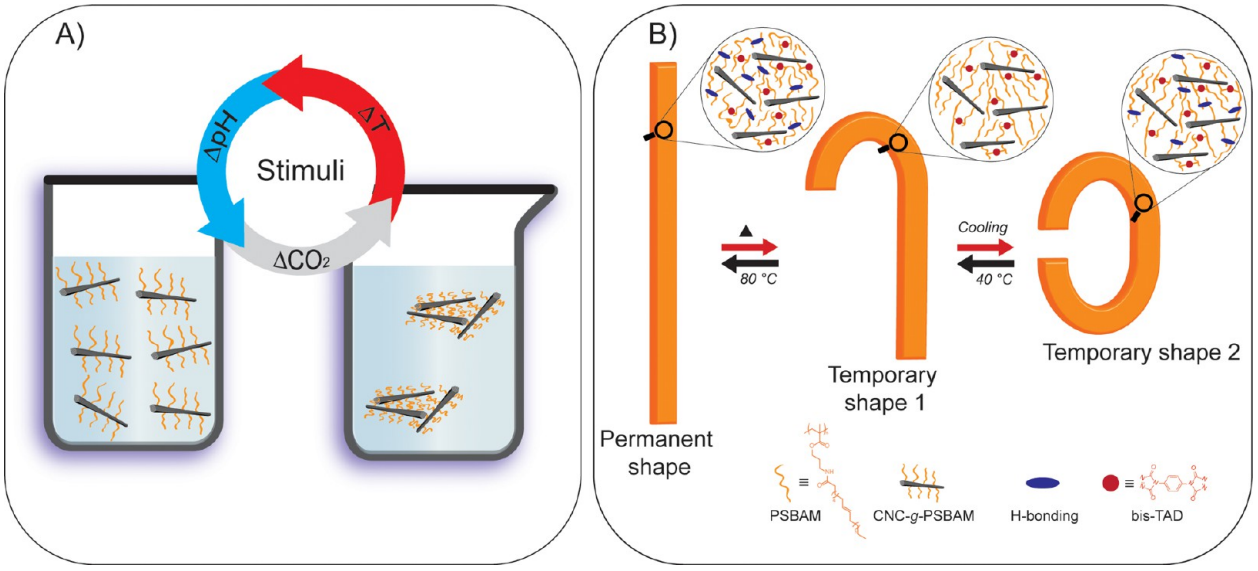

Figure 10. Schematic representation of stimuli-responsive hybrids based on polymer-grafted CNCs. (A) Transitions in solution of stimuli-responsive polymer modified CNCs from well dispersed to aggregates or vice versa as response to an external stimulus, such as pH, temperature or carbon dioxide (CO_2) atmosphere. (B) Thermally triggered triple shape memory behavior is achieved with poly(soybean amide methacrylate) (PSBAM) grafted CNCs dispersed in a PSBAM matrix in the presence of 4,4′-(1,4-phenylene)-bis(1,2,4-triazoline-3,5-dione) (bis-TAD) as cross-linker, where H-bonding between PSBAM chains is also at play.

that promote structural changes in response to the conditions in their surrounding environment.[197] These properties are based on highly cooperative interactions that provide a significant driving force for the response caused by small external changes. Similar adaptive behavior can be imparted to synthetic polymers by incorporating functional groups in their backbone capable of responding to diverse external chemical (pH, ionic factor or chemical agents) or physical stimuli (temperature, electronic or magnetic fields, light or mechanical stress) (Figure 10). These are known as stimuli-responsive or smart polymers. By grafting such polymers from the surface of CNCs, hybrid nanomaterials bearing reversible interfacial properties can be fabricated.

pH-Responsive Hybrids. Polymers that undergo chemical and morphological changes as a result of pH variations are known as pH-responsive polymers. They usually contain functional groups that can be protonated, resulting in a transition from a hydrophilic to a hydrophobic state or vice versa, which may induce precipitation in aqueous solutions. CNC-*g*-P4VP was reported to display a completely reversible pH-responsive behavior in water.[132] P4VP is a well-known polyelectrolyte with an acid dissociation constant (pK_a) of around 5, and is thus present in a hydrophilic protonated state at a pH of lower than 5, but it can be rendered hydrophobic at higher pH values due to the deprotonation of the pyridyl groups. Accordingly, suspensions of CNC-*g*-P4VP in water show good colloidal stability in acidic environments but flocculate above a pH of 5, due to the change from hydrophilic to hydrophobic character of the grafts.

In a different study, CNC-*g*-PAA also showed equivalent properties due to the nature of its brushes.[178] PAA is a weak polyelectrolyte, which undergoes pH-dependent conformation transition according to the ionization state of its carboxylic groups; i.e., the chains adopt a partial globular conformation in their protonated form (at low pH) and change to a coiled conformation when deprotonated at high pH.[198] The CNC-*g*-PAA suspensions showed lower UV−vis absorbance at pH values higher than 7 as consequence of the ionizations of the carboxylic groups present in the grafts, which promotes the complete solvation of polymer chains.[178]

pH variations of a colloid can also be promoted by its exposition to acidic or basic gases, such as CO_2 and N_2, respectively. In addition, it is known that polymers containing tertiary amines are easily protonated in the presence of water and CO_2, which involves the formation of carbonic acid and an increase in the hydrophilicity character of the polymer. The combination of these two concepts was applied to CNCs by decoration with PDMAEMA, PDEAEMA and PDMAPMAM either via S-NMP[181] or SI-ATRP.[171] The CO_2-responsiveness of these systems was evaluated by determining the ζ-potential versus pH in alternating CO_2/N_2 exposure cycles (Figure 11). In all cases, high ζ-potential values were observed for stable dispersion when grafts were protonated under CO_2 atmosphere (low pH), while low ζ-potential values were reported when the dispersion flocculated in the presence of N_2 (high pH). From the three hybrids studied, CNC-*g*-PDEAEMA clearly demonstrated the pH-switchability of the system due to its sole solubility in water under its protonated form, *i.e.*, in the presence of CO_2.

Temperature-Responsive Hybrids. Thermosensitive polymers respond to a change in their solvation state upon heating or cooling. According to the way the measurement is performed, the reported value should be cited as cloud point, upper (UCST) or lower critical solution temperature (LCST). The cloud point is an experimentally measured value at which the first appearance of turbidity or cloudiness are observed due to the phase separation of the components of a mixture as a response of a stimulus (i.e., temperature).[199] When plotting these cloud-point temperatures (CPT) vs the overall polymer concentration, the cloud-point curve is obtained, where the minimum point is known as the precipitation threshold (or LCST).[200] In this sense, the term LCST only refers to the lowest temperature at which phase separation can happen.

Decorating CNCs with thermosensitive polymers can lead to hybrid materials with temperature-responsive features. CNC-*g*-PNIPAM has demonstrated thermal behavior due to the ability

DOI: 10.1021/acs.macromol.8b00733
Macromolecules 2018, 51, 6157−6189

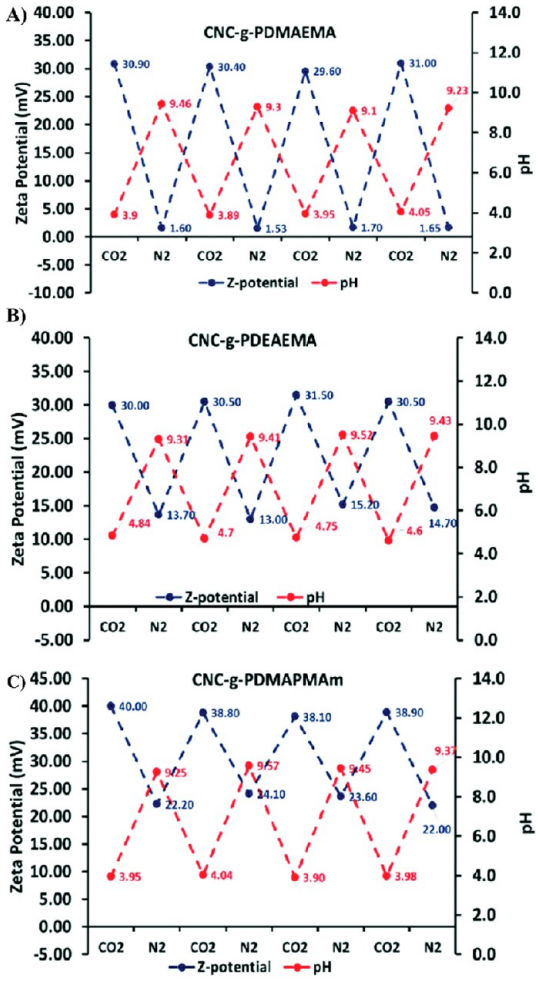

Figure 11. ζ-Potential and pH at room temperature of aqueous dispersions (1 mg·mL^{-1}) of (A) CNC-*g*-PDMAEMA, (B) CNC-*g*-PDEAEMA and (C) CNC-*g*-PDMAPMAM in alternating CO_2/N_2 exposure cycles. Adapted from ref 181. Copyright 2017, Royal Society of Chemistry.

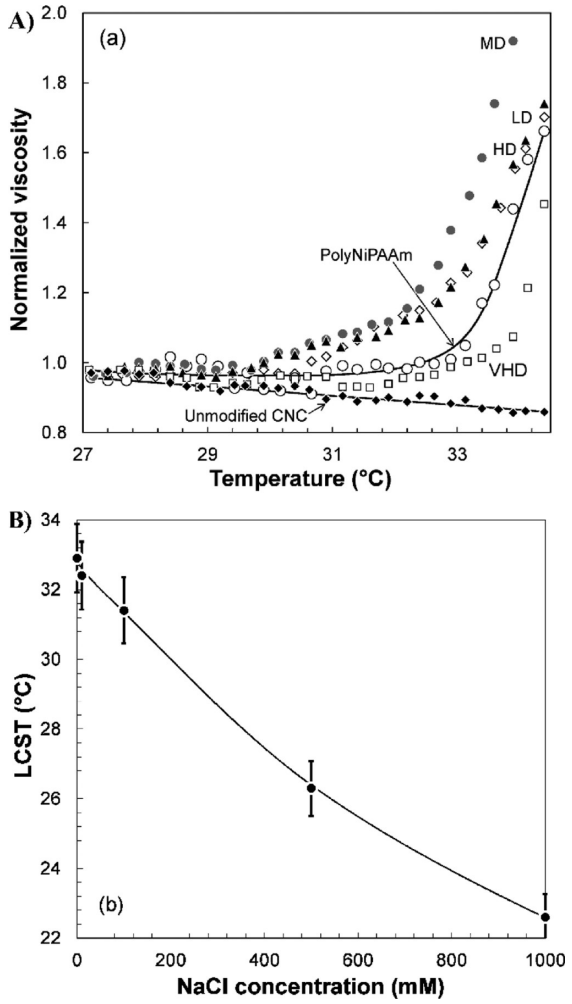

Figure 12. Thermoresponsive behavior of CNC-*g*-PNIPAM. (A) Viscosity of CNC-*g*-PNIPAM with various graft densities (i.e., VHD, very high; HD, high; MD, medium; and LD, low densities) at different temperature normalized by the viscosity of the corresponding dispersion at 25 °C. (B) LCST of aqueous dispersions of medium density CNC-*g*-PNIPAM at various NaCl concentrations. Adapted from ref 201. Copyright 2011, American Chemical Society.

of PNIPAM to undergo a coil-to-globule transition at about 32 °C.[164,178,201] Zoppe et al. reported for the first time the thermoresponsive behavior of such materials as a function of grafting density and degree of polymerization of PNIPAM, which was prepared by SI-ATRP.[201] In this study, suspensions of CNC-*g*-PNIPAM were shown to respond to temperature changes between 30 and 32 °C (CPT) by a significant increase in their viscosity (Figure 12A). The CPT of the hybrid materials was shown to approach the LCST of the free polymer as the grafting density was increased. In addition to the nature of the grafts, the CPT was also influenced by the differences in the steric repulsive forces between adjacent polymer-modified CNCs. The latter was also shown to affect the size of aggregates at temperatures higher than the LCST of free polymer. In the same study, the CPT of these materials also was shown to decrease upon increasing the ionic strength (i.e., by varying the concentration of NaCl), as is the case of free PNIPAM in aqueous solution (Figure 12B).

In another study, CNC-*g*-PNIPAM also demonstrated a sol−gel phase transition at about 34.3 °C, which may be exploited for embolization of hepatocellular carcinoma.[164] The weight-average molecular weight (M_w) of these grafts was more than 10 times lower than the one reported by Zoppe et al.[201] This indicates that the molecular weight of the grafts has a direct influence on the thermal behavior of the hybrid nanoparticles. Furthermore, Haqani et al. also reported the thermoresponsiveness of CNC-*g*-PNIPAM with a CPT around 29 °C.[178] Such differences in CPTs are often associated with differences in molecular weight, which is known for PNIPAM chains in solution,[202] and the grafting density of PNIPAM brushes.

CNC-*g*-PNVC was also reported to display a thermally induced phase transition above 36 °C from a stable colloidal aqueous suspension to collapsed PNVC brushes due to a change of the hydrophilicity of the grafts.[161] CNC-*g*-POEGMEMA[159] and CNC-*g*-poly(ethylene glycol)methyl acrylate[160] have exhibited tunable thermal behavior (between 23.8 and 63.8 °C and between 34 and 66 °C, respectively); the respective cloud points could readily be tailored by adjusting the comonomer ratio in the grafted polymers. In all cases, the transition was confirmed by changes in the viscoelastic properties of the materials.

A thermoresponsive enhanced fluorescence hybrid based on CNC-*g*-P(NIPAM-*co*-EANI) was recently synthesized. This

DOI: 10.1021/acs.macromol.8b00733
Macromolecules 2018, 51, 6157−6189

nanomaterial reacted to temperature variations while displaying a simultaneous increase in its fluorescence intensity.[154] The latter was attributed to the thermoresponsiveness of PNIPAM brushes, which altered the distance between the dye groups.

Dual pH- and Temperature-Responsive Hybrids. Contributions of polymeric chains bearing different stimuli-responsive properties can result in copolymers with multiple response functions. In the domain of polymer-grafted CNCs, the first example of hybrids reporting such dual-responsiveness was CNC-*g*-P(NIPAM-*ran*-AA) containing different amounts of AA, which responded to pH and temperature variations.[142] The CPT of this system was tuned by three factors: polymer tethering to CNCs, AA content, and pH (Figure 13). The CPT increased

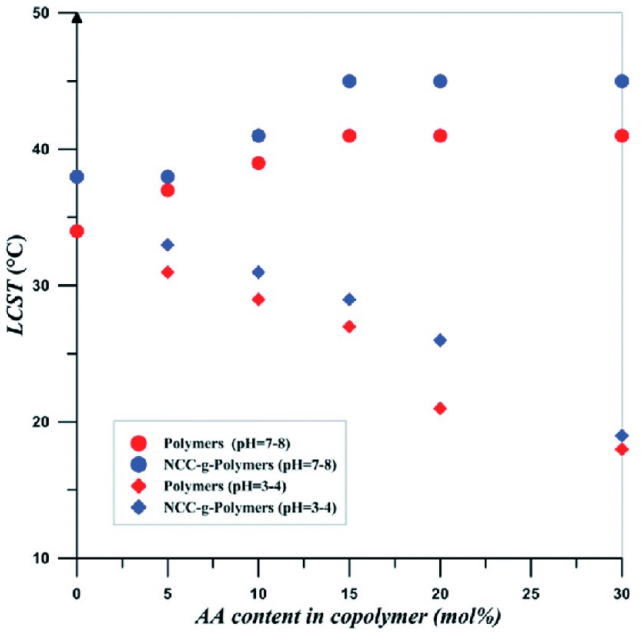

Figure 13. LCST diagram of 0.2 wt % aqueous suspensions of P(NIPAM-*ran*-AA) as free copolymer (red) or grafted to CNCs (blue) bearing different AA content at low and high pH values. Reprinted with permission of ref 142. Copyright 2014, Royal Society of Chemistry.

from 38 to 45 °C at high pH (*ca.* 7−8) while it decreased from 30 to 18 °C at lower pH values (*ca.* 3−4), when the AA content of the grafts was increased from 5 to 30 mol %. The reduction observed in the CPT was mainly attributed to the hydrophobic behavior of AA in protic media. In addition, a comparison between free and CNC-grafted copolymers demonstrated that tethering copolymers to CNCs resulted in an increase up to 6 °C in the CPT, with respect to the LCST of free copolymer.

Using the same monomers, albeit with block rather than random distribution of comonomers and varying the inner and outer block, Haqani et al. also reported thermoresponsive systems. A dual-sensitive characteristic was only observed when the PAA was at the outer block, i.e. CNC-*g*-PNIPAM-*block*-PAA.[178] Furthermore, Tang et al. developed a hybrid, containing POEGMA and PMAA grafted-CNCs, in order to control the stability of particle-stabilized emulsions manipulated by pH and temperature.[135] PMAA brushes formed hydrogen bonds with POEGMA at low pH values (<4.5), leading to the formation of aggregates, while the presence of electrostatic repulsions at higher pH disrupted hydrogen bonding to yield stable dispersions. Additionally, POEGMA chains exhibited temperature-dependent conformational changes that influenced the stability of the emulsion.

Shape-Memory Hybrids. Shape-memory polymers (SMPs) are those capable of being deformed and returned to their original state through a specific stimulus, for example, via thermal transitions or activation−deactivation of supramolecular interactions, often in elastomeric systems. Wang et al. proposed a shape-memory nanocomposite derived from biomass, i.e., soybean oil and CNC.[156] The system was composed of CNC-*g*-PSBAM (synthesized via SI-ATRP with a theoretical M_n = 22 kDa) and bis-TAD using PSBAM as a matrix (Figure 10B). The network of the hybrid was formed by using two types of cross-links within the material: one covalently linked by bis-TAD and another dynamic physically cross-linked via hydrogen bonding with the plant oil functional groups (and also the bis-TAD moiety). Here, the covalently bonded network was responsible for the permanent shape of the material, while the physical network provided multiresponsive and multi shape-memory properties. The material showed triple-shape-memory with two recovery steps performed at staged temperatures of 40 and 80 °C, respectively. Additionally, water and THF induced the shape-recovery of the material within 30 and 5 min of immersion, respectively.

The properties exhibited by the above-mentioned stimuli-responsive nanohybrids are mainly attributed to the type of polymer grafted on the CNC surface. Thus, the main function of the CNCs is to provide either mechanical reinforcement[156] to the material or enhance their solubility[142] in polar solvents due to the large amount of −OH groups at the surface of CNCs. Most of these investigations have been focused on the synthesis of stimuli-responsive materials and their behavior upon application of different stimuli, but little is known about the minimum amount of grafted polymer required to observe such stimuli-responsive behavior. Furthermore, it is in many cases unclear how the grafting density of the polymer influences the responsiveness of the material.

4.3. Nanocomposites. Nanocomposites are materials composed of two or more components, often a matrix and a filler, in the solid or gel-like state, the filler being on the nanoscale. There are different processing routes reported in the literature for the production of cellulose nanocomposites, such as solution casting, melt extrusion, compression molding, injection molding, ball milling, or even precipitation methods.[4,5,7,203] The outstanding mechanical properties and the high specific area suggest that CNCs would provide good reinforcement to other polymeric materials. The reinforcement potential of CNCs was first reported by Favier et al., who incorporated tunicate-derived CNCs into a copolymer of Sty and BA (P(Sty-*co*-BA)).[204,205] The reinforcement effect of CNCs is often explained by the formation of a rigid percolating network in which the filler nanoparticles interact via hydrogen bonding.[5] The experimental evidence and statistical models stipulate that the matrix, the filler characteristics, such as aspect ratio, dispersion and volume fraction, and their interactions (filler−matrix and filler−filler) all influence the mechanical properties of the nanocomposites.[3]

Even though unmodified CNCs have been reported to offer reinforcement in some materials,[204−206] the hydrophilicity of the CNC surface makes their dispersion difficult in polymer matrices, especially those that are nonpolar or hydrophobic. In addition, the numerous −OH groups at their surface promotes the agglomeration of CNCs via hydrogen bonding limiting the extent of mechanical reinforcement. In that regard, surface modification of CNCs is a viable approach to create good interfacial

DOI: 10.1021/acs.macromol.8b00733
Macromolecules 2018, 51, 6157−6189

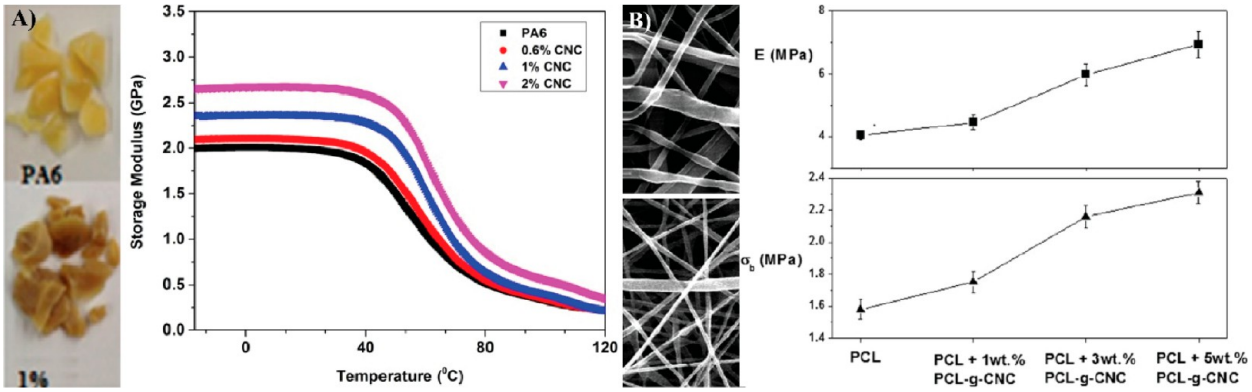

Figure 14. Reinforcement on the mechanical properties of nanocomposites by the incorporation of polymer-grafted CNCs. (A) Pictures of neat PCL (top left) and 1 wt % CNC-*g*-PCL/PCL (bottom left) and the storage modulus of CNC-*g*-PCL/PCL nanocomposites with different wt % of the hybrid (right). (B) Scanning electron microscopy (SEM) images of electrospun mats of neat PCL (top left) and 5 wt % CNC-*g*-PCL/PCL (bottom left), and the elastic modulus (E) and tensile at break (σ_b) of samples bearing up to 5 wt % of CNC-*g*-PCL. Reprinted with permission from references 207 (A) and 80 (B) Copyright 2016, John Wiley and Sons.

adhesion between CNCs and a (hydrophobic) polymer matrix, ideally without compromising the intrinsic properties of the CNCs and their filler−filler interactions. Many efforts have focused on the modification of the CNC surface in order to enhance their compatibility with hydrophobic media.[4]

The first nanocomposite containing polymers grafted from the surface of CNCs was reported by Habibi et al. in 2008, based on CNC-*g*-PCL dispersed in a PCL matrix.[30] Nanocomposites of PCL-grafted CNCs incorporated into PCL,[30,80,88,207,208] PLA,[81] PCL/PLA 50/50 w/w %,[104] poly(butylene succinate-*co*-adipate) (PBSA),[82] and segmented polyurethane (PCL/PU)[209] matrices have also been investigated. The above-mentioned systems generally reported good filler−matrix compatibility due to the hydrophobicity of modified CNCs, with the exception of the PCL/PU matrix,[209] where microphase separation was observed. For example, the incorporation of 2 wt % of CNC-*g*-PCL in PCL matrix showed an increase on the storage modulus (E': going from 1.95 to 2.6 GPa and 0.52 to 0.74 GPa at 30 and 80 °C, respectively) attributed to the gain in rigidity of the matrix through restriction of the mobility of the brushes (Figure 14A).[207]

In another study, the reinforcement effect of CNC-*g*-PCL was confirmed by 140% increase of Young's modulus (E) when 2 wt % or a higher amount of modified CNCs were added to PCL/PU matrix.[209] The incorporation of homopolyester (PCL or PLA) or diblock copolymer (PCL-*block*-PLA) grafted-CNCs into PCL or PCL/PLA matrices enhanced the shear storage modulus (G'), recorded at low-frequency, by a factor 10−100 relative to the PCL/PLA blend loaded with unmodified CNCs.[104]

Electrospun nanocomposites, based on CNC-*g*-PCL in PCL matrix, also demonstrated an improvement in stiffness (from 4 to 7 GPa) and strength (from 1.6 to 2.3 MPa) upon an increase in modified CNC content from 0 to 5 wt % (Figure 14B).[80] The improvements in mechanical behavior were attributed to the addition of modified CNCs in the nanofiber and the higher molecular weight of the grafted PCL chains, which perhaps cocrystallized with the PCL nanofiber matrix.

The effects of incorporating polymer-modified CNCs in polymer matrices were not only observed by mechanical testing, but also by DSC. For PLA reinforced by CNC-*g*-PLA, a reduction between 3 and 5 °C in thermal stability, with respect to neat PLA, was observed and attributed to either a plasticizing effect of short PLA chains[88] or residual catalyst from the polymerization step.[90,91] However, this was not the case when D-LA was used as the monomer and loaded up to 5 wt % CNC-*g*-PLA in a PLA matrix.[109] The incorporation of CNC-*g*-PLA in poly(*β*-hydroxybutyrate) (PHB) resulted in a substantial reduction of the crystallization temperature of PHB varying from 2 to 8 °C with respect to the neat polymer, while the lamellar structure of the latter was unaffected.[113] In another study, the grafting of P(MMA-*co*-BA) from the surface of CNCs resulted in self-reinforced thermoplastic elastomers, whose T_g increased by a remarkable 19 °C in comparison to the free copolymer, as a consequence of the restricted mobility of the copolymer brushes on the surface of CNCs.[169]

Polymer-grafted CNCs used in the preparation of nanocomposites have been mainly synthesized via SI-ROP. Nevertheless, some examples have also been reported for SI-FRP[94,133] and SI-ATRP.[157] PGMA[133] and PSty[94] brushes showed a contribution in the increase of compatibility with PLA matrices. In addition, CNC-*g*-PGMA also showed a slight increase in the tensile strength (from 47.8 ± 0.6 to 52 ± 2 MPa) compared to equivalent nanocomposite made with unmodified CNC in PLA matrix.[133] In another study, CNC-*g*-PSty was incorporated in PMMA matrix exhibiting better dispersibility and thermal stability (50 °C higher than CNC/PMMA nanocomposite).[157] It is worth mentioning that the reinforcement effect in nanocomposites based on polymer-grafted CNCs cannot always be explained by percolation theory, due to the disturbance of hydrogen bonding interactions between chemically modified CNCs, which may hinder their percolation.[5] Therefore, the reinforcement may involve other factors, such as better interfacial adhesion between filler and matrix or cocrystallization of grafted polymers with the polymer matrix.

With the aim to fabricate viable alternatives to petroleum-based composites, PLA-modified CNCs have gained interest due to their biodegradability, renewability and nontoxicity. Biodegradable CNC-based nanocomposites containing CNCs grafted with homo-[88,90,91,104,106−109,133] and random copolymers[105] dispersed in PLA matrices have been reported. As common characteristics, these all showed good interfacial adhesion between modified-CNCs and the matrix, stereocomplexation from cocrystallization with the matrix, efficient nucleation induced by grafted CNCs, as well as enhancement in the mechanical properties.

DOI: 10.1021/acs.macromol.8b00733
Macromolecules 2018, 51, 6157−6189

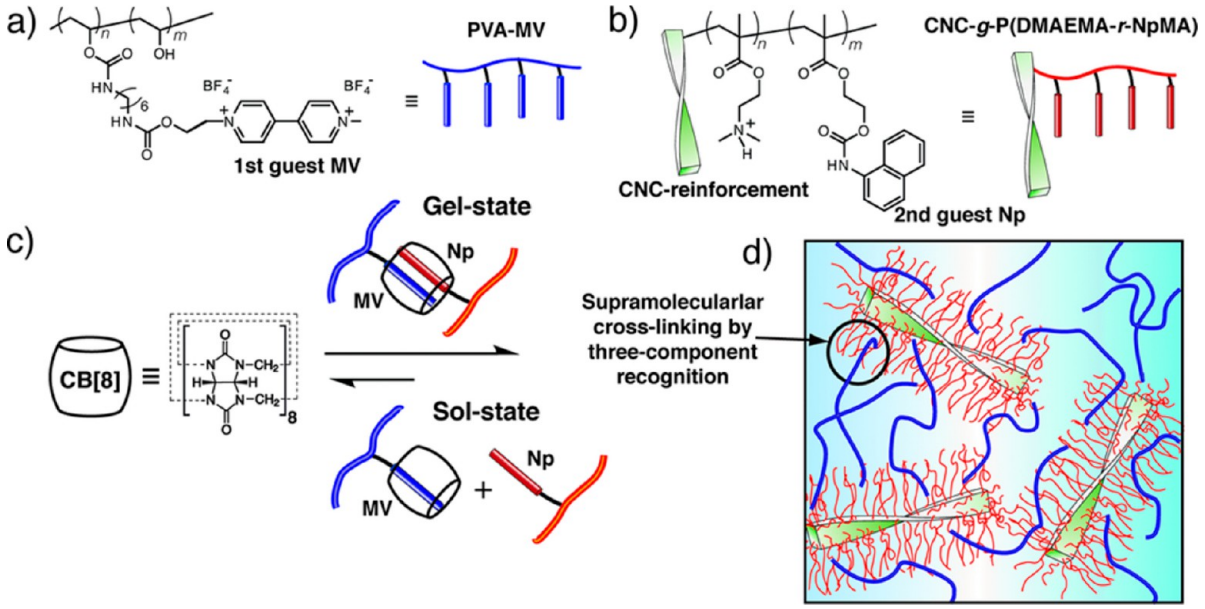

Figure 15. Three-component CNC-reinforced hydrogel based on (a) PVA containing methyl viologen functionalities as first-guest units, (b) CNC-*g*-P(DMAEMA-*ran*-NpMA) bearing NpMA units as second-guest and (c) the CB[8] host motif. The latter shows simultaneous binding of the guest entities resulting in the formation of (d) a dynamic hydrogel with supramolecular cross-linking. Reprinted with permission from ref 166. Copyright 2014, John Wiley and Sons.

A new class of nanocomposites based on polymer-modified CNCs, referred to as one-component nanocomposites (OCNs) or cocontinuous composites, has recently started to attract attention. In contrast to conventional composites these materials feature (as the name implies) only one component, i.e., CNCs from which a significant amount of polymer chains have been grafted that serves as the "matrix". As the polymer is covalently attached to CNCs, these systems do not typically suffer from phase separation or mixing problems, like conventional nanocomposites, while beneficing properties to which both components contribute.

The first example was reported by Chen et al. through the grafting of PCL chains from the surface of CNCs, via SI-ROP, as a thermoformable material.[112] The molecular weight of the grafts was unknown, however the content of the polymer brushes was calculated to be between 92 and 96 wt % for CNC-*g*-PCL, depending on the reaction time and the two different microwave irradiation powers (160 and 320 W) employed. In addition, a nonlinear dependence was observed in the mechanical properties of these OCNs, indicating that the reaction conditions may influence the number and length of the grafted chains.

Recently, another study showed that OCN materials based on CNC-*g*-PMMA displayed properties superior to equivalent conventional two-component nanocomposites for two different compositions, i.e., 10 and 20 wt % of CNC.[93] For example, the E' at 25 °C of CNC_{10}-*g*-PMMA was 3168 MPa versus 3018 for 10% w/w PMMA/CNC conventional nanocomposite. The authors suggested that the stress-transfer is mediated by the polymer chains attached to the CNCs. Indeed, OCNs are promising materials due to their easy-to-process characteristics, which also offer a unique combination of high stiffness, strength, and toughness.[93]

4.4. Hydrogels. Hydrogels are soft cross-linked three-dimensional networks mainly based on hydrophilic polymeric materials that have the capability of holding large amounts of water or biological solutions. Such soft materials have many potential applications, especially in the biomedical field.[128] The hydrophilic character and the intrinsic properties of CNC make them an attractive candidate for the formation of reinforced or structured hydrogel nanocomposites.[210] Hydrogels based on polymer-grafted CNCs have generally reported enhanced mechanical properties due to the critical role of CNCs acting as multifunctional cross-linkers and bridges for the neighboring polymer chains.

Zhou et al. reported the synthesis of hydrogels from CNC-*g*-PAM in the presence of NMBA as cross-linker.[128] The grafted CNCs accelerated the formation of hydrogels and increased the effective cross-link density of the material. The interfacial interactions between PAM and CNCs were significantly improved and the reinforcement effect was confirmed by an increase in the compression stress of 2.5-fold for hydrogels containing 6.7 wt % of CNC-*g*-PMA. Later, a three-component supramolecular nanocomposite hydrogel showing high stiffness, rapid sol−gel transition and self-healing properties was reported.[166] The system was composed of poly(vinyl alcohol) (PVA) containing methyl viologen functionalities, CNC-*g*-P(DMAEMA-*ran*-NpMA) and cucurbit[8]uril (CB[8]) supramolecular cross-links, where CB[8] (host) selectively and simultaneously binded methyl viologen- and naphthyl-based guest units under stoichiometric molar ratio (Figure 15).

Even though the use of external cross-linkers is a known practice in the synthesis of CNC-based hydrogels, it can be avoided by designing a CNC-based system containing building blocks capable of physically or chemically cross-linking in three-dimensional networks. The first example of such systems was based on CNC-*g*-PMA.[138] This hydrogel presents elastomeric features, due to the properties of the PMA brushes, and high toughness, thanks to a unique core/shell network structure, where CNCs behave as multifunctional cross-links, resulting in unique mechanical properties.

Recently, an elastic macroporous composite hydrogel was prepared via aqueous phase polymerization of CNC-*g*-PUPyMA containing acrylamide and gelating methacrylate.[123] Their swelling ratio, pore size and mechanical strength

DOI: 10.1021/acs.macromol.8b00733
Macromolecules 2018, 51, 6157−6189

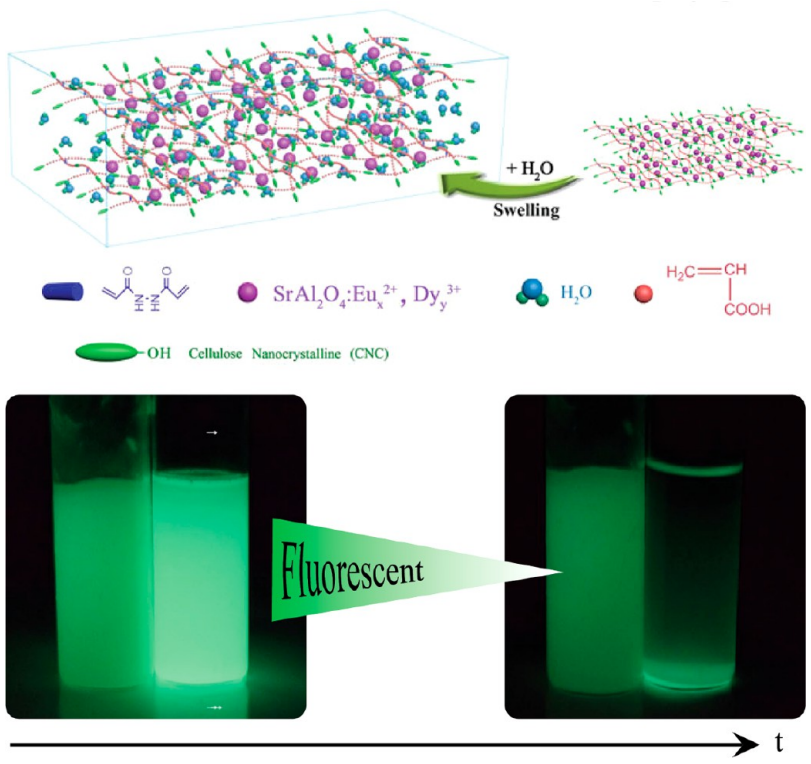

Figure 16. Hydrogel based on phosphorescent Eu^{2+}/Dy^{3+}-doped $SrAl_2O_4$ and CNC-*g*-PAA (top) showing fluorescent properties just after water absorption (bottom left), which get reduced with time (25 min later, bottom right). Adapted from ref 124. Copyright 2017, Springer Nature.

were tunable by controlling the incorporated concentration of CNC-*g*-PUPyMA. The material achieved a swelling ratio of 70% within 10 min, while the pore size was reduced from 62 to 30 μm by increasing the concentration of modified CNCs from 0.1 to 0.5 wt %, respectively. The mechanical strength also significantly increased at higher CNC content, about 50 kPa when the concentration of CNC-*g*-PUPyMA was varied from 0.1 to 0.5 wt %. In addition, these materials exhibited good biocompatibility and promising cell adhesion and proliferation under *in vitro* cell culture.

Furthermore, a fluorescent nanohybrid hydrogel for water detection was developed by Wu et al. (Figure 16).[124] The structure was composed of a cross-linked CNC-*g*-PAA network in which Eu^{2+}/Dy^{3+}-doped $SrAl_2O_4$ NPs were fixed by the polymer chains through coordinate bonds preventing the aggregation and quenching in water. The fluorescence intensity of the material showed a direct linear relationship with water absorption and an excellent fluorescence stability, making them a suitable sensor material for water detection. In the domain of injectable hydrogels, CNC-*g*-PNIPAM could be potentially used for wound dressing due to the good drug-loading capacity at room temperature and a burst drug release at 37 °C, as shown by Zubik et al.[129]

5. SUMMARY AND OUTLOOK

Since the seminal work of Habibi et al. in 2008 on SI-ROP of ε-CL from CNCs,[30] the scientific interest in utilizing surface-initiated polymerization from CNCs as a means to tailor their properties has manifested itself in over one hundred publications. Most investigations have dealt with the synthetic protocols to modify CNCs with high density polymer brushes, an objective appropriately reached using grafting from techniques. Upon a review of the literature, it appears that each of these approaches has distinct advantages and disadvantages regarding number of reaction steps, conditions and polymer brush characteristics.

SI-ROP, for example, is advantageous in that it does not typically require the prior immobilization of initiators on the CNC surface, as SI-ROP can be conducted directly from the CNC −OH groups albeit in a dry organic solvent. Although there is only very limited information regarding the molecular weight and dispersity of such polymer grafts, relatively short polymer chains have been reported, *e.g.*, DP = 12.[107] In contrast, high polymer contents (up to 96 wt %) were reported by others,[112] which could suggest high grafting density, high molecular weight, or both were obtained.

Analogously, SI-FRP can also be utilized without the prior immobilization of initiators on CNC surfaces at higher temperatures, however it is assumed that higher molecular weights are obtained, based on bulk FRP kinetics. In addition, the use of radical initiators attached to the surface of CNCs may be an alternative when high DP is desired despite the poor control over the molecular weight.[93] As many researchers have focused on using SI-FRP in order to produce nanocomposite hydrogels,[123,124,128,129,137,138] little is known about the molecular weight and dispersity of the grafted polymers.

SI-CRP approaches can be used to grow polymer brushes with controlled molecular weight and dispersity, however usually require an appropriate initiator or CTA to be attached to the CNC surface beforehand. An exception to this is an S-RAFT approach in which the polymerization is conducted in the presence of a free macro-RAFT agent and initiated by CAN.[96,180] Although initiator immobilization is a prerequisite to conduct Cu-mediated SI-CRP from CNCs, it has been shown that such initiators can be covalently attached *in situ* during the sulfuric acid hydrolysis process to produce functionalized CNCs.[95]

DOI: 10.1021/acs.macromol.8b00733
Macromolecules 2018, 51, 6157−6189

In these Cu-mediated systems, the inherent surface chemistry of the CNCs, *i.e.* sulfate half-ester groups, also plays a role in the polymerization kinetics when performed in aqueous media, due to the formation of electrical double layers of Cu/ligand species.[173] Regarding SI-NMP, the synthetic strategy is simple in that, once the NMP initiator is grafted to the CNC surface, only monomer and heat are required to initiate polymerization.[143,181] Although information on the polymer graft characteristics is still lacking, free polymers synthesized *in situ* during SI-NMP had M_n values in excess of 100 kDa.[143] In most cases of SI-CRP, molecular weight >100 kDa may be obtained with the appropriate reaction conditions. In general, there are few reports on the analysis of polymers cleaved from the surface of CNCs in order to accurately determine their molecular weight and grafting density,[96,115,154,163,176] suggesting that there is much to be understood regarding polymer brush growth kinetics from CNCs compared to analogous solution polymerizations.

As the kinetics of surface-initiated polymerizations from other types of planar and curved interfaces are very often reported to differ significantly from solution polymerizations,[28] this also likely applies to polymer brush growth from CNCs and will depend highly on the polymerization technique, monomer, solvent, reactions conditions, etc. Utilizing cleavable functional groups for covalent attachment of initiator species[28,115] and applying new techniques to determine polymer brush grafting density[211] are promising approaches to address this challenge.

In addition to the development of appropriate strategies for the chemical synthesis of polymer-modified CNCs and fundamental investigations of polymer brush growth kinetics, a majority of these research efforts have focused on exploiting the unique thermomechanical properties of CNCs as a reinforcing filler in hydrophobic polymer matrices through surface functionalization. Such nanocomposites have been primarily processed by solution casting and various forms of melt processing.

A few works have sought to fabricate nanocomposites that do not suffer some of the processing limitations associated with blending hydrophilic CNCs with hydrophobic polymers by removing the polymer matrix component altogether; so-called OCNs.[93,112] These systems are advantageous in that they are less affected by phase separation of the components and can offer superior mechanical properties provided the molecular weight of polymer grafts is sufficient to allow chain entanglements between neighboring hybrid nanoparticles. One of the challenges in this regard is obtaining such high molecular weight polymer grafts without compromising the structural integrity of the CNCs. Due to the limited molecular weight that is often obtained using SI-ROP,[107] it may not be ideal for this type of application. In comparison to SI-CRP, it is already clear that this goal is probably best realized through SI-FRP techniques, since good control over polymer graft dispersity may not be as critical. However, there are many open research questions; what is the relationship between internanoparticle chain entanglements, anisotropy, molecular weight and grafting density? How does the dispersity of grafted polymers affect the thermomechanical properties of OCNs of rod-shaped nanoobjects? Furthermore, one can imagine OCNs composed of block or statistical copolymer grafts with dissimilar, *e.g.*, hard and soft phases, which might show interesting phase separation behaviors.

From the standpoint of LC research, anisotropic colloidal hybrid materials are useful models for elucidating the relationship between building block properties and self-assembly. Among this class, CNCs are unique in that they retain their chiral LC assemblies in the solid-state upon evaporation-induced self-assembly (EISA), which has opened new doors for the preparation of mesoporous inorganic solids with long-range chiral order.[191] Such chiral materials have great implications in enantioselective separations, asymmetric catalysis and chiral optics. Thus, far, such templating processes have been mostly limited to aqueous systems, and this puts a number of restraints on the types of chiral mesoporous solids one can fabricate. Moreover, the pitch of chiral nematic phases of CNCs is sensitive to the presence of additives, pH, ionic strength, external fields, and evaporation rate, due to the complex interplay between surface charge density, CNC chirality, aspect ratio, and dispersity.[31,212−214] Such factors have often been employed as a means to control the optical properties of CNC LC phases both in solution and in free-standing films. However, these means are not typically reversible processes, which are better realized by incorporating stimuli-responsive polymer systems.

In this regard, surface chemical modification with tethered polymers has not been widely explored. This is probably due to the disturbance that the macromolecular layers could cause on the self-assembly process. Nevertheless, simulations have shown that this effect is dependent on the packing density of the polymer tethers on the rods.[215] Therefore, selective modification at the reducing ends of CNCs could allow sufficient packing density and the formation of chiral nematic phases. Even though there is no experimental data for the formation of chiral nematic phases with such polymer end-group modified CNCs, Horsch et al. reported theoretical descriptions on chiral nematic phases of achiral end-tethered nanorods.[215−217] Furthermore, as described in section 3.4, Zoppe et al. proposed the starting point for symmetric (perhaps using CNCs from the cellulose II polymorph) and asymmetric CNCs (cellulose I polymorph) as new colloidal building blocks for self-assembled structures.[172] Moreover, much work remains in addressing some of the research challenges ranging from the synthesis of such polymer-modified CNCs to their self-assembly and applications.

In addition, CNC aspect ratio and polymer:tether length ratio will likely play a critical role in their self-assembly. Other questions include; what is the most promising approach to reduce the size distribution of CNCs? How does cellulose polymorph structure affect their native chiral morphology and assembly? Will end-tethered polymers allow polymer-modified CNCs to form chiral LC phases without sulfate half-ester groups? Will they phase separate into defined morphologies? These challenges will be investigated in our future research and we encourage others in the field to join us on this invigorating research path. Overall, our hope is that such end group-modified polymer-modified CNCs will open new avenues toward the fundamental understanding of the processes that govern the self-assembly of anisotropic colloids and a wide range of new nanocomposites and functional materials with programmed chirality.

■ ASSOCIATED CONTENT

Supporting Information

The Supporting Information is available free of charge on the ACS Publications website at DOI: 10.1021/acs.macromol.8b00733.

Overview of all polymers grafted from CNCs cited in this Perspective summarized in a table by the polymerization technique employed, including substrate, monomer(s),

DOI: 10.1021/acs.macromol.8b00733
Macromolecules 2018, 51, 6157−6189

reaction conditions, resulting properties, and applications (PDF)

AUTHOR INFORMATION

Corresponding Author

*(J.O.Z.) E-mail: justin.zoppe@unifr.ch. Telephone: +41 26 300 9563.

ORCID

Wim Thielemans: 0000-0003-4451-1964
Christoph Weder: 0000-0001-7183-1790
Justin O. Zoppe: 0000-0002-3599-9227

Author Contributions

The manuscript was written through contributions of all authors. All authors have given approval to the final version of the manuscript.

Notes

The authors declare no competing financial interest.

Biographies

Originally from Venezuela, Sandra Wohlhauser received her Master's degree in chemical engineering from the University of Carabobo, Venezuela, in 2005. After a few years of professional experience, she returned to academia and completed a Master's degree in chemistry from the University of Fribourg, Switzerland, in 2015 while studying the potential mechano-responsive behavior of poly(sulfonate ester)s. She then joined the group of Prof. C. Weder in the Adolphe Merkle Institute at the University of Fribourg as a Ph.D. student, where she is currently working on the surface modification of CNCs with polymer chains to develop unique one-component nanocomposites in the solid state, which combine high strength, stiffness, and toughness.

Gwendoline Delepierre obtained her Bachelor's degree at KU Leuven, where she worked in The Renewable Materials and Nanotechnology Research Group under the supervision of Prof. Wim Thielemans for various research projects involving cellulose nanocrystals. During her Master's studies, she did an internship at Cambridge University in the research group of Dr. Silvia Vignolini. She worked on a project in collaboration with Dr. Wadood Hamad from FP Innovations on size sorting of cellulose nanocrystals. She went to Uppsala University for her Master's thesis to work on a collaboration between Dr. Lukazs Pilarski's group in Biomedicinskt centrum (BMC) and that of Dr. Anders Thapper at Uppsala's Ångström laboratory. She finished her Master's program in KU Leuven and started her Ph.D. work in the Adolphe Merkle Institute in October 2017 under the supervision of Dr. Justin Zoppe and Prof. Christoph Weder.

Marianne Labet is a research associate working at KU Leuven (Belgium). She received her MEng in paper science, printing, and converting from the French Graduate School of Engineering in Paper, Print Media, and Biomaterials and her MRes in materials science and engineering from Grenoble INP in 2006. She obtained her Ph.D. in chemistry and chemical engineering from the University of Nottingham (U.K.) working on the SI-ROP of ϵ-caprolactone from polysaccharide nanocrystals under the supervision of Wim Thielemans. She then worked as a postdoctoral researcher with Chris Breen of the Materials and Engineering Research Institute at Sheffield Hallam University (U.K.) and with Xavier Coqueret of the Institut de Chimie Moléculaire de Reims at the University of Reims (France). Her research interests include cellulose based composites, the recycling of polymer-based materials and the development of materials for packaging applications.

Gaëlle Morandi was born in Le Mans, France, and received her Ph.D. in polymer chemistry and physical chemistry in 2007 from the Université du Maine under the supervision of Prof. L. Fontaine. She then joined W. Thielemans' group in Nottingham, U.K., as a postdoctoral fellow, to develop cellulose nanocrystals grafted with polymeric chains through a SI-ATRP process. Since 2009, she is an assistant professor in INSA Rouen Normandie. Her research interests include the controlled

DOI: 10.1021/acs.macromol.8b00733
Macromolecules 2018, 51, 6157–6189

synthesis of stimuli-sensitive amphiphilic copolymers and their association into mixed micelles of tunable stability.

Wim Thielemans is Professor, Odysseus Fellow, and Province Chair of Advanced Materials at KU Leuven, Belgium where he leads the Renewable Materials and Nanotechnology research group. Wim received his Master in Chemical Engineering from KU Leuven (BE) in 1999 and his Ph.D. in Chemical Engineering from the University of Delaware (USA) in 2004. After postdoctoral work as a Marie Curie research fellow at the School of Engineering in Paper, Print Media, and Biomaterials of the National Polytechnic Institute of Grenoble (France), he became a lecturer, then associate professor at the University of Nottingham (U.K.) in 2006. In 2013, Wim completed the circle by moving back to KU Leuven with an Odysseus fellowship from Research Foundation Flanders as associate professor and was promoted to professor in 2017. Wim is currently also an honorary professor with the University of Nottingham and an affiliate professor with the University of Auburn. His research group focusses on the development of renewable (nano)materials.

Christoph Weder is Professor for Polymer Chemistry and Materials and Director of the Adolphe Merkle Institute (AMI) at the University of Fribourg (Switzerland). He also directs the Swiss National Center of Competence in Research Bio-Inspired Materials. Chris studied chemistry at ETH Zurich where he also earned his doctoral degree. After a postdoctoral stay at MIT, he held positions at ETH Zurich and Case Western Reserve University, before joining the AMI in 2009. Chris' current research efforts are focused on stimuli-responsive polymers and nanomaterials. He coauthored some 250 research papers and book chapters and is coinventor of 20 patents. Chris has as mentored about 70 Ph.D. students and postdoctoral researchers. He serves as an Associate Editor of ACS Macro Letters and as codirector of the Swiss Chemical Society's Polymer and Colloid Division and is a member of the Swiss Academy of Technical Sciences and a Fellow of the American Chemical Society's Division of Polymer Chemistry.

Justin O. Zoppe was born in Flint, Michigan (USA) in 1983 and graduated from the University of North Carolina at Wilmington with a Bachelor of Science degree in chemistry and a minor in mathematics. He was awarded a Ph.D. in 2011 from the Department of Forest Biomaterials at North Carolina State University under the supervision of Prof. Orlando Rojas. He then joined the Polymer Technology group of Prof. Jukka Seppälä at Aalto University as a postdoc before working as a Research Scientist at Clariant Specialty Chemicals in Frankfurt, Germany, in 2013. From 2014-2017, Dr. Zoppe was an EPFL Fellow cofunded by Marie Curie in the Polymers Laboratory of Prof. Harm-Anton Klok at the Swiss Federal Institute of Technology in Lausanne. Dr. Zoppe moved to the Polymer Chemistry & Materials Laboratory of Prof. Christoph Weder at the Adolphe Merkle Institute, University of Fribourg, in 2017 as a Group Leader and Ambizione Fellow funded by the Swiss National Science Foundation. In addition to surface modification of cellulose nanomaterials, he is interested in the fundamentals of transition metal-mediated SI-CRP carried out in polar media, surface forces, and colloidal liquid crystal assembly.

■ ACKNOWLEDGMENTS

Financial support from the Swiss National Science Foundation (SNSF) (Ambizione Grant No. PZ00P2_167900; J.O.Z. and G.D.) is gratefully acknowledged. S.W. and C.W. acknowledge financial support through the Army Research Office under Grant No. W911NF-15-1-0190. M.L. and W.T. acknowledge funding from Flanders Innovation & Entrepreneurship through the Plast-i-Com project (IWT 135100). W.T. also thanks the Provincie West-Vlaanderen for his Chair in Advanced Materials and Research Foundation Flanders for his Odysseus Fellowship (Grant G.0C60.13N).

■ ABBREVIATIONS

^{13}C,carbon isotope 13; ^{1}H NMR,proton nuclear magnetic resonance; 4-SS,sodium 4-vinylbenzenesulfonate; A(R)GET,activators (re)generated by electron transfer; AA,acrylic acid; Ac,sodium triacetoxyborohydride; ACVA,4,4′-azobis(4-cyanovaleric acid); AEM,2-aminoethyl methacrylate; AEMA,2-aminoethyl methacrylamide; AgNPs,silver nanoparticles; AGU,anhydroglucopyranose unit; AIBN,2,2′-azobis(2-methylpropionitrile); AM,acrylamide; (AMIM)Cl,1-allyl-3-methylimidazolium chloride; APS,ammonium persulfate; ATRP,atom transfer radical polymerization; AuNPs,gold nanoparticles; BA,butyl acrylate; BIBA,α-bromoisobutyric acid; bis-TAD,4,4′-(1,4-phenylene)-bis(1,2,4-triazoline-3,5-dione); BlocBuilder,4-(diethoxyphosphinyl)-2,2,5,5-tetramethyl-3-azahexane-*N*-oxyl; Br,bromine; BiBB,2-bromoisobutyryl bromide; CAN,ceric(IV) ammonium nitrate; CB[8],cucurbit[8]uril; $CDCl_3$,deuterated chloroform; Ce^{4+},ceric ion; Cl,chlorine; Cn,sodium cyanoborohydride;

DOI: 10.1021/acs.macromol.8b00733
Macromolecules 2018, 51, 6157−6189

CNC,cellulose nanocrystal; CNC-1,cellulose nanocrystals with high surface density of sulfate half-ester groups; CNC-2,cellulose nanocrystals with low surface density of sulfate half-ester groups; CNC−COOH,carboxylate functionalized cellulose nanocrystals; CNC-SH,thiolated cellulose nanocrystals; CNF,cellulose nanofibrils; CO_2,carbon dioxide; CPADB,4-cyano-4-(phenylcarbonothioylthio)pentanoic acid; CP-MAS,-cross-polarization magic angle spinning; CPT,cloud-point temperature; CSC,cellulose synthase complex; CTA,chain transfer agent; Cu,copper; DCC,*N,N′*-dicyclohexylcarbodiimide; DDMAT,2-(dodecylthiocarbonothioylthio)-2-methylpropionic acid; DEAEMA,2-(diethylamino)ethyl methacrylate; DEPN,*N*-*tert*-butyl-*N*-[1-diethylphosphono-(2,2-dimethylpropyl)] nitroxide; D-LA,D-lactide; DLS,dynamic light scattering; DMAEMA,2-(dimethylamino)ethyl methacrylate; DMAM,*N,N*-dimethylacrylamide; DMAP,4-dimethylaminopyridine; DMAPMAM,N-[3-(dimethylamino)propyl]-methacrylamide; DMF,*N,N*-dimethylformamide; DMSO,dimethyl sulfoxide; DMSO-d_6,deuterated dimethyl sulfoxide; DP,degree of polymerization; DSC,differential scanning calorimetry; *E*,elastic modulus; *E′*,storage modulus; EANI,4-ethoxy-9-allyl-1,8-naphthalimide; EBiB,ethyl α-bromoisobutyrate; EDA,ethylenediamine; EDC,*N*-(3-(dimethylamino)propyl)-*N*-ethylcarbodiimide hydrochloride; EGDMA,2-(2-methylacryloyloxy)ethyl 2-methyl-acrylate; EISA,evaporation-induced self-assembly; Fe_3O_4,magnetite; FRP,free radical polymerization; FTIR,Fourier transformed infrared; *G′*,shear storage modulus; *gg*,gauche−gauche; *gt*,gauche−trans; HBr,hydrobromic acid; HCl,hydrochloric acid; KPS,potassium persulfate; LC,liquid crystal; LCEs,liquid crystal elastomers; LCST,lower critical solution temperature; L-LA,L-lactide; MA,methyl acrylate; MADIX,macromolecular design via the interchange of xanthates; METAC,[2-(methacryloyloxy)ethyl]-trimethylammonium chloride; MgH_2,magnesium hydride; MMA,-methyl methacrylate; MMAZO,6-[4-(4-methoxyphenylazo)-phenoxy] hexyl methacrylate; M_n,number-average molecular weight; *Đ*,dispersity; $Mo(CO)_6$,molybdenumhexacarbonyl; MPC,2-methacryloyloxyethyl phosphorylcholine; M_w,weight-average molecular weight; N_2,nitrogen; NaCl,sodium chloride; $NaClO_2$,sodium chlorite; $NH_2(CH_2)_6SH{\cdot}HCl$,6-amino-1-hexanethiol hydrochloride; NHS,*N*-hydroxysuccinimide; NHS-BiB,2-bromoisobutanoic acid *N*-hydroxysuccinimide ester; NIPAM,*N*-isopropylacrylamide; NMBA,*N,N′*-methylenebis-(acrylamide); NMP,nitroxide-mediated polymerization; NMR,nuclear magnetic resonance; NPs,nanoparticles; NpMA,-naphtyl methacrylate; NVC,*N*-vinylcaprolactam; OCNs,one-component nanocomposites; OEGMA,oligoethylene glycol methacrylate; OEGMEMA,oligoethylene glycol methyl ether acrylate; −OH,hydroxyl; P(MAA-*co*-VSA),poly(methacrylic acid-*co*-vinylsulfonic acid); P4VP,poly(4-vinylpyridine); PAA,poly(acrylic acid); PAM,polyacrylamide; PBSA,poly-(butylene succinate-*co*-adipate); Pc,2-picoline−borane complex; PCL,poly(ε-caprolactone); PDMAEMA,poly-[(dimethylamino)ethyl methacrylate]; PGMA,poly(glycidyl methacrylate); pH,potential of hydrogen; PHB,poly(β-hydroxybutyrate); PHEMA,poly(2-hydroxyethyl methacrylate); PHMA,poly(hexyl methacrylate); pK_a,acid dissociation constant; PLA,poly(lactic acid); PMMA,poly(methyl methacrylate); PMAA,poly(methacrylic acid); PNVC,*N*-vinylcaprolactam; POEGMA,poly(oligoethylene glycol) methacrylate; POEGMEMA,poly[(oligoethylene glycol) methyl ether acrylate]; POM,polarized optical microscopy; PPEGEEMA,poly-[poly(ethylene glycol)ethyl ether methacrylate]; PSBAM,poly-(soybean amide methacrylate); PSty,polystyrene; PtBA,poly-(*tert*-butyl acrylate); PU,polyurethane; PVA,poly(vinyl alcohol); PVAc,poly(vinyl acetate); RAFT,reversible addition−fragmentation chain transfer; ROP,ring-opening polymerization; S,sulfur; SARA ATRP,supplemental activator and reducing agent atom transfer radical polymerization; SBAM,-soybean amide methacrylate; SBS,sodium bisulfite; SEC,size-exclusion chromatography; SEM,scanning electron microscopy; SET LRP,single-electron transfer living radical polymerization; SI-AGET-ATRP,surface-initiated activators generated by electron transfer atom transfer radical polymerization; SI-ATRP,surface-initiated atom transfer radical polymerization; SI-CRP,surface-initiated controlled radical polymerization; SI-FRP,surface-initiated free radical polymerization; SI-NMP,surface-initiated nitroxide-mediated polymerization; SI-ROP,surface-initiated ring-opening polymerization; SMA,stearyl methacrylate; SMPs,shape-memory polymers; $Sn(Oct)_2$,tin(II) 2-ethylhexanoate; S-RAFT,surface reversible addition−fragmentation chain transfer; Sty,styrene; tBA,*tert*-butyl acrylate; T_d,degradation temperature; TEM,transmission electron microscopy; TEMPO,(2,2,6,6-tetramethylpiperidin-1-yl)oxy; T_g,glass transition temperature; *tg*,trans−gauche; TGA,thermogravimetric analysis; THF,tetrahydrofuran; TMEDA,*N,N,N′,N′*-tetramethylethane-1,2-diamine; UCST,upper critical solution temperature; UPyMA,2-(3-(6-methyl-4-oxo-1,4-dihydropyrimidin-2-yl)ureido)ethyl methacrylate; UV,ultraviolet; VAc,vinyl acetate; wt %,weight percent; XPS,X-ray photoelectron spectroscopy; ΔC_p,heat capacity variation; ε-CL,ε-caprolactone; σ_b,tensile at break

REFERENCES

(1) Sanchez, C.; Belleville, P.; Popall, M.; Nicole, L. Applications of advanced hybrid organic-inorganic nanomaterials: from laboratory to market. *Chem. Soc. Rev.* **2011**, *40* (2), 696−753.

(2) Dufresne, A. *Nanocellulose: from nature to high performance tailored materials*; Walter de Gruyter GmbH: Berlin, 2012.

(3) Eichhorn, S. J. Cellulose nanowhiskers: promising materials for advanced applications. *Soft Matter* **2011**, *7* (2), 303−315.

(4) Eichhorn, S. J.; Dufresne, A.; Aranguren, M.; Marcovich, N. E.; Capadona, J. R.; Rowan, S. J.; Weder, C.; Thielemans, W.; Roman, M.; Renneckar, S.; Gindl, W.; Veigel, S.; Keckes, J.; Yano, H.; Abe, K.; Nogi, M.; Nakagaito, A. N.; Mangalam, A.; Simonsen, J.; Benight, A. S.; Bismarck, A.; Berglund, L. A.; Peijs, T. Review: current international research into cellulose nanofibres and nanocomposites. *J. Mater. Sci.* **2010**, *45* (1), 1−33.

(5) Habibi, Y.; Lucia, L. A.; Rojas, O. J. Cellulose Nanocrystals: Chemistry, Self-Assembly, and Applications. *Chem. Rev.* **2010**, *110* (6), 3479−3500.

(6) Klemm, D.; Kramer, F.; Moritz, S.; Lindstroem, T.; Ankerfors, M.; Gray, D.; Dorris, A. Nanocelluloses: A New Family of Nature-Based Materials. *Angew. Chem., Int. Ed.* **2011**, *50* (24), 5438−5466.

(7) Moon, R. J.; Martini, A.; Nairn, J.; Simonsen, J.; Youngblood, J. Cellulose nanomaterials review: structure, properties and nanocomposites. *Chem. Soc. Rev.* **2011**, *40* (7), 3941−3994.

(8) Kontturi, E.; Laaksonen, P.; Linder, M. B.; Nonappa; Gröschel, A. H.; Rojas, O. J.; Ikkala, O. Advanced Materials through Assembly of Nanocelluloses. *Adv. Mater.* **2018**, *30*, 1703779.

(9) Klemm, D.; Heublein, B.; Fink, H.-P.; Bohn, A. Cellulose: Fascinating biopolymer and sustainable raw material. *Angew. Chem., Int. Ed.* **2005**, *44* (22), 3358−3393.

(10) Sacui, I. A.; Nieuwendaal, R. C.; Burnett, D. J.; Stranick, S. J.; Jorfi, M.; Weder, C.; Foster, E. J.; Olsson, R. T.; Gilman, J. W. Comparison of the Properties of Cellulose Nanocrystals and Cellulose Nanofibrils Isolated from Bacteria, Tunicate, and Wood Processed Using Acid, Enzymatic, Mechanical, and Oxidative Methods. *ACS Appl. Mater. Interfaces* **2014**, *6* (9), 6127−6138.

DOI: 10.1021/acs.macromol.8b00733
Macromolecules 2018, 51, 6157−6189

(11) Salas, C.; Nypelö, T.; Rodriguez-Abreu, C.; Carrillo, C.; Rojas, O. J. Nanocellulose properties and applications in colloids and interfaces. *Curr. Opin. Colloid Interface Sci.* **2014**, *19* (5), 383−396.
(12) Grishkewich, N.; Mohammed, N.; Tang, J.; Tam, K. C. Recent advances in the application of cellulose nanocrystals. *Curr. Opin. Colloid Interface Sci.* **2017**, *29*, 32−45.
(13) Herbert, K. M.; Schrettl, S.; Rowan, S. J.; Weder, C. 50th Anniversary Perspective: Solid-State Multistimuli, Multiresponsive Polymeric Materials. *Macromolecules* **2017**, *50* (22), 8845−8870.
(14) Montero de Espinosa, L.; Meesorn, W.; Moatsou, D.; Weder, C. Bioinspired Polymer Systems with Stimuli-Responsive Mechanical Properties. *Chem. Rev.* **2017**, *117* (20), 12851−12892.
(15) Endes, C.; Mueller, S.; Kinnear, C.; Vanhecke, D.; Foster, E. J.; Petri-Fink, A.; Weder, C.; Clift, M. J. D.; Rothen-Rutishauser, B. Fate of Cellulose Nanocrystal Aerosols Deposited on the Lung Cell Surface In Vitro. *Biomacromolecules* **2015**, *16* (4), 1267−1275.
(16) Endes, C.; Camarero-Espinosa, S.; Mueller, S.; Foster, E. J.; Petri-Fink, A.; Rothen-Rutishauser, B.; Weder, C.; Clift, M. J. D. A critical review of the current knowledge regarding the biological impact of nanocellulose. *J. Nanobiotechnol.* **2016**, *14* (1), 78.
(17) Camarero-Espinosa, S.; Endes, C.; Mueller, S.; Petri-Fink, A.; Rothen-Rutishauser, B.; Weder, C.; Clift, M.; Foster, E. J. Elucidating the Potential Biological Impact of Cellulose Nanocrystals. *Fibers* **2016**, *4* (3), 21.
(18) Majoinen, J.; Haataja, J. S.; Appelhans, D.; Lederer, A.; Olszewska, A.; Seitsonen, J.; Aseyev, V.; Kontturi, E.; Rosilo, H.; Osterberg, M.; Houbenov, N.; Ikkala, O. Supracolloidal Multivalent Interactions and Wrapping of Dendronized Glycopolymers on Native Cellulose Nanocrystals. *J. Am. Chem. Soc.* **2014**, *136* (3), 866−869.
(19) Majoinen, J.; Hassinen, J.; Haataja, J. S.; Rekola, H. T.; Kontturi, E.; Kostiainen, M. A.; Ras, R. H. A.; Torma, P.; Ikkala, O. Chiral Plasmonics Using Twisting along Cellulose Nanocrystals as a Template for Gold Nanoparticles. *Adv. Mater.* **2016**, *28* (26), 5262.
(20) Usov, I.; Nystrom, G.; Adamcik, J.; Handschin, S.; Schutz, C.; Fall, A.; Bergstrom, L.; Mezzenga, R. Understanding nanocellulose chirality and structure-properties relationship at the single fibril level. *Nat. Commun.* **2015**, *6* (1), 7564.
(21) Camarero-Espinosa, S.; Kuhnt, T.; Foster, E. J.; Weder, C. Isolation of Thermally Stable Cellulose Nanocrystals by Phosphoric Acid Hydrolysis. *Biomacromolecules* **2013**, *14* (4), 1223−1230.
(22) Nicharat, A.; Sapkota, J.; Weder, C.; Foster, E. J. Melt processing of polyamide 12 and cellulose nanocrystals nanocomposites. *J. Appl. Polym. Sci.* **2015**, *132* (45), 42752.
(23) Trache, D.; Hussin, M. H.; Haafiz, M. K. M.; Thakur, V. K. Recent progress in cellulose nanocrystals: sources and production. *Nanoscale* **2017**, *9* (5), 1763−1786.
(24) Eyley, S.; Thielemans, W. Surface modification of cellulose nanocrystals. *Nanoscale* **2014**, *6* (14), 7764−7779.
(25) Habibi, Y. Key advances in the chemical modification of nanocelluloses. *Chem. Soc. Rev.* **2014**, *43* (5), 1519−1542.
(26) Natterodt, J. C.; Petri-Fink, A.; Weder, C.; Zoppe, J. O. Cellulose Nanocrystals: Surface Modification, Applications and Opportunities at Interfaces. *Chimia* **2017**, *71* (6), 376−383.
(27) Roy, D.; Semsarilar, M.; Guthrie, J. T.; Perrier, S. Cellulose modification by polymer grafting: a review. *Chem. Soc. Rev.* **2009**, *38* (7), 2046−2064.
(28) Zoppe, J. O.; Ataman, N. C.; Mocny, P.; Wang, J.; Moraes, J.; Klok, H. A. Surface-Initiated Controlled Radical Polymerization: State-of-the-Art, Opportunities, and Challenges in Surface and Interface Engineering with Polymer Brushes. *Chem. Rev.* **2017**, *117* (3), 1105−1318.
(29) Barbey, R.; Lavanant, L.; Paripovic, D.; Schuwer, N.; Sugnaux, C.; Tugulu, S.; Klok, H.-A. Polymer Brushes via Surface-Initiated Controlled Radical Polymerization: Synthesis, Characterization, Properties, and Applications. *Chem. Rev.* **2009**, *109* (11), 5437−5527.
(30) Habibi, Y.; Goffin, A.-L.; Schiltz, N.; Duquesne, E.; Dubois, P.; Dufresne, A. Bionanocomposites based on poly(ε-caprolactone)-grafted cellulose nanocrystals by ring-opening polymerization. *J. Mater. Chem.* **2008**, *18* (41), 5002−5010.
(31) Parker, R. M.; Guidetti, G.; Williams, C. A.; Zhao, T.; Narkevicius, A.; Vignolini, S.; Frka-Petesic, B. The Self-Assembly of Cellulose Nanocrystals: Hierarchical Design of Visual Appearance. *Adv. Mater.* **2018**, *30*, 1704477.
(32) Kulasinski, K.; Guyer, R.; Derome, D.; Carmeliet, J. Water Adsorption in Wood Microfibril-Hemicellulose System: Role of the Crystalline−Amorphous Interface. *Biomacromolecules* **2015**, *16* (9), 2972−2978.
(33) French, A. D. Glucose, not cellobiose, is the repeating unit of cellulose and why that is important. *Cellulose* **2017**, *24* (11), 4605−4609.
(34) Wertz, J.-L.; Mercier, J.-P.; Bédué, O. *Cellulose Science and Technology*, 1st ed.; EPFL Press: Lausanne, Switzerland, 2010.
(35) Hardy, B. J.; Sarko, A. Molecular dynamics simulations and diffraction-based analysis of the native cellulose fibre: Structural modelling of the I-alpha and I-beta phases and their interconversion. *Polymer* **1996**, *37* (10), 1833−1839.
(36) Perez, S.; Samain, D. Structure and Engineering of Celluloses. *Adv. Carbohydr. Chem. Biochem.* **2010**, *64*, 25−116.
(37) Vietor, R. J.; Newman, R. H.; Ha, M.-A.; Apperley, D. C.; Jarvis, M. C. Conformational features of crystal-surface cellulose from higher plants. *Plant J.* **2002**, *30* (6), 721−731.
(38) Newman, R. H.; Davidson, T. C. Molecular conformations at the cellulose-water interface. *Cellulose* **2004**, *11* (1), 23−32.
(39) Nishiyama, Y.; Langan, P.; Chanzy, H. Crystal structure and hydrogen-bonding system in cellulose 1 beta from synchrotron X-ray and neutron fiber diffraction. *J. Am. Chem. Soc.* **2002**, *124* (31), 9074−9082.
(40) Sugiyama, J.; Vuong, R.; Chanzy, H. Electron-Diffraction Study on the 2 Crystalline Phases Occurring in Native Cellulose from an Algal Cell-Wall. *Macromolecules* **1991**, *24* (14), 4168−4175.
(41) Wada, M.; Okano, T.; Sugiyama, J. Synchrotron-radiated X-ray and neutron diffraction study of native cellulose. *Cellulose* **1997**, *4* (3), 221−232.
(42) Wang, T.; Phyo, P.; Hong, M. Multidimensional solid-state NMR spectroscopy of plant cell walls. *Solid State Nucl. Magn. Reson.* **2016**, *78*, 56−63.
(43) Wang, T.; Yang, H.; Kubicki, J. D.; Hong, M. Cellulose Structural Polymorphism in Plant Primary Cell Walls Investigated by High-Field 2D Solid-State NMR Spectroscopy and Density Functional Theory Calculations. *Biomacromolecules* **2016**, *17* (6), 2210−22.
(44) Debzi, E. M.; Chanzy, H.; Sugiyama, J.; Tekely, P.; Excoffier, G. The I-Alpha-]I-Beta Transformation of Highly Crystalline Cellulose by Annealing in Various Media. *Macromolecules* **1991**, *24* (26), 6816−6822.
(45) Wada, M.; Kondo, T.; Okano, T. Thermally induced crystal transformation from cellulose I-alpha to I-beta. *Polym. J. (Tokyo, Jpn.)* **2003**, *35* (2), 155−159.
(46) Yamamoto, H.; Horii, F. CP/MAS 13C NMR Analysis of the Crystal Transformation Induced for Valonia Cellulose by Annealing at HighTemperatures. *Macromolecules* **1993**, *26* (6), 1313−1317.
(47) French, A. D.; Johnson, G. P. Cellulose and the twofold screw axis: modeling and experimental arguments. *Cellulose* **2009**, *16* (6), 959−973.
(48) Huber, K. C.; McDonald, A.; BeMiller, J. N. Carbohydrate Chemistry. *Handbook of Food Science, Technology, and Engineering* **2006**, *1*, 1−23.
(49) Kovalenko, V. I. Crystalline Cellulose: Structure and Hydrogen Bonds. *Russ. Chem. Rev.* **2010**, *79* (3), 231.
(50) Tsuji, M.; Manley, R. S. Image-Analysis in the Electron-Microscopy of Cellulose Protofibrils. *Colloid Polym. Sci.* **1984**, *262* (3), 236−244.
(51) Brown, R. M.; Montezinos, D. Cellulose Microfibrils - Visualization of Biosynthetic and Orienting Complexes in Association with Plasma-Membrane. *Proc. Natl. Acad. Sci. U. S. A.* **1976**, *73* (1), 143−147.
(52) Kimura, S.; Laosinchai, W.; Itoh, T.; Cui, X.; Linder, C. R.; Brown, R. M. Immunogold labeling of rosette terminal cellulose-

DOI: 10.1021/acs.macromol.8b00733
Macromolecules 2018, 51, 6157−6189

synthesizing complexes in the vascular plant Vigna angularis. *Plant Cell* **1999**, *11* (11), 2075−2085.
(53) Brown, R. M. The biosynthesis of cellulose. *J. Macromol. Sci., Part A: Pure Appl.Chem.* **1996**, *A33* (10), 1345−1373.
(54) Mueller, S. C.; Brown, R. M. Evidence for an Intramembrane Component Associated with a Cellulose Microfibril-Synthesizing Complex in Higher-Plants. *J. Cell Biol.* **1980**, *84* (2), 315−326.
(55) Fernandes, A. N.; Thomas, L. H.; Altaner, C. M.; Callow, P.; Forsyth, V. T.; Apperley, D. C.; Kennedy, C. J.; Jarvis, M. C. Nanostructure of cellulose microfibrils in spruce wood. *Proc. Natl. Acad. Sci. U. S. A.* **2011**, *108* (47), E1195−E1203.
(56) Nishiyama, Y. Structure and properties of the cellulose microfibril. *J. Wood Sci.* **2009**, *55* (4), 241−249.
(57) Nishiyama, Y.; Sugiyama, J.; Chanzy, H.; Langan, P. Crystal structure and hydrogen bonding system in cellulose 1(alpha), from synchrotron X-ray and neutron fiber diffraction. *J. Am. Chem. Soc.* **2003**, *125* (47), 14300−14306.
(58) Cosgrove, D. J. Re-constructing our models of cellulose and primary cell wall assembly. *Curr. Opin. Plant Biol.* **2014**, *22*, 122−131.
(59) Wang, T.; Hong, M. Solid-state NMR investigations of cellulose structure and interactions with matrix polysaccharides in plant primary cell walls. *J. Exp. Bot.* **2016**, *67* (2), 503−14.
(60) Kono, H.; Yunoki, S.; Shikano, T.; Fujiwara, M.; Erata, T.; Takai, M. CP/MAS 13C NMR study of cellulose and cellulose derivatives. 1. Complete assignment of the CP/MAS 13C NMR spectrum of the native cellulose. *J. Am. Chem. Soc.* **2002**, *124* (25), 7506−7511.
(61) Rowland, S. P.; Howley, P. S. Hydrogen-Bonding on Accessible Surfaces of Cellulose from Various Sources and Relationship to Order within Crystalline Regions. *J. Polym. Sci., Part A: Polym. Chem.* **1988**, *26* (7), 1769−1778.
(62) Eyley, S.; Shariki, S.; Dale, S. E. C.; Bending, S.; Marken, F.; Thielemans, W. Ferrocene-Decorated Nanocrystalline Cellulose with Charge Carrier Mobility. *Langmuir* **2012**, *28* (16), 6514−6519.
(63) Wakelyn, P. J.; Bertoniere, N. R.; French, A. D.; Thibodeaux, D. P.; Triplett, B. A.; Rousselle, M.-A.; Goynes, W. R.; Edwards, J. V.; Hunter, L.; McAlister, D. D.; Gamble, G. R. Cotton Fibers: Chemical properties of cotton. *Handbook of Fiber Chemistry* **2007**, *20061511*, 584−628.
(64) Atkins, P.; de Paula, J. *Physical Chemistry*, 8th ed.; W. H. Freeman and Company: New York, 2006.
(65) Beck, S.; Méthot, M.; Bouchard, J. General procedure for determining cellulose nanocrystal sulfate half-ester content by conductometric titration. *Cellulose* **2015**, *22* (1), 101−116.
(66) Jiang, F.; Esker, A. R.; Roman, M. Acid-Catalyzed and Solvolytic Desulfation of H2SO4-Hydrolyzed Cellulose Nanocrystals. *Langmuir* **2010**, *26* (23), 17919−17925.
(67) Kloser, E.; Gray, D. G. Surface Grafting of Cellulose Nanocrystals with Poly(ethylene oxide) in Aqueous Media. *Langmuir* **2010**, *26* (16), 13450−13456.
(68) Habibi, Y.; Chanzy, H.; Vignon, M. R. TEMPO-mediated surface oxidation of cellulose whiskers. *Cellulose* **2006**, *13* (6), 679−687.
(69) Lee, S.-Y.; Mohan, D. J.; Kang, I.-A.; Doh, G.-H.; Lee, S.; Han, S. O. Nanocellulose reinforced PVA composite films: Effects of acid treatment and filler loading. *Fibers Polym.* **2009**, *10* (1), 77−82.
(70) Filson, P. B.; Dawson-Andoh, B. E.; Schwegler-Berry, D. Enzymatic-mediated production of cellulose nanocrystals from recycled pulp. *Green Chem.* **2009**, *11* (11), 1808−1814.
(71) Lu, Q.; Cai, Z.; Lin, F.; Tang, L.; Wang, S.; Huang, B. Extraction of Cellulose Nanocrystals with a High Yield of 88% by Simultaneous Mechanochemical Activation and Phosphotungstic Acid Hydrolysis. *ACS Sustainable Chem. Eng.* **2016**, *4* (4), 2165−2172.
(72) Leung, A. C. W.; Hrapovic, S.; Lam, E.; Liu, Y.; Male, K. B.; Mahmoud, K. A.; Luong, J. H. T. Characteristics and Properties of Carboxylated Cellulose Nanocrystals Prepared from a Novel One-Step Procedure. *Small* **2011**, *7* (3), 302−305.
(73) Zhou, Y.; Saito, T.; Bergström, L.; Isogai, A. Acid-Free Preparation of Cellulose Nanocrystals by TEMPO Oxidation and Subsequent Cavitation. *Biomacromolecules* **2018**, *19*, 633−639.
(74) Van den Berg, O.; Capadona, J. R.; Weder, C. Preparation of Homogeneous Dispersions of Tunicate Cellulose Whiskers in Organic Solvents. *Biomacromolecules* **2007**, *8* (4), 1353−1357.
(75) Beck, S.; Bouchard, J.; Berry, R. Dispersibility in Water of Dried Nanocrystalline Cellulose. *Biomacromolecules* **2012**, *13* (5), 1486−1494.
(76) Foster, E. J.; Moon, R. J.; Agarwal, U. P.; Bortner, M. J.; Bras, J.; Camarero-Espinosa, S.; Chan, K. J.; Clift, M. J. D.; Cranston, E. D.; Eichhorn, S. J.; Fox, D. M.; Hamad, W. Y.; Heux, L.; Jean, B.; Korey, M.; Nieh, W.; Ong, K. J.; Reid, M. S.; Renneckar, S.; Roberts, R.; Shatkin, J. A.; Simonsen, J.; Stinson-Bagby, K.; Wanasekara, N.; Youngblood, J. Current characterization methods for cellulose nanomaterials. *Chem. Soc. Rev.* **2018**, *47* (8), 2609−2679.
(77) Carlsson, L.; Ingverud, T.; Blomberg, H.; Carlmark, A.; Larsson, P. T.; Malmström, E. Surface characteristics of cellulose nanoparticles grafted by surface-initiated ring-opening polymerization of ε-caprolactone. *Cellulose* **2015**, *22* (2), 1063−1074.
(78) Labet, M.; Thielemans, W. Improving the reproducibility of chemical reactions on the surface of cellulose nanocrystals: ROP of ε-caprolactone as a case study. *Cellulose* **2011**, *18* (3), 607−617.
(79) Labet, M.; Thielemans, W. Citric acid as a benign alternative to metal catalysts for the production of cellulose-grafted-polycaprolactone copolymers. *Polym. Chem.* **2012**, *3* (3), 679−684.
(80) Bellani, C. F.; Pollet, E.; Hebraud, A.; Pereira, F. V.; Schlatter, G.; Averous, L.; Bretas, R. E. S.; Branciforti, M. C. Morphological, thermal, and mechanical properties of poly(ε-caprolactone)/poly(ε-caprolactone)-grafted-cellulose nanocrystals mats produced by electrospinning. *J. Appl. Polym. Sci.* **2016**, *133* (21), 43445.
(81) Lin, N.; Chen, G.; Huang, J.; Dufresne, A.; Chang, P. R. Effects of polymer-grafted natural nanocrystals on the structure and mechanical properties of poly(lactic acid): A case of cellulose whisker-graft-polycaprolactone. *J. Appl. Polym. Sci.* **2009**, *113* (5), 3417−3425.
(82) Simao, J. A.; Bellani, C. F.; Branciforti, M. C. Thermal properties and crystallinity of PCL/PBSA/cellulose nanocrystals grafted with PCL chains. *J. Appl. Polym. Sci.* **2017**, *134* (8), 44493.
(83) Tian, C.; Fu, S.; Chen, J.; Meng, Q.; Lucia, L. A. Graft polymerization of ε-caprolactone to cellulose nanocrystals and optimization of grafting conditions utilizing a response surface methodology. *Nord. Pulp Pap. Res. J.* **2014**, *29* (01), 058−068.
(84) Braun, B.; Dorgan, J. R.; Hollingsworth, L. O. Supra-Molecular EcoBioNanocomposites Based on Polylactide and Cellulosic Nanowhiskers: Synthesis and Properties. *Biomacromolecules* **2012**, *13* (7), 2013−2019.
(85) Peltzer, M.; Pei, A.; Zhou, Q.; Berglund, L.; Jimenez, A. Surface modification of cellulose nanocrystals by grafting with poly(lactic acid). *Polym. Int.* **2014**, *63* (6), 1056−1062.
(86) Tian, C.; Fu, S.; Habibi, Y.; Lucia, L. A. Polymerization Topochemistry of Cellulose Nanocrystals: A Function of Surface Dehydration Control. *Langmuir* **2014**, *30* (48), 14670−14679.
(87) Bitinis, N.; Verdejo, R.; Bras, J.; Fortunati, E.; Kenny, J. M.; Torre, L.; López-Manchado, M. A. Poly(lactic acid)/natural rubber/cellulose nanocrystal bionanocomposites Part I. Processing and morphology. *Carbohydr. Polym.* **2013**, *96* (2), 611−620.
(88) Goffin, A.-L.; Raquez, J.-M.; Duquesne, E.; Siqueira, G.; Habibi, Y.; Dufresne, A.; Dubois, P. From Interfacial Ring-Opening Polymerization to Melt Processing of Cellulose Nanowhisker-Filled Polylactide-Based Nanocomposites. *Biomacromolecules* **2011**, *12* (7), 2456−2465.
(89) Wu, H.; Nagarajan, S.; Zhou, L.; Duan, Y.; Zhang, J. Synthesis and characterization of cellulose nanocrystal-graft-poly(d-lactide) and its nanocomposite with poly(l-lactide). *Polymer* **2016**, *103*, 365−375.
(90) Lizundia, E.; Vilas, J. L.; Leon, L. M. Crystallization, structural relaxation and thermal degradation in Poly(l-lactide)/cellulose nanocrystal renewable nanocomposites. *Carbohydr. Polym.* **2015**, *123*, 256−265.
(91) Lizundia, E.; Fortunati, E.; Dominici, F.; Vilas, J. L.; Leon, L. M.; Armentano, I.; Torre, L.; Kenny, J. M. PLLA-grafted cellulose nanocrystals: Role of the CNC content and grafting on the PLA bionanocomposite film properties. *Carbohydr. Polym.* **2016**, *142*, 105−113.

DOI: 10.1021/acs.macromol.8b00733
Macromolecules 2018, 51, 6157−6189

(92) Tang, J.; Sisler, J.; Grishkewich, N.; Tam, K. C. Functionalization of cellulose nanocrystals for advanced applications. *J. Colloid Interface Sci.* **2017**, *494*, 397−409.
(93) Wohlhauser, S.; Meesorn, W.; Montero de Espinosa, L.; Weder, C. One-component nanocomposites based on homopolymer-grafted cellulose nanocrystals. Manuscript in preparation, 2018.
(94) Espino-Perez, E.; Gilbert, R. G.; Domenek, S.; Brochier-Salon, M. C.; Belgacem, M. N.; Bras, J. Nanocomposites with functionalised polysaccharide nanocrystals through aqueous free radical polymerisation promoted by ozonolysis. *Carbohydr. Polym.* **2016**, *135*, 256−266.
(95) Boujemaoui, A.; Mongkhontreerat, S.; Malmström, E.; Carlmark, A. Preparation and characterization of functionalized cellulose nanocrystals. *Carbohydr. Polym.* **2015**, *115* (SupplementC), 457−464.
(96) Liu, T.; Xue, F.; Ding, E. Cellulose nanocrystals grafted with polyacrylamide assisted by macromolecular RAFT agents. *Cellulose* **2016**, *23* (6), 3717−3735.
(97) Coulembier, O.; Dubois, P. Polyesters from beta-lactones. *Handbook of Ring-Opening Polymerization* **2009**, 227−254.
(98) Albertsson, A.-C.; Varma, I. K.; Srivastava, R. K. Polyesters from large lactones. *Handbook of Ring-Opening Polymerization* **2009**, 287−306.
(99) Dechy-Cabaret, O.; Martin-Vaca, B.; Bourissou, D. Polyesters from dilactones. *Handbook of Ring-Opening Polymerization* **2009**, 255−286.
(100) Roda, J. Polyamides. *Handbook of Ring-Opening Polymerization* **2009**, 165−195.
(101) Keul, H. Polycarbonates. *Handbook of Ring-Opening Polymerization* **2009**, 307−327.
(102) Hoogenboom, R. Polyethers and polyoxazolines. *Handbook of Ring-Opening Polymerization* **2009**, 141−164.
(103) Goffin, A.-L.; Raquez, J.-M.; Duquesne, E.; Siqueira, G.; Habibi, Y.; Dufresne, A.; Dubois, P. Poly(ϵ-caprolactone) based nanocomposites reinforced by surface-grafted cellulose nanowhiskers via extrusion processing: Morphology, rheology, and thermo-mechanical properties. *Polymer* **2011**, *52* (7), 1532−1538.
(104) Goffin, A.-L.; Habibi, Y.; Raquez, J.-M.; Dubois, P. Polyester-Grafted Cellulose Nanowhiskers: A New Approach for Tuning the Microstructure of Immiscible Polyester Blends. *ACS Appl. Mater. Interfaces* **2012**, *4* (7), 3364−3371.
(105) Muiruri, J. K.; Liu, S.; Teo, W. S.; Kong, J.; He, C. Highly Biodegradable and Tough Polylactic Acid-Cellulose Nanocrystal Composite. *ACS Sustainable Chem. Eng.* **2017**, *5* (5), 3929−3937.
(106) Ma, P.; Jiang, L.; Xu, P.; Dong, W.; Chen, M.; Lemstra, P. J. Rapid Stereocomplexation between Enantiomeric Comb-Shaped Cellulose-g-poly(l-lactide) Nanohybrids and Poly(d-lactide) from the Melt. *Biomacromolecules* **2015**, *16* (11), 3723−3729.
(107) De Paula, E. L.; Roig, F.; Mas, A.; Habas, J.-P.; Mano, V.; Pereira, F. V.; Robin, J.-J. Effect of surface-grafted cellulose nanocrystals on the thermal and mechanical properties of PLLA based nanocomposites. *Eur. Polym. J.* **2016**, *84*, 173−187.
(108) Miao, C.; Hamad, W. Y. In-situ polymerized cellulose nanocrystals (CNC)-poly(L-lactide) (PLLA) nanomaterials and applications in nanocomposite processing. *Carbohydr. Polym.* **2016**, *153*, 549−558.
(109) Habibi, Y.; Aouadi, S.; Raquez, J.-M.; Dubois, P. Effects of interfacial stereocomplexation in cellulose nanocrystal-filled polylactide nanocomposites. *Cellulose* **2013**, *20* (6), 2877−2885.
(110) Ma, P.; Shen, T.; Lin, L.; Dong, W.; Chen, M. Cellulose-g-poly(D-lactide) nanohybrids induced significant low melt viscosity and fast crystallization of fully bio-based nanocomposites. *Carbohydr. Polym.* **2017**, *155*, 498−506.
(111) Carlmark, A.; Larsson, E.; Malmstroem, E. Grafting of cellulose by ring-opening polymerization - A review. *Eur. Polym. J.* **2012**, *48* (10), 1646−1659.
(112) Chen, G.; Dufresne, A.; Huang, J.; Chang, P. R. A Novel Thermoformable Bionanocomposite Based on Cellulose Nanocrystal-graft-Poly(ε-caprolactone). *Macromol. Mater. Eng.* **2009**, *294* (1), 59−67.
(113) Chen, J.; Wu, D.; Tam, K. C.; Pan, K.; Zheng, Z. Effect of surface modification of cellulose nanocrystal on nonisothermal crystallization of poly(β-hydroxybutyrate) composites. *Carbohydr. Polym.* **2017**, *157*, 1821−1829.
(114) Hansson, S.; Antoni, P.; Bergenudd, H.; Malmstrom, E. Selective cleavage of polymer grafts from solid surfaces: assessment of initiator content and polymer characteristics. *Polym. Chem.* **2011**, *2* (3), 556−558.
(115) Morandi, G.; Thielemans, W. Synthesis of cellulose nanocrystals bearing photocleavable grafts by ATRP. *Polym. Chem.* **2012**, *3* (6), 1402−1407.
(116) Klok, H.-A.; Genzer, J. Expanding the Polymer Mechanochemistry Toolbox through Surface-Initiated Polymerization. *ACS Macro Lett.* **2015**, *4* (6), 636−639.
(117) Sheiko, S. S.; Panyukov, S.; Rubinstein, M. Bond Tension in Tethered Macromolecules. *Macromolecules* **2011**, *44* (11), 4520−4529.
(118) Anzlovar, A.; Huskic, M.; Zagar, E. Modification of nanocrystalline cellulose for application as a reinforcing nanofiller in PMMA composites. *Cellulose* **2016**, *23* (1), 505−518.
(119) Casas, J.; Persson, P. V.; Iversen, T.; Córdova, A. Direct Organocatalytic Ring-Opening Polymerizations of Lactones. *Adv. Synth. Catal.* **2004**, *346* (9−10), 1087−1089.
(120) Hafrén, J.; Córdova, A. Direct Organocatalytic Polymerization from Cellulose Fibers. *Macromol. Rapid Commun.* **2005**, *26* (2), 82−86.
(121) Dadkhah Tehrani, A.; Neysi, E. Surface modification of cellulose nanowhisker throughout graft polymerization of 2-ethyl-2-oxazoline. *Carbohydr. Polym.* **2013**, *97* (1), 98−104.
(122) Odian, G. *Principles of Polymerization*, 4th ed.; John Wiley & Sons, Inc.: Hoboken, NJ, 2004.
(123) Liu, S.; Jin, M.; Chen, Y.; Gao, H.; Shi, X.; Cheng, W.; Ren, L.; Wang, Y. High internal phase emulsions stabilized by supramolecular cellulose nanocrystals and their application as cell-adhesive macroporous hydrogel monoliths. *J. Mater. Chem. B* **2017**, *5* (14), 2671−2678.
(124) Wu, Y.; Wang, L.; Qing, Y.; Yan, N.; Tian, C.; Huang, Y. A green route to prepare fluorescent and absorbent nano-hybrid hydrogel for water detection. *Sci. Rep.* **2017**, *7* (1), 4380.
(125) Anirudhan, T. S.; Rejeena, S. R.; Binusree, J. Adsorptive Separation of Myoglobin from Aqueous Solutions Using Iron Oxide Magnetic Nanoparticles Modified with Functionalized Nanocrystalline Cellulose. *J. Chem. Eng. Data* **2013**, *58* (5), 1329−1339.
(126) Tang, J.; Lee, M. F. X.; Zhang, W.; Zhao, B.; Berry, R. M.; Tam, K. C. Dual Responsive Pickering Emulsion Stabilized by Poly[2-(dimethylamino)ethyl methacrylate] Grafted Cellulose Nanocrystals. *Biomacromolecules* **2014**, *15* (8), 3052−3060.
(127) Sarac, A. S. Redox polymerization. *Prog. Polym. Sci.* **1999**, *24* (8), 1149−1204.
(128) Zhou, C.; Wu, Q.; Yue, Y.; Zhang, Q. Application of rod-shaped cellulose nanocrystals in polyacrylamide hydrogels. *J. Colloid Interface Sci.* **2011**, *353* (1), 116−123.
(129) Zubik, K.; Singhsa, P.; Wang, Y.; Manuspiya, H.; Narain, R. Thermo-Responsive Poly(N-Isopropylacrylamide)-Cellulose Nanocrystals Hybrid Hydrogels for Wound Dressing. *Polymers* **2017**, *9* (4), 119.
(130) Feng, X. D.; Guo, X. Q.; Qiu, K. Y. Study of the initiation mechanism of the vinyl polymerization with the system persulfate/N,N,N′,N′-tetramethylethylenediamine. *Makromol. Chem.* **1988**, *189* (1), 77−83.
(131) Feng, X. D. The role of amine in vinyl radical polymerization. *Makromol. Chem., Macromol. Symp.* **1992**, *63* (1), 1−18.
(132) Kan, K. H. M.; Li, J.; Wijesekera, K.; Cranston, E. D. Polymer-Grafted Cellulose Nanocrystals as pH-Responsive Reversible Flocculants. *Biomacromolecules* **2013**, *14* (9), 3130−3139.
(133) Pracella, M.; Haque, M. M.-U.; Puglia, D. Morphology and properties tuning of PLA/cellulose nanocrystals bio-nanocomposites by means of reactive functionalization and blending with PVAc. *Polymer* **2014**, *55* (16), 3720−3728.
(134) Kedzior, S. A.; Graham, L.; Moorlag, C.; Dooley, B. M.; Cranston, E. D. Poly(methyl methacrylate)-grafted cellulose nano-

DOI: 10.1021/acs.macromol.8b00733
Macromolecules 2018, 51, 6157−6189

crystals: One-step synthesis, nanocomposite preparation, and characterization. *Can. J. Chem. Eng.* **2016**, *94* (5), 811−822.
(135) Tang, J.; Berry, R. M.; Tam, K. C. Stimuli-Responsive Cellulose Nanocrystals for Surfactant-Free Oil Harvesting. *Biomacromolecules* **2016**, *17* (5), 1748−1756.
(136) Arthur, J. C.; Baugh, P. J.; Hinojosa, O. ESR study of reactions of cellulose initiated by the ceric ion method. *J. Appl. Polym. Sci.* **1966**, *10* (10), 1591−1606.
(137) Yang, J.; Han, C.-R.; Duan, J.-F.; Ma, M.-G.; Zhang, X.-M.; Xu, F.; Sun, R.-C.; Xie, X.-M. Studies on the properties and formation mechanism of flexible nanocomposite hydrogels from cellulose nanocrystals and poly(acrylic acid). *J. Mater. Chem.* **2012**, *22* (42), 22467−22480.
(138) Yang, J.; Han, C.-R.; Duan, J.-F.; Ma, M.-G.; Zhang, X.-M.; Xu, F.; Sun, R.-C. Synthesis and characterization of mechanically flexible and tough cellulose nanocrystals−polyacrylamide nanocomposite hydrogels. *Cellulose* **2013**, *20* (1), 227−237.
(139) Lee, Y. R.; Park, D.; Choi, S. K.; Kim, M.; Baek, H. S.; Nam, J.; Chung, C. B.; Osuji, C. O.; Kim, J. W. Smart Cellulose Nanofluids Produced by Tunable Hydrophobic Association of Polymer-Grafted Cellulose Nanocrystals. *ACS Appl. Mater. Interfaces* **2017**, *9*, 31095.
(140) Dorman, G.; Prestwich, G. D. Benzophenone Photophores in Biochemistry. *Biochemistry* **1994**, *33* (19), 5661−5673.
(141) Yi, J.; Xu, Q.; Zhang, X.; Zhang, H. Chiral-nematic self-ordering of rodlike cellulose nanocrystals grafted with poly(styrene) in both thermotropic and lyotropic states. *Polymer* **2008**, *49* (20), 4406−4412.
(142) Zeinali, E.; Haddadi-Asl, V.; Roghani-Mamaqani, H. Nanocrystalline cellulose grafted random copolymers of N-isopropylacrylamide and acrylic acid synthesized by RAFT polymerization: effect of different acrylic acid contents on LCST behavior. *RSC Adv.* **2014**, *4* (59), 31428−31442.
(143) Roeder, R. D.; Garcia-Valdez, O.; Whitney, R. A.; Champagne, P.; Cunningham, M. F. Graft modification of cellulose nanocrystals via nitroxide-mediated polymerisation. *Polym. Chem.* **2016**, *7* (41), 6383−6390.
(144) Matyjaszewski, K. Atom Transfer Radical Polymerization (ATRP): Current Status and Future Perspectives. *Macromolecules* **2012**, *45* (10), 4015−4039.
(145) Jakubowski, W.; Min, K.; Matyjaszewski, K. Activators Regenerated by Electron Transfer for Atom Transfer Radical Polymerization of Styrene. *Macromolecules* **2006**, *39* (1), 39−45.
(146) Min, K.; Gao, H.; Matyjaszewski, K. Use of Ascorbic Acid as Reducing Agent for Synthesis of Well-Defined Polymers by ARGET ATRP. *Macromolecules* **2007**, *40* (6), 1789−1791.
(147) Bai, L.; Zhang, L.; Cheng, Z.; Zhu, X. Activators generated by electron transfer for atom transfer radical polymerization: recent advances in catalyst and polymer chemistry. *Polym. Chem.* **2012**, *3* (10), 2685−2697.
(148) Rosen, B. M.; Percec, V. Single-Electron Transfer and Single-Electron Transfer Degenerative Chain Transfer Living Radical Polymerization. *Chem. Rev.* **2009**, *109* (11), 5069−5119.
(149) Konkolewicz, D.; Wang, Y.; Zhong, M.; Krys, P.; Isse, A. A.; Gennaro, A.; Matyjaszewski, K. Reversible-Deactivation Radical Polymerization in the Presence of Metallic Copper. A Critical Assessment of the SARA ATRP and SET-LRP Mechanisms. *Macromolecules* **2013**, *46* (22), 8749−8772.
(150) Lligadas, G.; Grama, S.; Percec, V. Single-Electron Transfer Living Radical Polymerization Platform to Practice, Develop, and Invent. *Biomacromolecules* **2017**, *18* (10), 2981−3008.
(151) Xu, Q.; Yi, J.; Zhang, X.; Zhang, H. A novel amphotropic polymer based on cellulose nanocrystals grafted with azo polymers. *Eur. Polym. J.* **2008**, *44* (9), 2830−2837.
(152) Yi, J.; Xu, Q.; Zhang, X.; Zhang, H. Temperature-induced chiral nematic phase changes of suspensions of poly(N,N-dimethylaminoethyl methacrylate)-grafted cellulose nanocrystals. *Cellulose* **2009**, *16* (6), 989−997.
(153) Hemraz, U. D.; Lu, A.; Sunasee, R.; Boluk, Y. Structure of poly(N-isopropylacrylamide) brushes and steric stability of their grafted cellulose nanocrystal dispersions. *J. Colloid Interface Sci.* **2014**, *430*, 157−165.
(154) Wu, W.; Huang, F.; Pan, S.; Mu, W.; Meng, X.; Yang, H.; Xu, Z.; Ragauskas, A. J.; Deng, Y. Thermo-responsive and fluorescent cellulose nanocrystals grafted with polymer brushes. *J. Mater. Chem. A* **2015**, *3* (5), 1995−2005.
(155) Hemraz, U. D.; Campbell, K. A.; Burdick, J. S.; Ckless, K.; Boluk, Y.; Sunasee, R. Cationic Poly(2-aminoethylmethacrylate) and Poly(N-(2-aminoethylmethacrylamide)) Modified Cellulose Nanocrystals: Synthesis, Characterization, and Cytotoxicity. *Biomacromolecules* **2015**, *16* (1), 319−325.
(156) Wang, Z.; Zhang, Y.; Yuan, L.; Hayat, J.; Trenor, N. M.; Lamm, M. E.; Vlaminck, L.; Billiet, S.; Du Prez, F. E.; Wang, Z.; Tang, C. Biomass Approach toward Robust, Sustainable, Multiple-Shape-Memory Materials. *ACS Macro Lett.* **2016**, *5* (5), 602−606.
(157) Yin, Y.; Tian, X.; Jiang, X.; Wang, H.; Gao, W. Modification of cellulose nanocrystal via SI-ATRP of styrene and the mechanism of its reinforcement of polymethylmethacrylate. *Carbohydr. Polym.* **2016**, *142*, 206−212.
(158) Hatton, F. L.; Kedzior, S. A.; Cranston, E. D.; Carlmark, A. Grafting-from cellulose nanocrystals via photoinduced Cu-mediated reversible-deactivation radical polymerization. *Carbohydr. Polym.* **2017**, *157*, 1033−1040.
(159) Grishkewich, N.; Akhlaghi, S. P.; Zhaoling, Y.; Berry, R.; Tam, K. C. Cellulose nanocrystal-poly(oligo(ethylene glycol) methacrylate) brushes with tunable LCSTs. *Carbohydr. Polym.* **2016**, *144*, 215−222.
(160) Zhang, X.; Zhang, J.; Dong, L.; Ren, S.; Wu, Q.; Lei, T. Thermoresponsive poly(poly(ethylene glycol) methylacrylate)s grafted cellulose nanocrystals through SI-ATRP polymerization. *Cellulose* **2017**, *24*, 4189.
(161) Zhang, J.; Wu, Q.; Li, M.-C.; Song, K.; Sun, X.; Lee, S.-Y.; Lei, T. Thermoresponsive Copolymer Poly(N-Vinylcaprolactam) Grafted Cellulose Nanocrystals: Synthesis, Structure, and Properties. *ACS Sustainable Chem. Eng.* **2017**, *5* (8), 7439−7447.
(162) Morandi, G.; Heath, L.; Thielemans, W. Cellulose Nanocrystals Grafted with Polystyrene Chains through Surface-Initiated Atom Transfer Radical Polymerization (SI-ATRP). *Langmuir* **2009**, *25* (14), 8280−8286.
(163) Zoppe, J. O.; Habibi, Y.; Rojas, O. J.; Venditti, R. A.; Johansson, L.-S.; Efimenko, K.; Osterberg, M.; Laine, J. Poly(N-isopropylacrylamide) Brushes Grafted from Cellulose Nanocrystals via Surface-Initiated Single-Electron Transfer Living Radical Polymerization. *Biomacromolecules* **2010**, *11* (10), 2683−2691.
(164) Chen, X.; Huang, L.; Sun, H.-J.; Cheng, S. Z. D.; Zhu, M.; Yang, G. Stimuli-Responsive Nanocomposite: Potential Injectable Embolization Agent. *Macromol. Rapid Commun.* **2014**, *35* (5), 579−584.
(165) Majoinen, J.; Walther, A.; McKee, J. R.; Kontturi, E.; Aseyev, V.; Malho, J. M.; Ruokolainen, J.; Ikkala, O. Polyelectrolyte Brushes Grafted from Cellulose Nanocrystals Using Cu-Mediated Surface-Initiated Controlled Radical Polymerization. *Biomacromolecules* **2011**, *12* (8), 2997−3006.
(166) McKee, J. R.; Appel, E. A.; Seitsonen, J.; Kontturi, E.; Scherman, O. A.; Ikkala, O. Healable, Stable and Stiff Hydrogels: Combining Conflicting Properties Using Dynamic and Selective Three-Component Recognition with Reinforcing Cellulose Nanorods. *Adv. Funct. Mater.* **2014**, *24* (18), 2706−2713.
(167) Rosilo, H.; McKee, J. R.; Kontturi, E.; Koho, T.; Hytonen, V. P.; Ikkala, O.; Kostiainen, M. A. Cationic polymer brush-modified cellulose nanocrystals for high-affinity virus binding. *Nanoscale* **2014**, *6* (20), 11871−11881.
(168) Malho, J.-M.; Morits, M.; Lobling, T. I.; Nonappa; Majoinen, J.; Schacher, F. H.; Ikkala, O.; Groschel, A. H. Rod-Like Nanoparticles with Striped and Helical Topography. *ACS Macro Lett.* **2016**, *5* (10), 1185−1190.
(169) Yu, J.; Wang, C.; Wang, J.; Chu, F. In situ development of self-reinforced cellulose nanocrystals based thermoplastic elastomers by atom transfer radical polymerization. *Carbohydr. Polym.* **2016**, *141*, 143−150.

DOI: 10.1021/acs.macromol.8b00733
Macromolecules 2018, 51, 6157−6189

(170) Wang, H.-D.; Roeder, R. D.; Whitney, R. A.; Champagne, P.; Cunningham, M. F. Graft modification of crystalline nanocellulose by Cu(0)-mediated SET living radical polymerization. *J. Polym. Sci., Part A: Polym. Chem.* **2015**, *53* (24), 2800−2808.
(171) Arredondo, J.; Jessop, P. G.; Champagne, P.; Bouchard, J.; Cunningham, M. F. Synthesis of CO2-responsive cellulose nanocrystals by surface-initiated Cu(0)-mediated polymerisation. *Green Chem.* **2017**, *19*, 4141.
(172) Zoppe, J. O.; Dupire, A. V. M.; Lachat, T. G. G.; Lemal, P.; Rodriguez-Lorenzo, L.; Petri-Fink, A.; Weder, C.; Klok, H.-A. Cellulose Nanocrystals with Tethered Polymer Chains: Chemically Patchy versus Uniform Decoration. *ACS Macro Lett.* **2017**, *6*, 892−897.
(173) Zoppe, J. O.; Xu, X.; Kanel, C.; Orsolini, P.; Siqueira, G.; Tingaut, P.; Zimmermann, T.; Klok, H.-A. Effect of Surface Charge on Surface-Initiated Atom Transfer Radical Polymerization from Cellulose Nanocrystals in Aqueous Media. *Biomacromolecules* **2016**, *17* (4), 1404−1413.
(174) Turgman-Cohen, S.; Genzer, d. J. Simultaneous Bulk- and Surface-Initiated Controlled Radical Polymerization from Planar Substrates. *J. Am. Chem. Soc.* **2011**, *133* (44), 17567−17569.
(175) Tang, W.; Kwak, Y.; Braunecker, W.; Tsarevsky, N. V.; Coote, M. L.; Matyjaszewski, K. Understanding atom transfer radical polymerization: Effect of ligand and initiator structures on the equilibrium constants. *J. Am. Chem. Soc.* **2008**, *130* (32), 10702−10713.
(176) Hu, H.; Hou, X.-J.; Wang, X.-C.; Nie, J.-J.; Cai, Q.; Xu, F.-J. Gold nanoparticle-conjugated heterogeneous polymer brush-wrapped cellulose nanocrystals prepared by combining different controllable polymerization techniques for theranostic applications. *Polym. Chem.* **2016**, *7* (18), 3107−3116.
(177) Matyjaszewski, K.; Pintauer, T.; Gaynor, S. Removal of Copper-Based Catalyst in Atom Transfer Radical Polymerization Using Ion Exchange Resins. *Macromolecules* **2000**, *33* (4), 1476−1478.
(178) Haqani, M.; Roghani-Mamaqani, H.; Salami-Kalajahi, M. Synthesis of dual-sensitive nanocrystalline cellulose-grafted block copolymers of N-isopropylacrylamide and acrylic acid by reversible addition-fragmentation chain transfer polymerization. *Cellulose* **2017**, *24* (5), 2241−2254.
(179) Boujemaoui, A.; Mazieres, S.; Malmstroem, E.; Destarac, M.; Carlmark, A. SI-RAFT/MADIX polymerization of vinyl acetate on cellulose nanocrystals for nanocomposite applications. *Polymer* **2016**, *99*, 240−249.
(180) Liu, T.; Ding, E.; Xue, F. Polyacrylamide and poly(N,N-dimethylacrylamide) grafted cellulose nanocrystals as efficient flocculants for kaolin suspension. *Int. J. Biol. Macromol.* **2017**, *103*, 1107−1112.
(181) Garcia-Valdez, O.; Brescacin, T.; Arredondo, J.; Bouchard, J.; Jessop, P. G.; Champagne, P.; Cunningham, M. F. Grafting CO2-responsive polymers from cellulose nanocrystals via nitroxide-mediated polymerisation. *Polym. Chem.* **2017**, *8* (28), 4124−4131.
(182) Olsen, B. D.; Segalman, R. A. Self-assembly of rod-coil block copolymers. *Mater. Sci. Eng., R* **2008**, *62* (2), 37−66.
(183) Lokanathan, A.; Nykänen, A.; Seitsonen, J.; Johansson, L.-S.; Campbell, J.; Rojas, O. J.; Ikkala, O.; Laine, J. Cilia-Mimetic Hairy Surfaces Based on End-Immobilized Nanocellulose Colloidal Rods. *Biomacromolecules* **2013**, *14* (8), 2807−2813.
(184) Arcot, L. R.; Lundahl, M.; Rojas, O. J.; Laine, J. Asymmetric cellulose nanocrystals: thiolation of reducing end groups via NHS−EDC coupling. *Cellulose* **2014**, *21* (6), 4209−4218.
(185) Hieta, K.; Kuga, S.; Usuda, M. Electron staining of reducing ends evidences a parallel-chain structure in Valonia cellulose. *Biopolymers* **1984**, *23* (10), 1807−1810.
(186) Sipahi-Sağlam, E.; Gelbrich, M.; Gruber, E. Topochemically Modified Cellulose. *Cellulose* **2003**, *10* (3), 237−250.
(187) Onsager, L. The Effects of Shape on the Interaction of Colloidal Particles. *Ann. N. Y. Acad. Sci.* **1949**, *51* (4), 627−659.
(188) Dumanli, A. G.; van der Kooij, H. M.; Kamita, G.; Reisner, E.; Baumberg, J. J.; Steiner, U.; Vignolini, S. Digital Color in Cellulose Nanocrystal Films. *ACS Appl. Mater. Interfaces* **2014**, *6* (15), 12302−12306.
(189) Lagerwall, J. P. F.; Schütz, C.; Salajkova, M.; Noh, J.; Hyun Park, J.; Scalia, G.; Bergström, L. Cellulose Nanocrystal-based materials: from liquid crystal self-assembly and glass formation to multifunctional thin films. *NPG Asia Mater.* **2014**, *6*, e80.
(190) Gençer, A.; Schütz, C.; Thielemans, W. Influence of the Particle Concentration and Marangoni Flow on the Formation of Cellulose Nanocrystal Films. *Langmuir* **2017**, *33* (1), 228−234.
(191) Shopsowitz, K. E.; Qi, H.; Hamad, W. Y.; MacLachlan, M. J. Free-standing mesoporous silica films with tunable chiral nematic structures. *Nature* **2010**, *468*, 422.
(192) Schlesinger, M.; Giese, M.; Blusch, L. K.; Hamad, W. Y.; MacLachlan, M. J. Chiral nematic cellulose-gold nanoparticle composites from mesoporous photonic cellulose. *Chem. Commun.* **2015**, *51* (3), 530−533.
(193) Rojas, O. J.; Lokanathan, A. R.; Kontturi, E.; Laine, J.; Bock, H. The unusual interactions between polymer grafted cellulose nanocrystal aggregates. *Soft Matter* **2013**, *9* (37), 8965−8973.
(194) Azzam, F.; Heux, L.; Jean, B. Adjustment of the Chiral Nematic Phase Properties of Cellulose Nanocrystals by Polymer Grafting. *Langmuir* **2016**, *32* (17), 4305−4312.
(195) White, T. J.; Broer, D. J. Programmable and adaptive mechanics with liquid crystal polymer networks and elastomers. *Nat. Mater.* **2015**, *14*, 1087.
(196) Lunn, D. J.; Finnegan, J. R.; Manners, I. Self-assembly of "patchy" nanoparticles: a versatile approach to functional hierarchical materials. *Chem. Sci.* **2015**, *6* (7), 3663−3673.
(197) Gil, E. S.; Hudson, S. M. Stimuli-reponsive polymers and their bioconjugates. *Prog. Polym. Sci.* **2004**, *29* (12), 1173−1222.
(198) Swift, T.; Swanson, L.; Geoghegan, M.; Rimmer, S. The pH-responsive behaviour of poly(acrylic acid) in aqueous solution is dependent on molar mass. *Soft Matter* **2016**, *12* (9), 2542−2549.
(199) IUPAC. Definition of terms related to polymer blends, composites, and multiphase polymeric materials (IUPAC Recommendations 2004). *Pure Appl. Chem.* **2004**, *76* (11), 1985.
(200) Boutris, C.; Chatzi, E. G.; Kiparissides, C. Characterization of the LCST behaviour of aqueous poly(N-isopropylacrylamide) solutions by thermal and cloud point techniques. *Polymer* **1997**, *38* (10), 2567−2570.
(201) Zoppe, J. O.; Osterberg, M.; Venditti, R. A.; Laine, J.; Rojas, O. J. Surface Interaction Forces of Cellulose Nanocrystals Grafted with Thermoresponsive Polymer Brushes. *Biomacromolecules* **2011**, *12* (7), 2788−2796.
(202) Xia, Y.; Burke, N. A. D.; Stover, H. D. H. End group effect on the thermal response of narrow-disperse poly(N-isopropylacrylamide) prepared by atom transfer radical polymerization. *Macromolecules* **2006**, *39* (6), 2275−2283.
(203) Natterodt, J. C.; Shirole, A.; Sapkota, J.; Zoppe, J. O.; Weder, C. Polymer nanocomposites with cellulose nanocrystals made by co-precipitation. *J. Appl. Polym. Sci.* **2018**, *135*, 45648.
(204) Favier, V.; Chanzy, H.; Cavaille, J.-Y. Polymer Nanocomposites Reinforced by Cellulose Whiskers. *Macromolecules* **1995**, *28* (18), 6365−6367.
(205) Favier, V.; Canova, G. R.; Cavaille, J.-Y.; Chanzy, H.; Dufresne, A.; Gauthier, C. Nanocomposite materials from latex and cellulose whiskers. *Polym. Adv. Technol.* **1995**, *6* (5), 351−355.
(206) Meesorn, W.; Shirole, A.; Vanhecke, D.; Montero de Espinosa, L.; Weder, C. A Simple and Versatile Strategy to Improve the Mechanical Properties of Polymer Nanocomposites with Cellulose Nanocrystals. *Macromolecules* **2017**, *50* (6), 2364−2374.
(207) Kashani Rahimi, S.; Otaigbe, J. U. Polyamide 6 nanocomposites incorporating cellulose nanocrystals prepared by In-situ ring opening polymerization: Viscoelasticity, creep behavior, and melt rheological properties. *Polym. Eng. Sci.* **2016**, *56* (9), 1045−1060.
(208) Kashani Rahimi, S.; Otaigbe, J. U. The role of particle surface functionality and microstructure development in isothermal and non-isothermal crystallization behavior of polyamide 6/cellulose nanocrystals nanocomposites. *Polymer* **2016**, *107*, 316−331.

DOI: 10.1021/acs.macromol.8b00733
Macromolecules 2018, 51, 6157−6189

(209) Tian, C.; Fu, S.; Meng, Q.; Lucia, L. A. New insights into the material chemistry of polycaprolactone-grafted cellulose nanofibrils/polyurethane nanocomposites. *Cellulose* **2016**, *23* (4), 2457−2473.
(210) De France, K. J.; Hoare, T.; Cranston, E. D. Review of Hydrogels and Aerogels Containing Nanocellulose. *Chem. Mater.* **2017**, *29* (11), 4609−4631.
(211) Michalek, L.; Barner, L.; Barner-Kowollik, C. Polymer on Top: Current Limits and Future Perspectives of Quantitatively Evaluating Surface Grafting. *Adv. Mater.* **2018**, *30*, 1706321.
(212) Beck, S.; Bouchard, J.; Chauve, G.; Berry, R. Controlled production of patterns in iridescent solid films of cellulose nanocrystals. *Cellulose* **2013**, *20* (3), 1401−1411.
(213) Frka-Petesic, B.; Guidetti, G.; Kamita, G.; Vignolini, S. Controlling the Photonic Properties of Cholesteric Cellulose Nanocrystal Films with Magnets. *Adv. Mater.* **2017**, *29* (32), 1701469.
(214) Frka-Petesic, B.; Radavidson, H.; Jean, B.; Heux, L. Dynamically Controlled Iridescence of Cholesteric Cellulose Nanocrystal Suspensions Using Electric Fields. *Adv. Mater.* **2017**, *29* (11), 1606208.
(215) Horsch, M. A.; Zhang, Z.; Glotzer, S. C. Simulation studies of self-assembly of end-tethered nanorods in solution and role of rod aspect ratio and tether length. *J. Chem. Phys.* **2006**, *125* (18), 184903.
(216) Horsch, M. A.; Zhang, Z.; Glotzer, S. C. Self-Assembly of Polymer-Tethered Nanorods. *Phys. Rev. Lett.* **2005**, *95* (5), 056105.
(217) Horsch, M. A.; Zhang, Z.; Glotzer, S. C. Self-assembly of end-tethered nanorods in a neat system and role of block fractions and aspect ratio. *Soft Matter* **2010**, *6* (5), 945−954.

DOI: 10.1021/acs.macromol.8b00733
Macromolecules 2018, 51, 6157−6189